Evaluation and Characterization of Hydraulic Pulsing Drilling Tools and Potential Impacts on Penetration Rate

by

© Yousef Gharibiyamchi

A Thesis submitted to the

School of Graduate Studies

in partial fulfillment of the requirements for the degree of

Master of Engineering

Faculty of Engineering and Applied Science

Memorial University of Newfoundland

May, 2014

St. John's Newfoundland

Abstract

Hydraulic pulse tools are one of the well-known tools to create vibrational forces in drill-strings. It is known that these vibrational forces applied behind the bit can affect the drilling rate in medium strength formations. This thesis investigates the action of these types of tools behind the bit through the series of Distinct Element Method (DEM) simulations.

Two types of hydraulic pulse tools are evaluated and characterized in this thesis. The Valved-flow tool (AGT) and the Hydropulse tool. A unique simulation scenario was designed to simulate these tools in the DEM environment. Then this scenario combined with simulation of drilling process to simulate the drilling with the AGT and the Hydropulse tool.

Results of the simulations showed significant increase in drilling performance when the AGT was used in the process. Simulation results of the two types of tools were analyzed and compared to each other. The results showed that the AGT tool with accompanying shock tool has better performance than the integrated Hydropulse tool and drilling bit. The shock tool produces axial compliance in the drill-string. Results of additional simulations revealed the effect of compliance on drilling performance. These results showed that if the AGT is deployed without accompanying shock tool, it can have strong negative effect on drilling rate. On the other hand, the results suggested the use of shock tool in Hydropulse tool assembly since the drilling performance improved when shock tool was used in combination with the Hydropulse tool. It was observed from the

simulation results that the drilling performance of the Hydropulse tool was increase by more than 100 % when shock tool was used in the assembly.

Acknowledgment

There are number of people without whom this thesis might never been written and to whom I am grateful.

To my family who supported me through my entire life. Without their encouragement and support I have never managed to complete this project.

To my supervisor Dr. Stephen D. Butt who provided me with financial support as well as guidance in numerical and experimental work, academic training and other experiences that I gained while completing my Master's degree.

To my co-supervisor Dr. Katna Munaswamy who assisted me in numerical work. His ideas about my numerical work helped me a lot in deciding different simulation scenarios and parameters.

To my friend and Project Manager, Farid Arvani for his great support and guidance throughout my Master's degree. His countless effort in assisting me with data analyses and providing useful information is appreciated and Project Engineer, Brock Gillis for his great help laboratory experiments and his ideas about my numerical work.

To my friend, Mohammad Mozaffari for his help and ideas in programming the simulations. Without his help, this work would never been completed.

To all members of Advanced Drilling Group for their cooperation, support, and friendly environment. Special thanks to Sadegh Babapour, Hossein Khorshidian, Ahmed Elnahas, Masoud Khademi, Pushpinder Rana, Lei Wang and Qian Gao.

This research was conducted at the Advanced Drilling Technology Laboratory at Memorial University of Newfoundland and was funded by the Atlantic Canada Opportunities Agency (AIF Contract no. 781-2636-1920044), the Research and Development Corporation of Newfoundland and Labrador, Husky Energy, and Suncor Energy.

Table of Content

List of Tables

List of Figures

List of Symbols, Nomenclature or Abbreviations

DEM	Distinct Element Method
UCS	Unconfined Compressive Strength
ROP	Rate of Penetration
TVD	Total Vertical Depth
UBD	Under-Balance Drilling
MPD	Managed Pressure Drilling
AGT	Axial oscillation Generator Tool
NOV	National Oil well Varco
PDC	Polycrystalline Diamond Compact
MRR	Material Removal Rate
MSE	Mechanical Specific Energy
WOB	Weight on Bit
TOB	Torque on Bit
DOC	Depth of Cut
POA	Pump Open Area
GPM	Gallon per Minute

IADC	International Association of Drilling Contractors
PPG	Pound per Gallon
OVA	Oscillating Valve Assembly
PDM	Positive Displacement Motor
MD	Molecular Dynamic
ED	Event-driven
PFC	Particle Flow Code
MWD	Measurement While Drilling
RPM	Revolution per Minute

Θ	Back rake angle
F^c_s	Horizontal force on cutter
F^c_n	Vertical force on cutter
ζ	Intrinsic specific energy
ψ	Interfacial friction angle
d	Depth of cut
E	Drilling specific energy
S	Drilling strength

μ	Coefficient of friction
γ	Bit constant
l	Contact length
σ	Contact strength
F^c	Face cutter force
F^{ch}	Chamfer force
F^b	Back cutter force
σ_0	Hydrostatic stress in crushed material
A_{ch}	Chamfer area
ω_d	Relief angle
a	Repression angle
ρ	Density
K_f	Bulk modulus
X_i	Position vector
U^n	Amount of overlap
R	Ball radius
g	Gravity
M	Moment

List of Appendices

Chapter 1 Introduction

1.1 Introduction

Drilling is one of the most expensive components of oil and gas exploration and production. For example at the Eagle Ford shale formation of Texas, drilling and completion cost per well are ranging from $5.5 to $9.5 million [1]. Offshore wells can cost higher than onshore wells. As a result, drilling engineers try to reduce these costs by increasing Rate of Penetration (ROP) and reducing rig time. In order to reach a reservoir, different types of drilling are used such as conventional, directional and extended reach drilling. Each of these drilling types has its own associated complications that limit ROP and reach of the well. Countless efforts have been made and numerous tools and technologies have been introduced in order to overcome these problems and ease the drilling process but as the bit goes deeper, new problems appear and the process becomes more complicated.

Conventional rotary drilling methods have existed since the 1950s [2]. One of the crucial problems associated with conventional drilling is the low ROP at greater depth. As Total Vertical Depth (TVD) increases, the ROP drops dramatically. The main reason for this phenomenon is bottom-hole pressure caused by the drilling mud column [3]. The bottom-hole drilling fluid pressure is typically kept about 10 % above formation pore pressure during conventional over-balanced drilling in order to stop the influx of formation pore fluid to the well bore. This differential pressure increases rock strength and inhibits the removal of cuttings from the bottom [3].

Figure 1.1 shows how the ROP decreases with an increase in differential pressure for drilling in Indiana limestone formation. Differential pressure is the pressure difference between hydrostatic pressure of the drilling fluid and formation pressure. Some techniques such as Under-Balanced Drilling (UBD) and Managed Pressure Drilling (MPD) and different tools such as down-hole pressure pulsation tools and down-hole vibration tools have been introduced in the past few years to overcome this issue. Nevertheless, this issue is still one of the most important and crucial issues in conventional drilling.

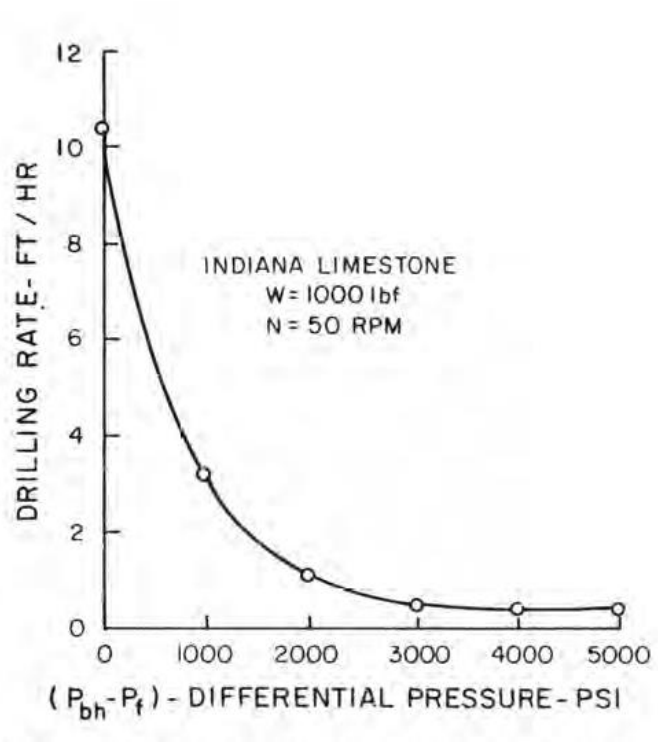

Figure 1.1: Penetration rate as a function of differential pressure for Indiana Limestone [4]

In the past few decades, drilling engineers have tried to overcome the problem of reduced ROP in pressurized wells. They have utilized different phenomena in nature to find a way to solve this problem. Numerous drilling methods using different mechanisms have been introduced to the industry so far. Researchers have examined different ideas such as drilling with hydraulic jets to the drilling with special drilling fluids which contains small explosive particles [5]. Among these ideas, the idea of varying force behind the bit is older than the others. The use of percussion drilling which utilizes a percussion hammer to produce impacts behind the bit was started from the early 1960s. Many tools have been introduced to the industries that create different profiles of varying force since then. Percussion tools increased rate of penetration significantly when drilling hard rocks, however, no significant effect was reported for down-hole hammers in drilling medium and weak formations. Recently, new down-hole tools such as Hydropulse and Valved-flow tools have been developed in order to increase ROP in the medium and weak formations. These tools produce high frequency variable force behind the bit through complete or partial stoppage of flow area. Different force profiles were generated by these tools. For example, the Hydropulse tool generates impulsive force profile using momentary obstruction of the flow area, while Valved-flow tools such as the Axial Oscillation Generator Tool (AGT) produces sinusoidal force profile through restriction of the flow area. Vibration drilling is the term that is used when drilling with these types of tools. Vibration drilling utilizes high frequency vibrations to increase ROP in the medium and low strength rocks.

1.2 Research Objectives and Scope

The use of down-hole pulse tools in order to produce axial variable force behind the bit has been investigated by several researchers in the past few decades. Pressure pulses produced by momentarily stopping the flow in the flow channel can act on bit cross sectional area and produce variable forces.

Kolle [3] conducted a comprehensive investigation of the effect of the produced pressure pulses on drilling performance and rock destruction. He developed a pressure confinement model to predict rock behavior at the bottom-hole condition. He attempted to develop a prototype tool called the Hydropulse tool in order to produce high frequency and high amplitude pressure pulses, using a complicated mechanism for stopping flow.

Recently, the National Oilwell Varco (NOV) Company has developed a Valved-flow tool called the Axial Oscillation Generator Tool (AGT) or the Agitator Tool that produces sinusoidal pressure pulses by restricting the flow passage. Its mechanism is very simple compared to the Hydropulse tool and at the same time it can produce a sinusoidal force profile instead of an impact profile.

The purpose of this research is to investigate the effect of sinusoidal and impact force profiles on the drilling performance of Polycrystalline Diamond Compact (PDC) bits in medium strength formations. As mentioned earlier, percussion hammers can increase ROP in hard formations. However, in order to increase the drilling rate in medium and weak formations, application of the other tools such as the Hydropulse and the Valved-flow tools can be investigated. For this purpose, an extensive literature review about penetration

mechanism of PDC bits and operating mechanism of the Hydropulse and Valved-flow tools was conducted in Chapter 2 of this thesis. Also a brief review of down-hole pulsating tools is presented in Chapter 2. At the end of Chapter 2 a brief introduction of the Distinct Element Method (DEM) is presented. A complete review of two down-hole pulsating tools (Hydropulse and AGT) is presented in Chapter 3 and detailed operating mechanism is reviewed. A simulation scenario for the AGT and corresponding simulation results and analyses are presented in Chapter 4. Simulation of the Hydropulse tool, results and analyses are presented in Chapter 5. Finally, the effect of shocks tools used in conjunction with hydraulic pulse tools is investigated in Chapter 6. A unique scenario is designed to simulate the effect of the shock tool behind the bit to investigate the effect of the shock tool's compliance on drilling rate.

1.3 Significance of Research

There is considerable literature research regarding the effect of percussion drilling on ROP. As mentioned earlier, percussion drilling is mostly used in hard rocks with Unconfined Compressive Strength (UCS) of 80 MPa and above [6]. However, in order to increase ROP in medium and soft formations (30 MPa<UCS < 80 MPa), vibration drilling is considered promising. The use of low magnitude and high frequency vibrations instead of high magnitude and low frequency impacts is investigated in this thesis. Simulation results presented in this thesis can provide proper analyses of the effect of sinusoidal and impact profile forces on ROP.

Secondly, this investigation presents the analyses of compliance effect on drilling rate for both sinusoidal and impact forces behind the bit. The displacement range generated as a result of force and compliance behind the bit is also analyzed.

Finally the effect of impact and sinusoidal force profiles on ROP in different down-hole pressures has been investigated. The performance of percussion hammers decreases dramatically in drilling deep wells where the hydrostatic pressure is higher. The reason for this is the ductile behavior of the rock in high pressure that prevents brittle breakage of the rock. The use of vibration drilling for this purpose is investigated in this research by simulating down-hole pressure and applying the vibration to the bit over a wide range of hydrostatic pressure. Simulations demonstrate that the vibration can increase ROP in highly pressurized formations through the different penetration mechanism than that of percussion drilling.

Chapter 2 Literature Review

A literature review for this investigation is presented in this chapter. A comprehensive literature review has been conducted concerning the penetration mechanism of drag bits and drilling performance of different hydraulic pulse tools as well as simulation of drilling process using the Distinct Element Method (DEM). In the first section of this chapter, the penetration mechanism of drag bits is presented. Different models that have been developed in the past few decades are reviewed. In the second part, case studies about different hydraulic pulse tools are presented. Three different types of hydraulic pulse tools and their drilling performance are reviewed. Finally, the DEM is summarized in the third part. Since this method is used to simulate the drilling process, a comprehensive review of the DEM modeling along with brief description of the simulation software are presented.

2.1 PDC bits and Penetration Mechanism

In drilling terminology, drag bits, or fixed cutter bits, are characterized by their fixed cutters mounted at the surface of the bit body. Since their introduction to the drilling industry, many modifications have been made by bit designers to improve their performance. From the simple design of the steel blades to the introduction of the PDC bits, engineers have tried to develop a bit that is capable of drilling fast and for a longer period. The early-generation drag bits such as steel blade bits were mostly used in soft and shallow formations because of their high wear rate. However, in order to drill harder formations,

harder materials such as tungsten carbide, compounds of diamonds and sintered carbide which had less wear rate, were used in the bit design. With the introduction of the PDC bits in the early 1970s, the drilling industry was revolutionized. The ROP in hard formations as well as bit life increased dramatically. This resulted in a lower drilling cost per foot and made most of the remote reservoirs economically feasible. Figure 2.1 shows a typical PDC bit made by the Schlumberger Company which is used in the industry [7]. These bits vary in geometry, number and size of cutters as well as in nozzle configuration.

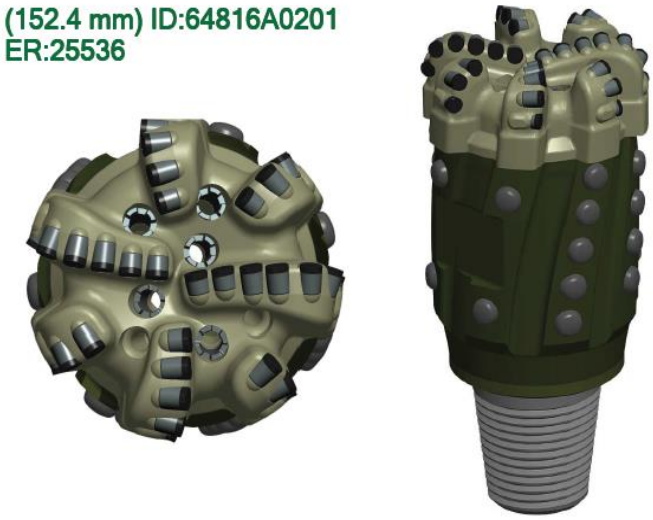

Figure 2.1: Smith bit standard 6 inch Mi 711 PDC [7]

Despite the numerous research papers about drag bit design and geometry, there are few papers published which discuss rock-cutter interaction in these bits. However, a few researchers have published some research in this area and different rock-bit interaction models have been introduced during the past two decades. These models are briefly described here.

In his paper on PDC wear, Glowka [8] stated that the cutter forces acting on the face of the cutter are nearly proportional to the wear flat area in contact with the rock. The wear flat area is the area beneath the cutter which is created as a result of bit wear. Its magnitude is proportional to the level of bit wear. Glowka concluded that the cross-sectional area in rock-cutter interaction plays a major role in determining the cutter forces.

Sellami [9] declared a negligible influence of in-situ stresses on the PDC penetration mechanism, especially in the presence of mud pressure. He concluded that the forces acting on the PDC cutter can be decomposed into two parts: i) the force require to produce rock failure (cutting forces) and ii) the frictional force developed as a result of normal force acting on the wear flat in contact with the rock.

Detournay [10] was one of the few researchers who made a big contribution to the understanding of the penetration mechanism of the drag bits. The cutter rock interaction model for the single cutter introduced by Detournay assumed one force acting on the cutter face. Figure 2.2 shows the force distribution for the perfectly sharp (ideal) cutter for Detournay's model. According to this model, the force acting on the face of the cutter is decomposed into vertical and horizontal components. The cutter's inclination with respect to the vertical axis is measured by the cutter's back rake angle Θ.

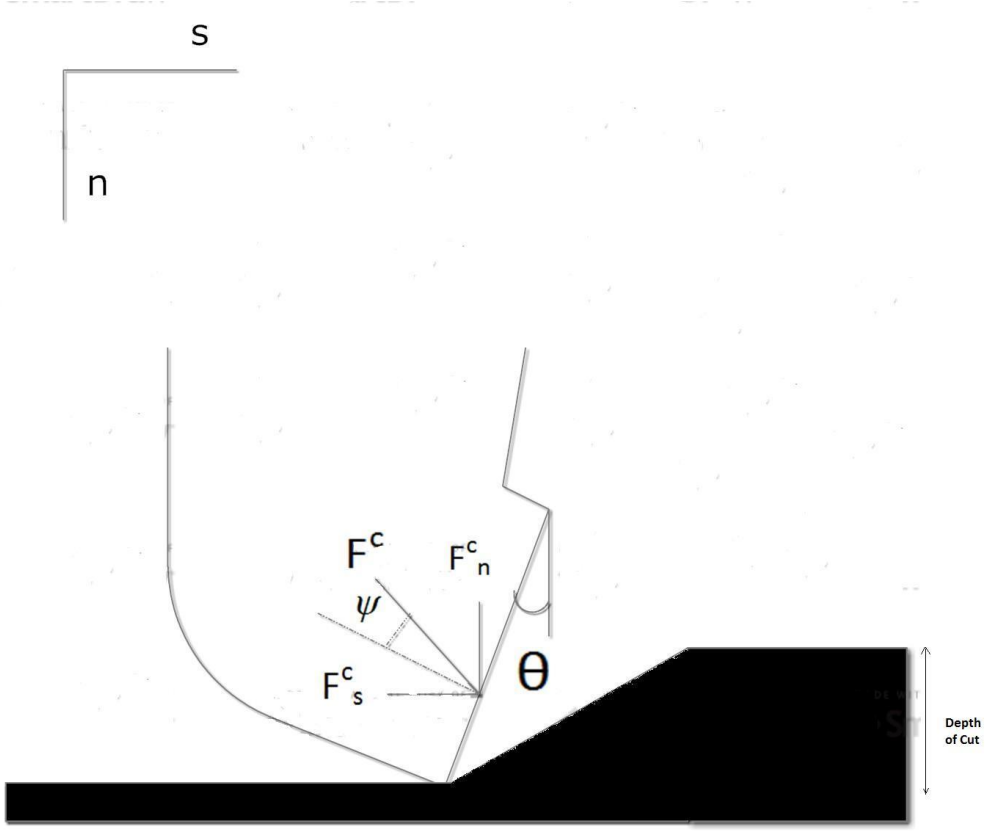

Figure 2.2**: Sharp (Ideal) cutter force distribution in Detournay's model**

This model assumes that the vertical and horizontal forces acting on the cutter are proportional to the cross-sectional area of the cut (A). The cross-sectional area of the cut is assumed to be the area in front of the cutter which is in direct contact with the rock. It is defined as a rectangle with length equal to the cutter length and width equal to the depth of cut.

$$F_s^c = \epsilon \mathrm{A} \qquad (2.1)$$

$$F_n^c = \zeta \epsilon \mathrm{A} \qquad (2.2)$$

Where ϵ is defined as the intrinsic specific energy or rock equivalent strength and ζ is the ratio of the vertical to horizontal force. The magnitude of ζ for the perfectly sharp cutter can be calculated as:

$$\zeta = \tan(\Theta + \psi) \qquad (2.3)$$

where ψ is the interfacial friction angle.

The force distribution and related equations for the blunt cutter (cutter with wear) in Detournay's model become more complicated since the friction forces due to the wear flat come into play. Figure 2.3 shows the force distribution for the blunt cutter.

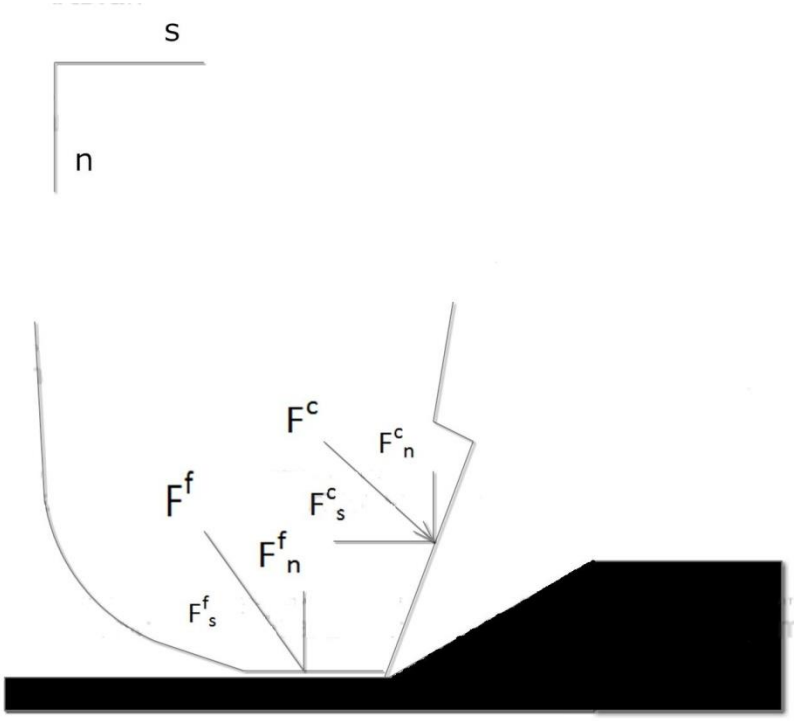

Figure 2.3: **Blunt cutter force distribution in Detournay's model**

According to Figure 2.3, normal and shear forces can be derived as below:

$$F_n = F_n^c + F_n^f \quad (2.4)$$

$$F_s = F_s^c + F_s^f \quad (2.5)$$

In the drilling application, Weight on Bit (W) and Torque on Bit (T) replace normal and shear forces, respectively. Therefore, Equations 2.4 and 2.5 become:

$$W = W^c + W^f \quad (2.6)$$

$$T = T^c + T^f \quad (2.7)$$

The cutting component of the weight on bit and the torque can be calculated using the ideal cutter equations as:

$$T^c = \epsilon d \quad (2.8)$$

$$W^c = \zeta \epsilon d \quad (2.9)$$

Where d denotes Depth of Cut (DOC) per revolution.

Introducing Drilling Specific Energy (E) and Drilling Strength (S) as:

$$E = T/d \quad (2.10)$$

and

$$S = WOB/d \quad (2.11)$$

Detournay suggested a linear relationship between the specific energy and the drilling strength.

$$E = E_0 + \mu\gamma S \qquad (2.12)$$

Using the E-S diagram, Detournay described the drilling process as a line which is called the "friction line". This diagram is shown in Figure 2.4. As shown in the diagram, the cutting process using an ideally sharp cutter is shown as a point called the "cutting point" in the friction line. This point represents a situation where the entire energy of the bit is transferred to the cutting process and there is no loss of energy due to friction. As we move up in the friction line, frictional forces increase due to the increase in wear. At any point in the friction line, the difference between E and the constant horizontal line of $\mathcal{E}$corresponds to the energy loss due to the friction between the wear flat and the rock surface. Detournay introduced μ (friction coefficient) and γ (bit constant) as two constraints that control the drilling process.

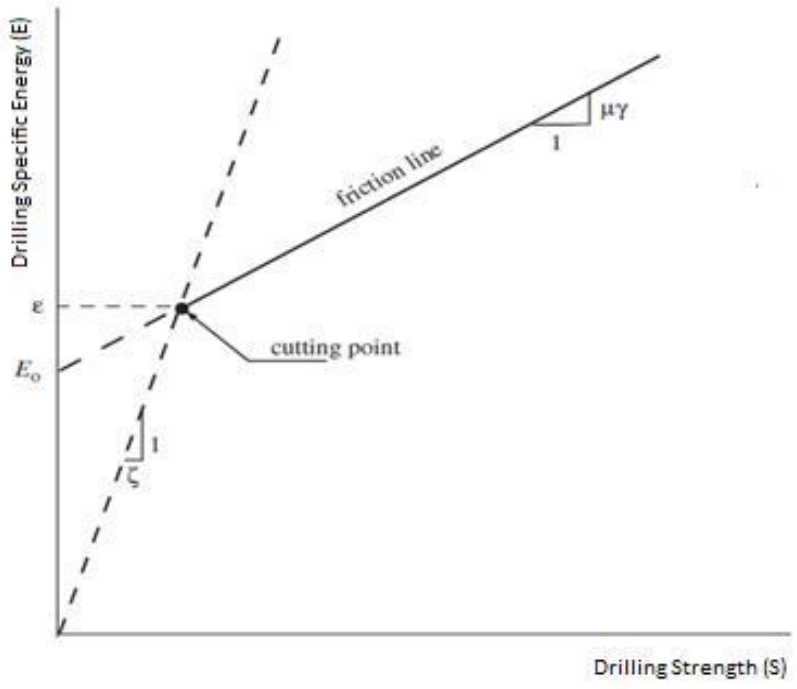

Figure 2.4: Schematic E-S diagram [11]

However, later, in his 2007 paper [11], Detournay modified his model and introduced two new quantities that can influence the bit response model: the characteristic contact length (l) and the contact strength (σ). Characteristic contact length shows the wear rate of the bit which is less than 1 mm for the ideal sharp cutter. Contact strength shows the limitation of the normal stress that can be transmitted by the wear flat. The Detournay divided the drilling process into three phases:

Phase 1 is when the forces under the cutter increase due to the increase in DOC and the drilling process is mostly controlled by the friction forces. Phase 2 starts when the friction forces reach maximum value (mobilized). In this phase the friction component of weight on bit is constant and the cutter behaves as a sharp cutter. Magnitude of the friction force in this phase is controlled by l and σ and is equal to: $W_f = l\,\sigma$. Finally, Phase 3 is when the effective contact length goes beyond the characteristic contact length due to poor cleaning. Depending on the loading path, the bit response will be different in this phase. Figure 2.5 shows these three phases.

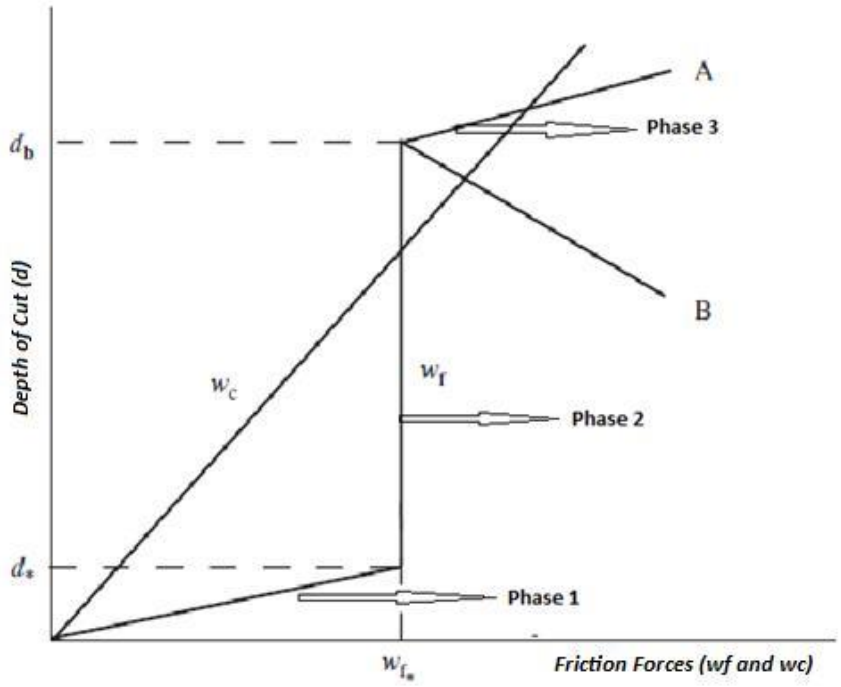

Figure 2.5**: Conceptual response of the bit in Detournay's model modified from [11]**

All three aforementioned models consider only one force acting on the face of the cutter. They decompose this force into vertical and horizontal components and derive equations based on these two components. These models give a good estimate of the cutter forces when the cutter is not chamfered. However, in the case of chamfered cutters, which are common in most of the new cutters, these models fail to predict the generated force on the cutter. Moreover, none of the previous models consider the force acting on the back of the cutter as a result of crushed materials squeezing from the bottom of the cutter and accumulating in the back of the cutter.

Gerbaud et al. [12] introduced a new model in 2006 which takes into account the forces acting on the back of the cutter as well as the forces acting on chamfer. The authors also introduced a region called the "Crushed Zone" which affects the force distribution on the cutter and the stress transfer from the cutter to the rock. Figure 2.6 shows their cutter-rock interaction model and the three types of forces acting on the cutter. The total force acting on the cutter consists of three loads: 1) forces acting on the cutter face (cutting face forces), 2) forces acting on the chamfer face (chamfer forces), and 3) forces acting on the back of the cutter (back cutter forces). Therefore, the total force on the cutter will be the sum of these forces:

$$F = F^c + F^{ch} + F^b \qquad (2.13)$$

The authors calculated the cutting forces using a build-up edge of the crushed material on the cutting face. They considered that the force applied by the cutting face is transferred to the rock through this build-up edge of crushed material. Therefore, they developed new sets of equations for the cutting forces using Mohr-Coulomb criteria.

$$F_c^c = \sigma_0 * (1+ k*\tan(\varphi) * \tan(\omega_c)) * A \qquad (2.14)$$

$$F_n^c = \sigma_0 * (\tan(\theta_f) + k * \tan(\omega_c)) * A \qquad (2.15)$$

Where φ is the friction angle between the crushed material and the virgin rock, $\sigma_0$is the hydrostatic stress in the crushed material, $\omega_c$is the back rake angle, θ_f is the rock-cutter friction angle and A is the cutting area.

For the chamfer forces the authors considered two scenarios. The first is when the DOC is greater than the chamfer height. In this case additional force is generated because of the

extra friction between the chamfer's flat area and the crushed material. These forces are calculated as below:

$$F_c^{ch} = \sigma_0 \tan(\varphi) A_{ch} \quad (2.16)$$

$$F_n^{ch} = \sigma_0 A_{ch} \quad (2.17)$$

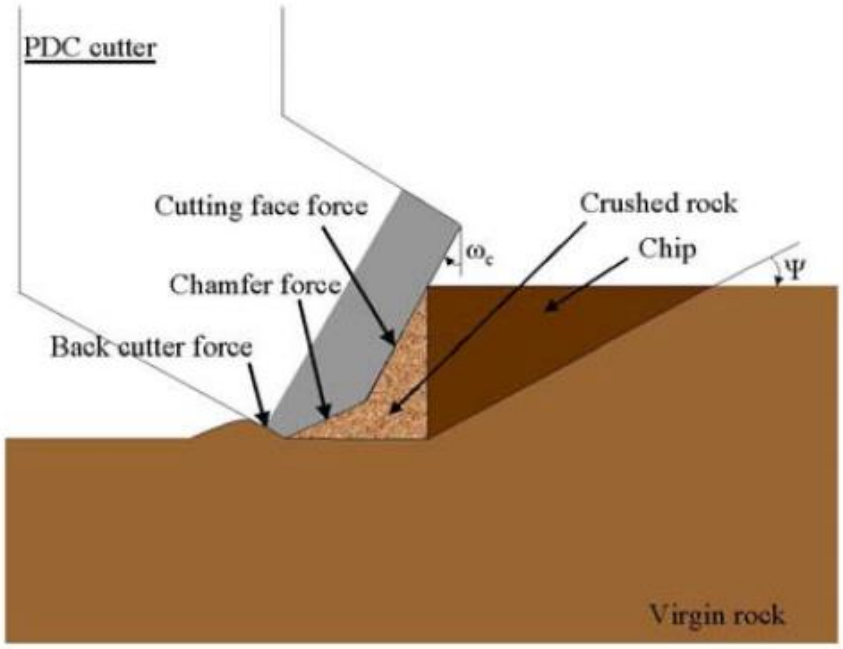

Figure 2.6: Model of forces acting upon PDC cutter [12]

The second scenario is when the DOC is less than the chamfer height. In this case the chamfer can be considered as a cutting face and the same equations for the cutting face can be derived for the chamfer face.

Finally, they calculated the back cutter forces as:

$$F_c^b = \sigma_0 \, \mathrm{f}\,(a, \mathrm{d}, \omega_d) \qquad (2.18)$$

$$F_n^b = F_c^b \, f_1\,(a, \mathrm{d}, \omega_d) \qquad (2.19)$$

Where d is the DOC, $\omega_d$is the relief angle and$a$ is the repression angle as shown in Figure 2.7.

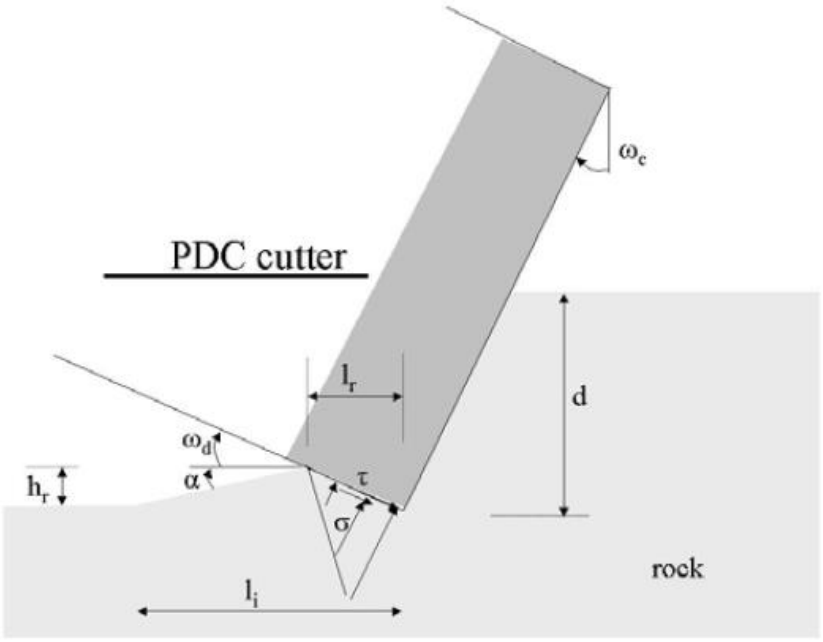

Figure 2.7: Stress distribution on the back cutter face [12]

In the case of drilling hard and abrasive formations, a wear flat appears in the cutter. In this case, the back cutter and the chamfer forces disappear and Detrournay's model can be applied to calculate the wear forces.

Ledgerwood [13] conducted series of experiments to investigate the effect of crushed particles beneath the cutter on drilling performance. He concluded that these particles once

they are under hydrostatic pressure have very high strength. He estimated the lowest strength of these particles to be as high as the strength of the virgin rock.

He also argued drillability of the formation rock under hydrostatic pressure. He concluded that inelastic properties of the rock have more effect on ROP than elastic properties such as UCS and friction angle.

2.2 Hydraulic Pulsing Drilling Tools

One of the major factors that differentiate the hydraulic pulsing tools from the hammer tools is the mechanism of force generation within the tool. Down-hole hammers utilize a piston that acts as a hammer in order to produce impact force behind the bit while the mechanism of force generation in hydraulic pulsing tools is quite different. The hydraulic pulsing tools generate pressure waves using sudden obstruction or restriction of flow area that travel both ways from the tool. These pressure waves are converted to the force when they act on the Pump Open Area (POA) of a shock tool or effective area of the bit. Depending on the type of the hydraulic pulsing tool, some tools are accompanied by the proper size shock tool and others are integrated with the bit. In the latter case, the bit's effective area acts as POA for the hydraulic pulsing tool. The force profiles produced by these tools are unique. For example, the Hydropulse drilling tool produces suction pulses that are translated to the impact forces behind the bit while the AGT produces sinusoidal pressure waves that act on the POA of the shock tool and generate a sinusoidal force profile. In this section, three different types of hydraulic pulsing tools are reviewed and related case

studies for each tool are presented. Detailed operating mechanisms for these tools are presented in Chapter 3.

2.2.1 Hydropulse Tool

The Hydropulse drilling tool is one of the down-hole drilling vibrators that is used in over-pressurized formations in order to increase ROP. Introduced and manufactured by Tempress Technology Inc. this tool is capable of producing suction pulses behind the bit that can be converted into impact forces when they act on the bit effective area. Figure 2.8 shows the schematics of the Hydropulse tool and generated suction pulses.

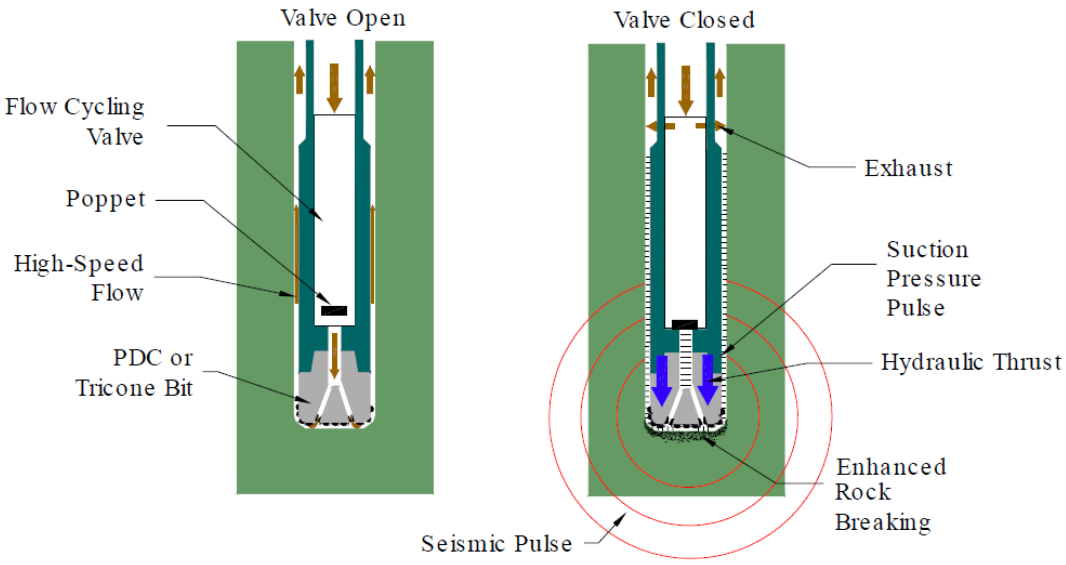

Figure 2.8: Hydropulse Tool Schematics [14]

As shown in the figure, a poppet valve periodically stops the flow through the flow course. This generates the intense suction pulses behind the bit that can transmit through the

nozzles and cause sudden pressure drop for a short period of time. This decrease in pressure causes upward tensile stresses in the rock surface which helps breakage of the rock. As well, these suction pulses act behind the bit which can be converted to the percussive mechanical forces. If the tool is appropriately decoupled from the drill-string, these percussive forces can create significant displacement below the bit. The percussive forces can also be used as seismic pulses for seismic applications [14].

Figure 2.9 demonstrates the typical pressure profiles generated by the Hydropulse tool. The pulse width is proportional to the length of the flow course. It is the two way travel time of the acoustic wave within the flow course. It is normally about 3 milliseconds at most of the applications but it can vary by varying the length of the flow course [14].

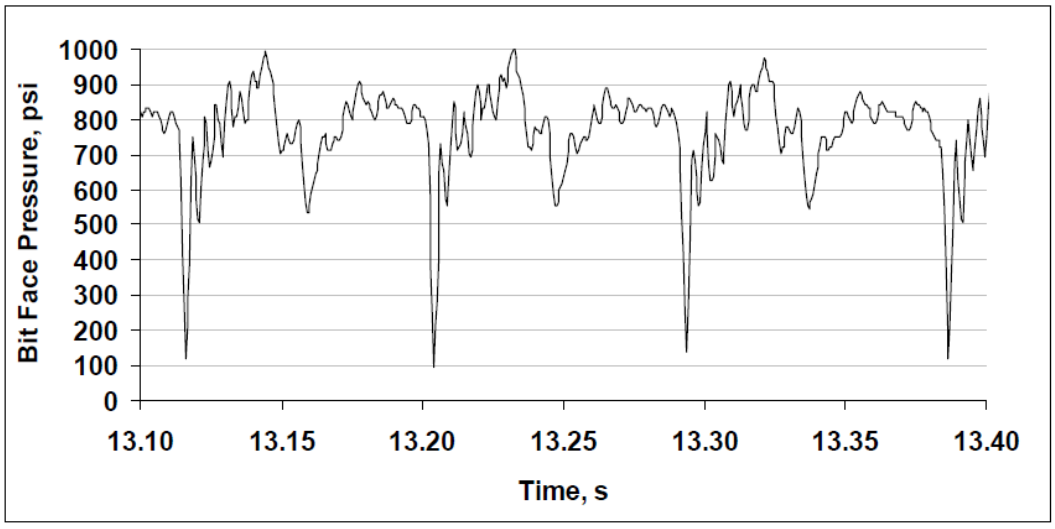

Figure 2.9: Bit face pressure profile generated by Hydropulse tool (Flow loop; 400 gpm water, no **bypass, 8.75"** test vessel) [14]

The amplitude of the pulses is proportional to the flow speed within the flow course and the fluid density. Using Joudowsky's equation for water hammer effect [15] the amplitude of the pressure drop can be calculated as follow:

$$\Delta P = v\sqrt{\rho K_f} \qquad (2.20)$$

Where ΔP is the amplitude of the suction pulse generated by the tool, v is the speed of the fluid through the flow course, ρ is the fluid density, and K_f is the bulk modulus of the drilling fluid. For water as a medium of the fluid, the bulk modulus is around 2.4 GPa at 35 Mpa [16].

Tempress Technology Inc. has conducted a series of micro-drilling and full-scale tests using a Hydropulse prototype in order to investigate the tool performance and its contribution to the ROP. Figure 2.10 shows the micro-drilling experiment that has been conducted by the Tempress Technology in Mancos Shale using 8.4 mm Micro-bit. They reported that a pulse amplitude of around 10 MPa increased ROP by a factor of 2 to 6 in sandstone, shale and granite [14].

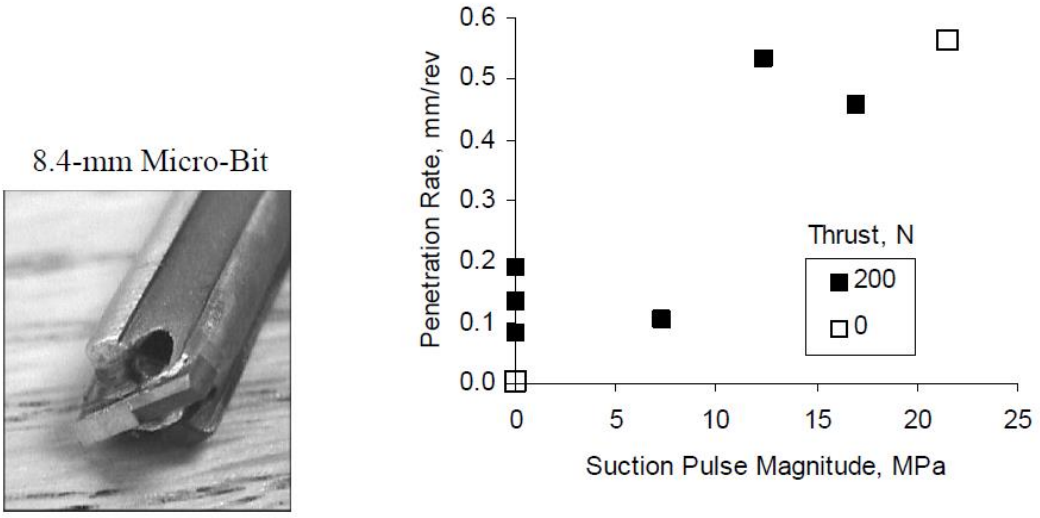

Figure 2.10: Effect of suction pulse amplitude on drilling rate with a micro-bit in Mancos Shale (Pulse amplitude of 10 Mpa = 1450 psi)) [14]

Full scale drilling experiments were conducted by Tempress Technology Inc. at Terra Tek facilities in Salt Lake City, USA, using Mancos shale and Crab Orchard sandstone to investigate the Hydropulse tool performance. An 8 1/8" IADC 537 insert bit in combination with a first generation tool was used in the experiments [14]. Results of the experiments showed 50 % to 200 % increase in ROP in Mancos shale when the Hydropulse tool was deployed. Figure 2.11 shows the drilling performance of the Hydropulse tool in comparison with baseline conventional drilling in Mancos shale.

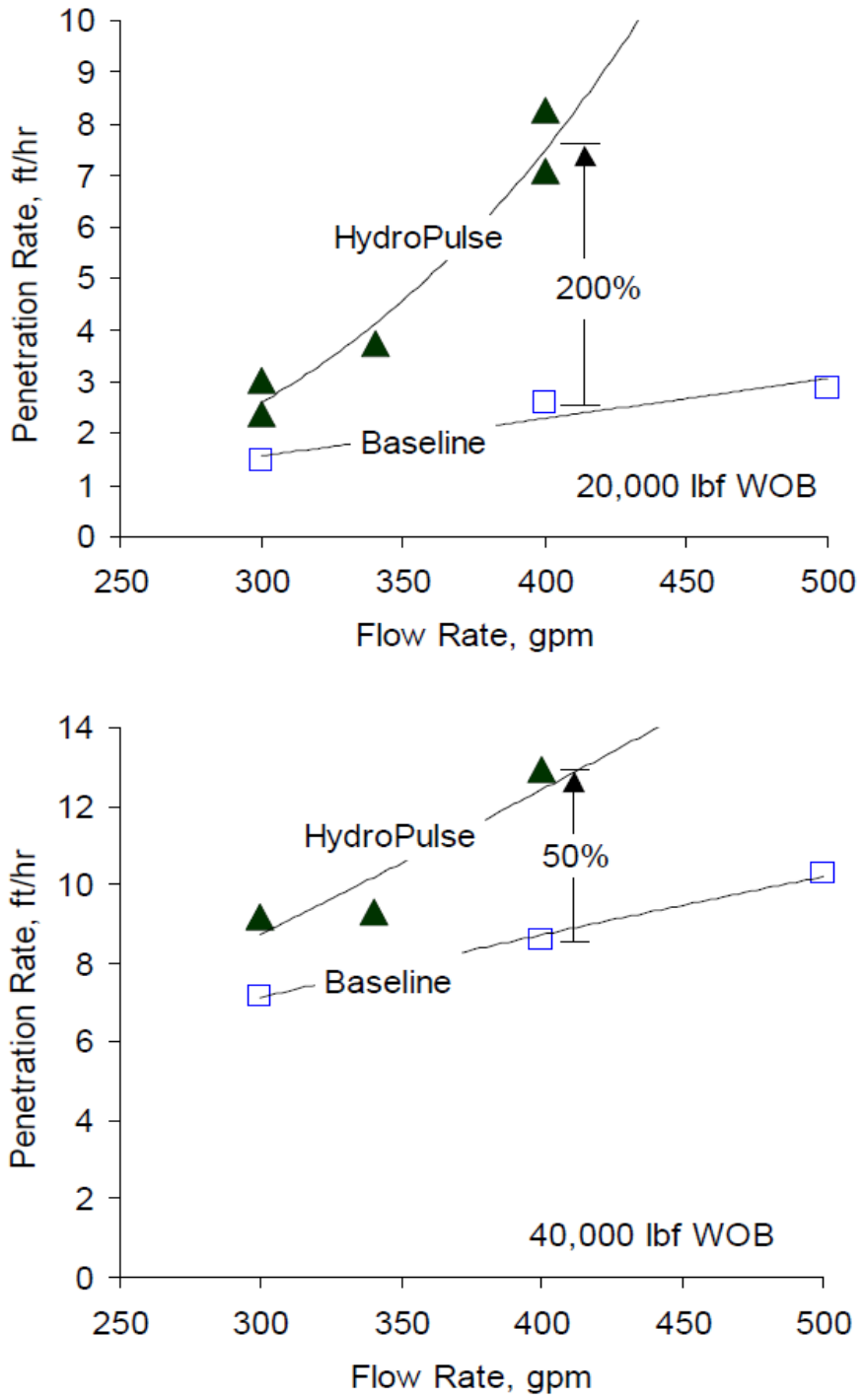

Figure 2.11: Mancos shale pressure drilling ROP comparison (14 ppg mud, 3000 psi borehole pressure, suction amplitude of 5.7 MPa (827 psi) at 400 GPM) [14]

2.2.2 AGT valved-flow tool

Valved-flow tools are types of hydraulic pulsing tools that generate pressure pulses through restricting the flow area rather than complete stoppage. The mechanism of these tools results in an output pressure profile is sinusoidal rather than impact profile. These tools are usually accompanied with a suitable shock tool. The pressure waves produced by the Valved-flow tools are transformed into mechanical forces when they act on the POA of the shock tool. The produced mechanical forces are then converted to displacement when they act on the compliance element of the shock tool.

The Axial Oscillation Generator Tool (AGT), or in some literature called the Agitator tool, is a Valved-flow tool that is capable of producing sinusoidal force oscillation. Introduced and manufactured by NOV, this tool has proved to be effective in increasing the ROP in vertical and horizontal wells. The tool produces pressure pulses by restricting the flow area. The flow restriction process is performed by the Oscillating Valve Assembly (OVA) and stationary plate [17]. The OVA is connected to the rotor. Figure 2.12 shows the valve assembly for the AGT. When the tool is not running, the hole in the oscillation valve is facing the hole in the stationary plate with the maximum flow area. The driving force for the valve assembly is supplied by the power section of the tool which is a progressive cavity positive displacement motor or PDM. The PDM uses drilling fluid to create eccentric motion. Based on the principle developed by Rene Moineau, the theory states that a helical rotor with one or more lobes will rotate eccentrically when the stator contains one or more lobes than the rotor [18]. The PDM rotates the rotor which is connected to the oscillating

valve assembly. As the rotor rotates, the oscillating valve assembly moves back and forth which causes the flow area to change from maximum to minimum. This cyclic motion of the valves produces pressure pulses within the tool. The tool is connected to the shock sub which converts pressure pulses to force and finally to displacement. Pressure pulses created by the valve section act on the POA of the shock sub that generates mechanical force. Frequency and magnitude of the oscillation are proportional to the flow rate of the fluid passing through the tool. The operating mechanism of this tool is explained in detail in Chapter 3.

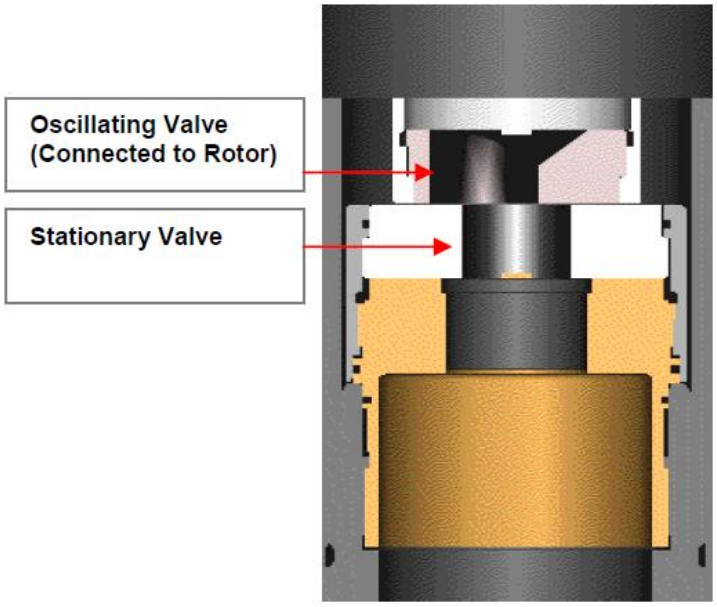

Figure 2.12: Oscillating Valve and Stationary Plate for the AGT modified from [19]

The AGT has frequently been tested in the laboratory and in the field scale. Drilling companies apply this tool as a friction reducer between the bore-hole wall and the drill-string, especially in horizontal drilling. It is normally installed around 800 ft from the bit to produce vibrations. These vibrations cause a reduction in friction and improve weight transfer to the bit.

Numerous case studies have been done over the past few years to investigate the AGT performance in drilling deep wells.

Skyles et al [20] conducted a case study with the AGT in the horizontal drilling of Barnett shale in Tarrant County, Texas. They found a 20 % increase in ROP when the AGT was used only in the curve section of the well and a 66 % improvement when the tool was deployed in the curve, lateral and build sections of the well.

Robertson et al [21] conducted a series of field tests in the Ullrig test facilities in Norway. They managed to reach 70 to 90 % improved weight transfer.

Rasheed et al [22] carried out a case study on the feasibility of extending the existing well while maintaining the tool face orientation, increasing weight transfer, and reducing motor stalling. The authors stated that there was an increase in ROP from 1.5 m/hr to 4.5 m/hr as well as improved steerable motor assembly performance.

In the West Sak field on the North Slope of Alaska, a previously drilled well was extended using the AGT up to a departure to depth ratio of more than six [23].

All of the aforementioned case studies investigating the AGT were done while the tool was positioned hundreds of feet from the bit in order to produce axial displacement

vibration in the drill-string. No research has been done so far to investigate the effect of the AGT when it is installed behind the bit. In this research, the feasibility of applying this tool behind the bit as a down-hole vibrator is examined through series of simulations. The operational mechanism of this tool is described in detail in Chapter 3.

2.2.3 Self-oscillation Pulse Percussive Rotary Tool

The Self-oscillation Pulse Rotary Percussive Tool is another hydraulic pulsing tool that produces high frequency and low magnitude pulses by utilizing a two-stage self-oscillator. This tool combines the technical advantages of pulse drilling and vibratory impact drilling [24]. Figure 2.13 illustrates the schematic view of the tool. As can be seen from the figure, the tool consists of two stage self-oscillators that create pressure waves using acoustic theory concept. These pressure waves travel down and act on the effective area of bit driving piston and cause vibratory force behind the bit. Hydraulic compliance is used in order to convert mechanical forces into the displacement. The pressure profile produced by this tool is shown in Figure 2.14.

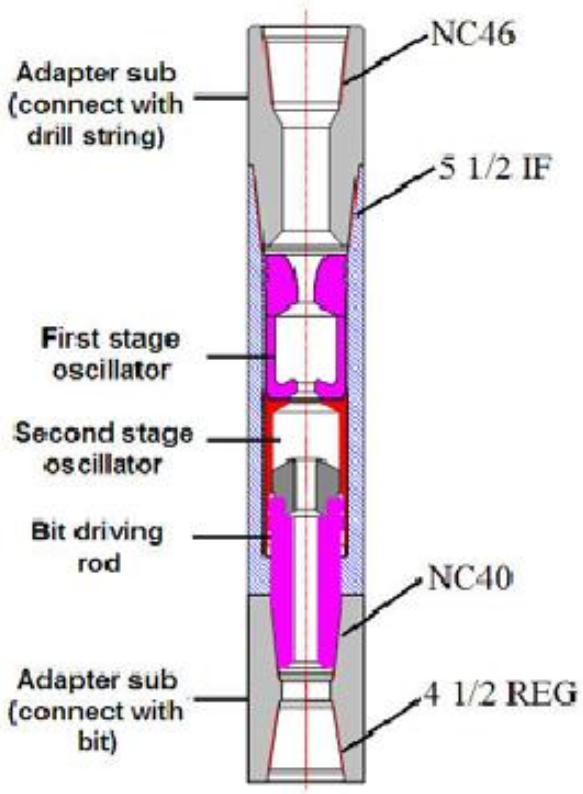

Figure 2.13: Schematics of self-oscillation pulse percussive rotary tool [24]

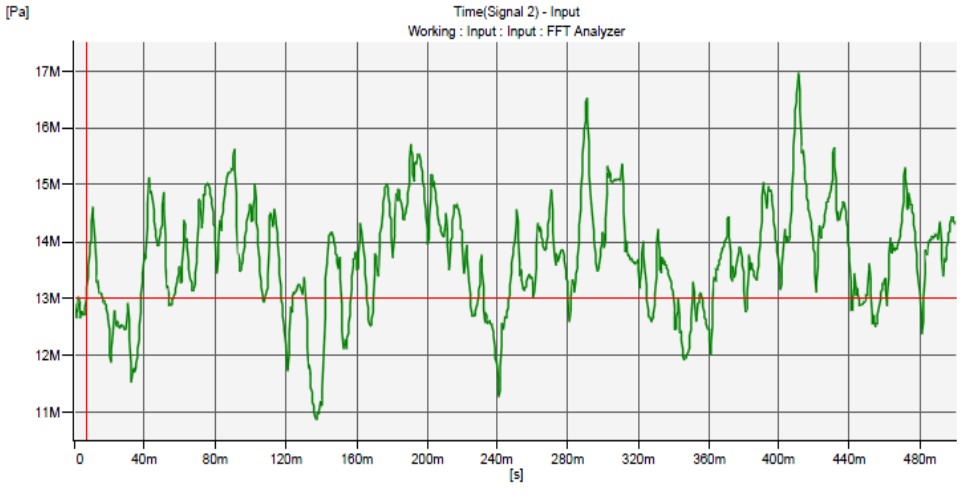

Figure 2.14: Pressure profile produced by self-oscillation pulse percussive rotary tool [24]

The Self-oscillation Pulse Percussive Rotary tool has been tested in different wells in China. It was tested for the first time in Songoliao Basin (China) which is verified as one of the most challenging zone for drilling in Northern China. Results of the test showed a 20 % increase in ROP compared to offset wells.

The tool was deployed in the Sichuan and Tarim basins and an ROP improvement of 20 % to 36 % was obtained by comparing the results to the offset wells.

2.3 Discrete Element Method (DEM)

DEM is a solid modeling approach that models the solid materials as a series of small balls connected together by cohesive and elastic bonds. The DEM method has shown considerable promise in modeling small scale deformation and fracturing processes in rock such as the penetration of cutters into the rock [25]. In the DEM, the interaction of the particles is treated as a dynamic process with states of equilibrium developing whenever the internal forces balance [26]. There are two general approaches in molecular dynamic simulations: the Soft sphere molecular dynamic (MD) approach (which is same as DEM) and Event-driven (ED) simulation. ED approach, which is different from DEM, simulates the collisions and impacts using a collision matrix that determines the momentum change on physical grounds [25]. However, in MD or DEM approach, the rigid particles overlap one another at contact points through the specified stiffness of the contact. This approach utilizes Newton's Second Law of Motion and the Force-Displacement Law to simulate the internal forces and displacements among the particles. DEM software uses these two laws

through the implementation of time stepping to simulate the behavior of granular materials. Simulation software used in this investigation (PFC2D) uses the DEM to simulate drilling rocks and granular materials such as soil and sand. The calculation method of this software as well as contact models and time stepping is described in this section. Material for this section is taken from the PFC2D software manual [26].

2.3.1 Calculation Method of DEM

In DEM, it is assumed that the particles that form the granular material can overlap each other. The amount of overlap is determined by contact forces and specified stiffness between the particles. In this method, Newton's Second Law and Force-Displacement Law are utilized alternatively to trace the movement of the individual particles and related contact forces. The dynamic behavior of the system is represented numerically by a time stepping algorithm in which it is assumed that the velocities and accelerations are constant within the each time step. Figure 2.15 illustrates the calculation cycle used in the soft contact approach of the DEM in order to simulate the movement of the particles and updating the contact forces.

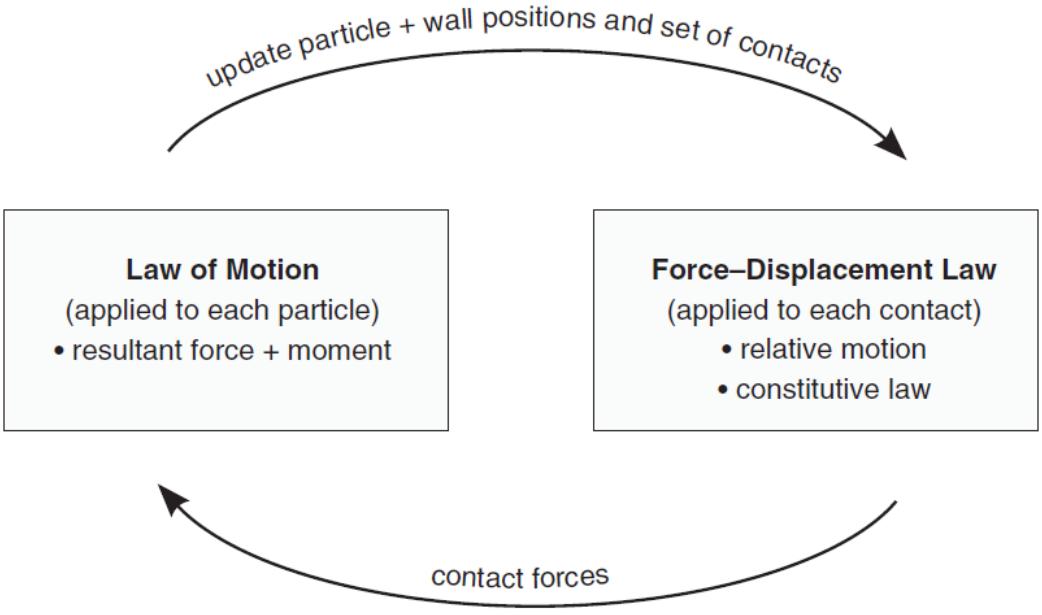

Figure 2.15: Calculation cycle in DEM [26]

Contacts between particles are formed and broken automatically during the course of a simulation. Each time step starts with updating a set of contacts from the known particle and wall position. Using force and displacement laws, contact forces are then updated based on the relative position of the two entities. In the next step, Newton's Law of Motion is applied to find the velocities and positions of the entities based on the previously obtained contact forces. These calculations are repeated in each time step as simulation time goes forward. In order to have better understanding of the process, both force-displacement and motion laws are described in details in the following sections.

2.3.2 Force-Displacement Law

The Force-Displacement Law relates the relative displacement between two entities at a contact to the contact force acting on the entities. Figure 2.16 shows the schematic the contact and notation used to describe the contact. In this figure, $R^{[A]}$ and $R^{[B]}$ are the radii of particle A and B, respectively, and d is the distance between the centers of the two particles. $x_i^{[A]}$ and $x_i^{[B]}$ and $x_i^{[C]}$are the position vectors of Particle A, Particle B and Contact C. U^n is the amount of overlap between two particles and n_i is the unit normal that defines the contact plane.

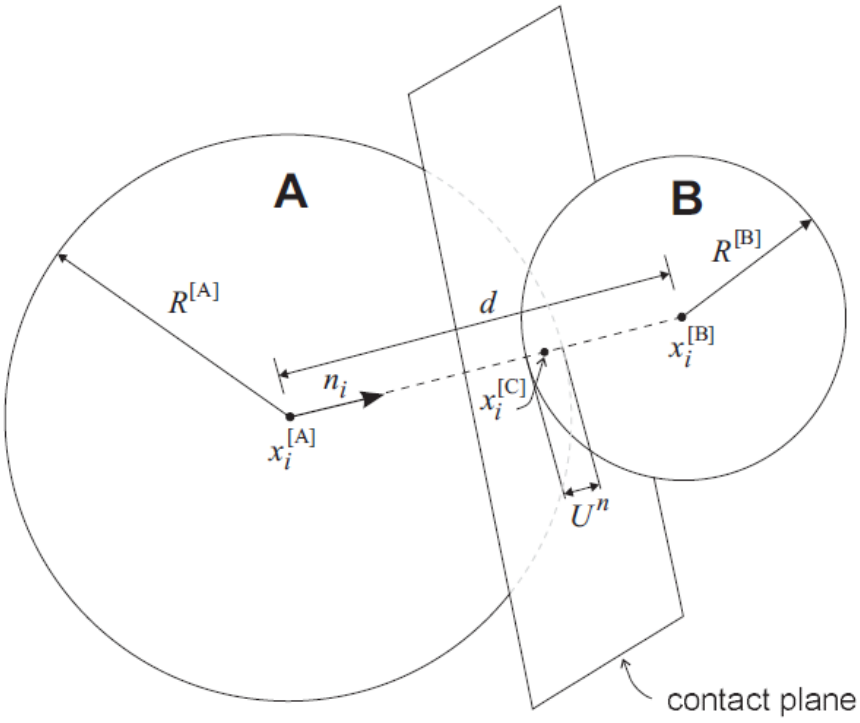

Figure 2.16: Notation used to describe ball-ball contact [26]

The unit normal can be defined as below:

$$n_i = \frac{x_i^{[B]} - x_i^{[A]}}{d} \qquad (2.21)$$

the distance between the particle centers is:

$$d = |x_i^{[B]} - x_i^{[A]}| = \sqrt{(x_i^{[B]} - x_i^{[A]})(x_i^{[B]} - x_i^{[A]})} \qquad (2.22)$$

and the amount of overlap can be defined as:

$$U^n = R^{[A]} + R^{[B]} - d \qquad (2.23)$$

therefore, the location of the contact point can be given by:

$$x_i^{[c]} = x_i^{[c]} + (x_i^{[A]} - \tfrac{1}{2} U^n)\, n_i \qquad (2.24)$$

Contact forces between the particles can be decomposed into two components of normal and shear forces:

$$F_i = F_i^n + F_i^s \qquad (2.25)$$

and their magnitude can be calculated as below:

$$F^n = K^n U^n \qquad (2.26)$$

$$F^s = - k^s \Delta U^s \qquad (2.27)$$

Where K^n and k^s are the normal and shear stiffness at the contact, respectively.

2.3.3 Law of Motion

According to the Newton's Second Law of Motion, the motion of a rigid body can be determined by the resultant force and moments acting upon it. This law can be described in terms of the translational motion of a point in the particle and the rotational motion of the particle. The key factors in the translational motion is the position of center of mass, x_i , velocity, $\dot{x}_\iota$, and acceleration, $\ddot{x}_\iota$ and the rotational motion is described in terms of its angular velocity, ω_i and acceleration, $\dot{\omega}_\iota$.

With these assumptions the equation of motion can be described as:

$$F_i = m\,(\ddot{x}_\iota - g_i) \qquad (2.28)$$

$$M_i = \dot{H}_\iota \qquad (2.29)$$

where F_i and M_i are the resultant force and moment acting on the particle, g_i is the body force acceleration vector (gravity), m is the total mass of the particle and $\dot{H}_\iota$ is the angular momentum of the particle.

The equations of motion mentioned above, are integrated using a centered finite-difference procedure which involves a time step of Δt. The quantities of $\dot{x}_\iota$ and ω_i are calculated at the mid-interval $(t \pm n\,\Delta t/2)$ of the time step while other quantities are computed at the start of intervals $(t \pm n\,\Delta t)$. Details of calculation cycle for the Law of Motion is very complex and is out of the scope of this thesis. However, it can be summarized as below:

Given the values of $\dot{x}_i^{(t-\Delta t/2)}$, $\omega_3^{(t-\Delta t/2)}$, $x_i^{(t)}$, $F_i^{(t)}$ and $M_3^{(t)}$, the values of $\dot{x}_i^{(t+\Delta t/2)}$ and $\omega_3^{(t+\Delta t/2)}$ are obtained. Then these values are used to obtain the value of $x_i^{(t+\Delta t)}$. The values of $F_i^{(t+\Delta t)}$ and $M_3^{(t+\Delta t)}$ to be used in the next cycle are obtained by application of the force-displacement law.

Note that the angular momentum of the particle consists of three components (M_1, M_2, and M_3) that lie along the three Principal Axes of Inertia. Since the used particles in the software are disk shaped, the axis remains in the out of plane direction. As a result, the angular velocities in the direction of first and second axis are zero. Consequently, instead of total moment and angular velocity only M_3 and ω_3 are used in the calculations.

DEM has many advantages in simulating solid materials. It can simulate forces and movements that are very hard and at some cases impossible to produce in laboratory experiments. Detail analyses of micro-forces and micro-movements are feasible by application of the DEM approach. This gives an opportunity to a scientist to understand the process thoroughly and justifies necessary modifications to the tools.

However, the DEM has some disadvantages that need to be mentioned. The most important disadvantage of the DEM is its inability to simulate hydraulics. In the drilling process, the hydraulics plays an important role such as: removing the drill cuttings, applying hydrostatic pressure on the rock, providing pore pressure within the rock and etc. Lack of ability to simulate fluid can cause some inconsistency between simulation and experimental results.

Chapter 3 Investigated Tools and Operational Mechanism

This chapter presents detailed descriptions of the two tools investigated in this study. After reviewing three different down-hole vibration tools, the Hydropulse and the NOV valved-flow tool (AGT) were selected for more investigations and analyses. Investigation of Cavitation Pulsing tools is being done by other members of the ADG research group. The rationale for choosing these two tools is to compare two different patterns of dynamic loading behind the bit and to investigate their influence on drilling performance. Another reason for this selection is to investigate the effect of application of axial compliance and resulting axial displacement behind the drilling bit. The AGT is typically used with accompanying shock tool which has considerable compliance while the Hydropulse tool is used without compliance. This chapter presents a detail description of the operational mechanism of both tools. The DEM simulation of these tools are discussed in Chapters 4 and 5.

3.1 NOV Valved-flow Tool (AGT)

The AGT is an axial oscillation generator tool that is usually accompanied by a shock tool that converts the pressure pulsations to force and finally displacement. The purpose of these axial oscillations is to keep the drill-string in motion while sliding in directional drilling. This reduces the friction between the drill-string and the bore-hole wall.

3.1.1 Tool Description

According to the AGT operating guidelines [27], different sizes of the tool have been manufactured for drilling and coiled tubing. Different sizes of the tool and their specifications are presented in Appendix A. In the coiled tubing application, the shock tool is not required for the AGT since the drill string has enough compliance and when the pressure pulses travel through the drill string, they can vibrate the drill string. However, for the drilling application, shock tool is required to convert pressure pulses to the displacement in order to vibrate the drill string.

Agitator tool frequency is linearly related to the flow rate of the fluid passing through. Different sizes of the agitator tool have been tested by NOV for frequency and pressure drop measurement. Figure 3.1 shows the graph of frequency vs. flow rate for different sizes of the tool.

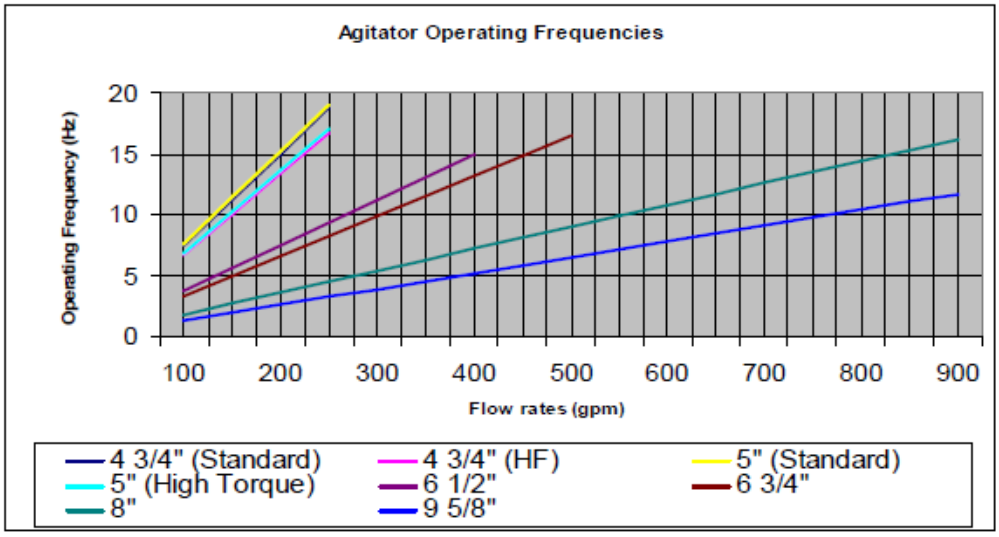

Figure 3.1: Frequency vs. Flow rate for different sizes of the AGT [27]

The tool creates sinusoidal pressure waves in its upstream and downstream by restricting the flow area through oscillating the built-in valve assembly. The amplitude of the sinusoidal pressure wave is related to the flow rate of the drilling fluid.

3.1.2 Operating Mechanism

The AGT consists of three main parts:

1. Power Section
2. Valve Assembly
3. Oscillating system (Shock Tool)

3.1.2.1 Power Section

The driving power of the AGTis a progressive cavity positive displacement power section. It consists of a rotor that is rotating inside a stator. When the drilling fluid passes through the power section, it causes the rotor to rotate in the opposite direction of the stator due to the friction of the fluid. The rotor is designed in a way that nutation motion is produced at the end of the rotor when it is rotating inside the stator. Figure 3.2 shows the assembly of the AGT.

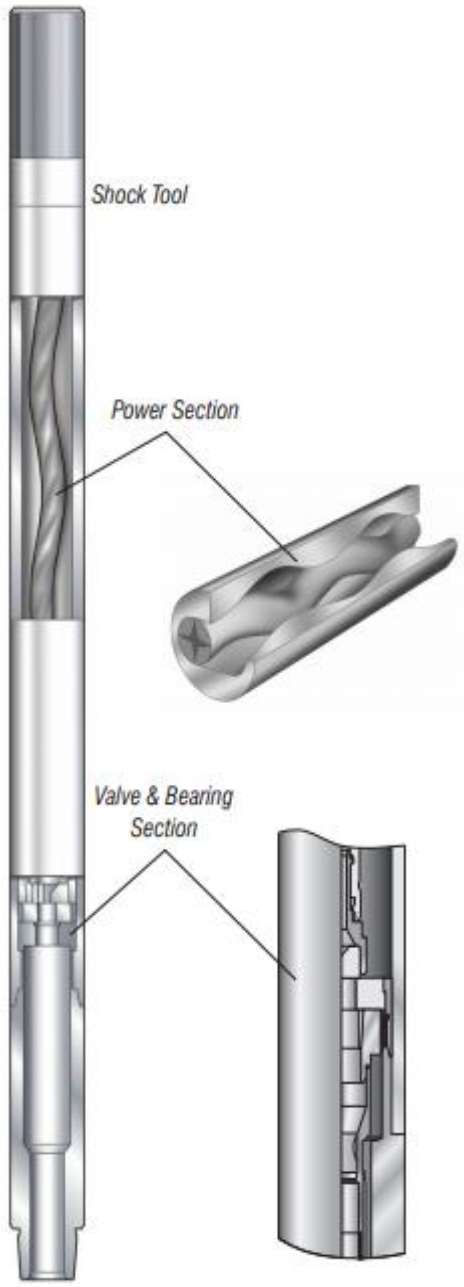

Figure 3.2: The AGT assembly [28]

3.1.2.2 Valve Assembly

The valve section of the AGT consists of two valves that are connected to the bottom of the power section. One is oscillating and is connected to the lower end of the rotor, while the other is stationary. When the rotor is rotating, nutation motion at the end of the rotor causes the oscillating valve to move back and forth. This motion of the oscillating valve causes restriction or in some cases, stoppage in the flow area. This cyclic restriction of the flow area causes pressure waves to be generated in both directions from the valves. These pressure waves travel in both directions, up through the power section and down to the drill-string. Figure 3.3 shows different positions of the rotary and stationary valves.

Figure 3.4 presents the schematic illustration of the valve assembly. Taken from the AGT patent [29], this figure shows the direction of the fluid passing through the tool and the operating mechanism of the valves. According to the figure, every time the rotor of the power section rotates, the lower end of the rotor moves back and forth in a linear motion. Since the end of the rotor is connected to the oscillating valve, this valve will move in the same pattern as the rotor. This displacement of the oscillatory valve over the stationary valve causes the flow area to change from minimum to maximum which generates pressure waves that propagate through the drilling fluid inside the drill-string.

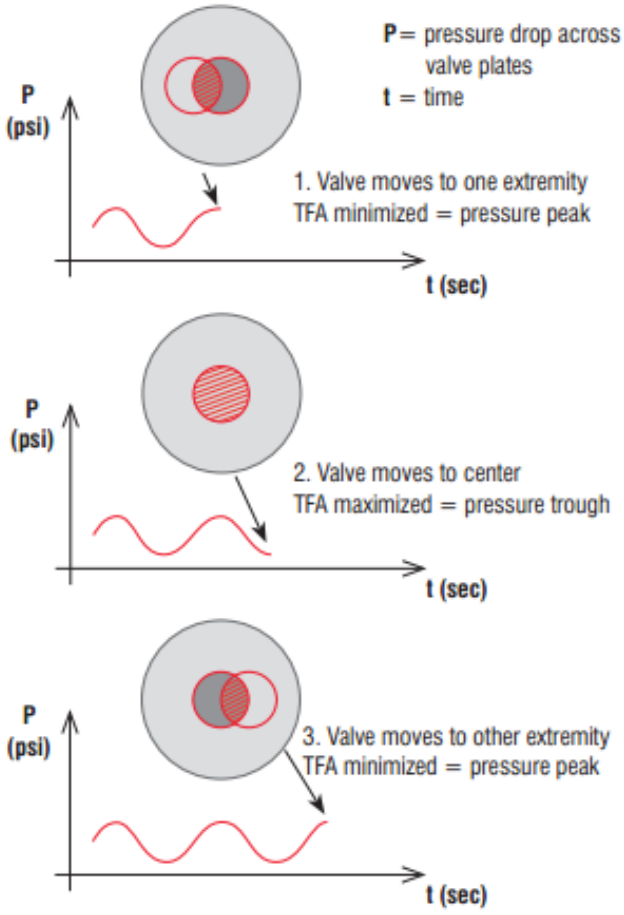

Figure 3.3: Different Positions of Rotary and Stationary Valves [28]

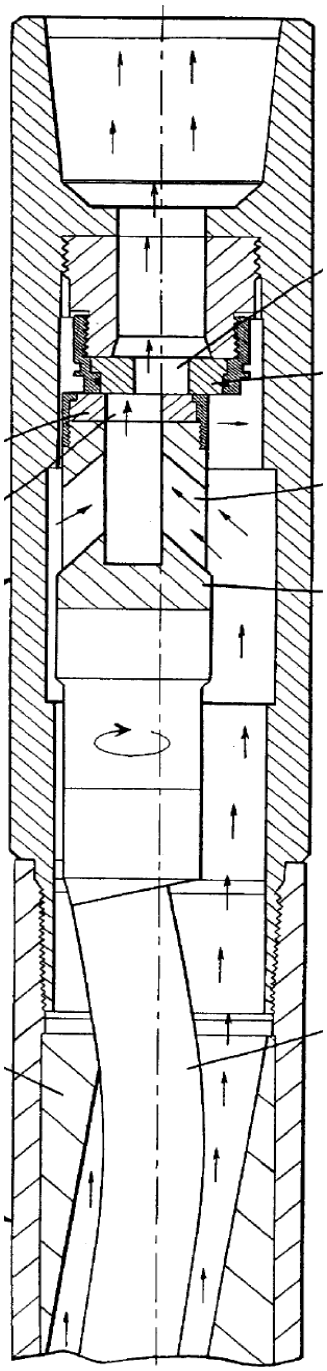

Figure 3.4: Schematic illustration of the valve assembly operating mechanism [29]

3.1.2.3 Oscillating System

The oscillating system is a shock tool that converts pressure pulses generated by the valve section to mechanical force and motion. It is generally installed on top of the power section. Figure 3.5 shows a typical shock tool. It contains an axially spring loaded mandrel which is sealed between the drill pipe pressure and annulus pressure. This mandrel creates a POA. Pressure pulses produced by the valve assembly act on this area and cause the mandrel to oscillate up and down. This oscillation transfers stress waves to the drill string and keeps the drill string in motion. The mandrel consists of Bellville springs which are disc shape washers attached together and act as one spring. They have frusto-conical shape which gives them a spring characteristic [30].

Figure 3.5: Oscillating System of the Agitator tool [20]

3.2 Hydropulse Tool

As stated earlier in Chapter 2, the Hydropulse tool increases ROP in high pressurized formations by creating suction pulses that cause sudden pressure drop at the bit face and at the same time generates impulsive load behind the bit. A brief description of the tool was presented in Chapter 2; however, detailed descriptions of the tool mechanism are presented in this section.

3.2.1 Operating Mechanism

Figure 3.6 shows more details about the tool operating mechanism. As shown in the figure, there is a poppet valve that stops the fluid flow momentarily. This sudden interruption of the fluid path cause suction pulses to be generated and travel downward. There are bypass valves that allows the fluid to flow during the stoppage time in order to prevent upward forces by the tool. These valves also ensure the circulation of the fluid in the event of valve malfunction. Figure 3.8 only shows a simplified diagram of the Hydropulse tool. The detailed diagram of the tool is very complicated and needs more description which is out of scope of this thesis. However, a brief description of valve operation is presented here.

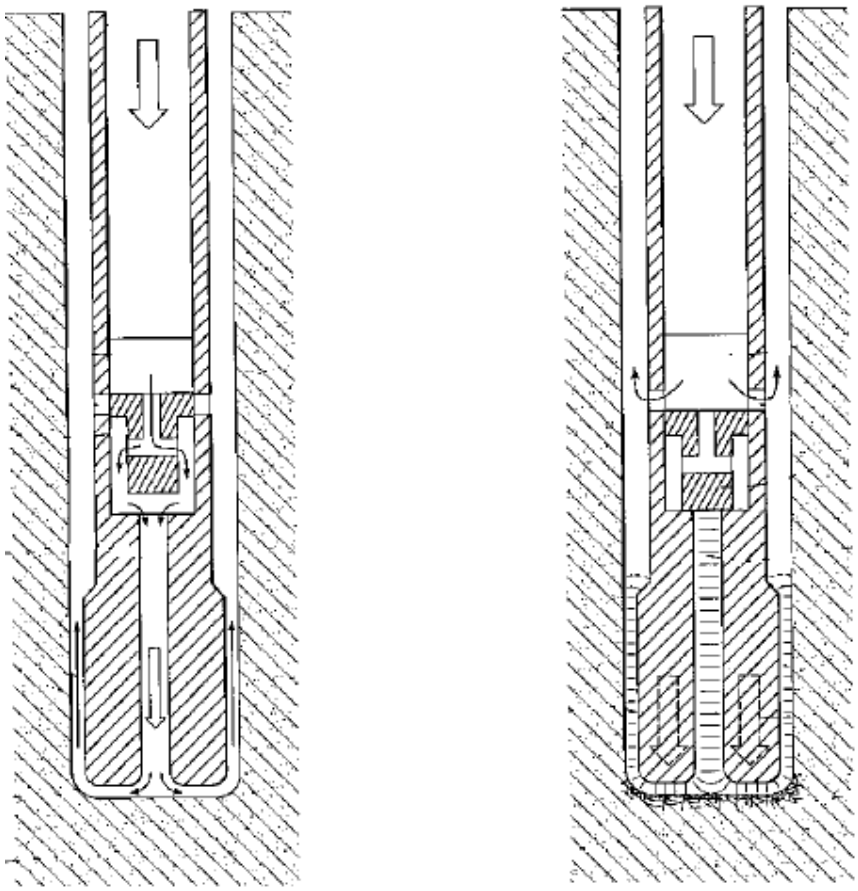

Figure 3.6: Hydropulse tool operating mechanism (right: closed position, left: open position) [31]

The valve section of the Hydropulse tool consists of two members. The first member is the main valve that reciprocates back and forth which causes the second member which is a poppet valve to interrupt flow path in cyclic motion. The flow interruption operation is illustrated in Figure 3.7. This figure schematically shows four states of the flow interruption valve during one complete cycle. Number 41 shows the main valve (left valve in the figure) and number 58 shows the poppet valve (right valve in the figure). For simplicity only the upper half of the two valves are shown here.

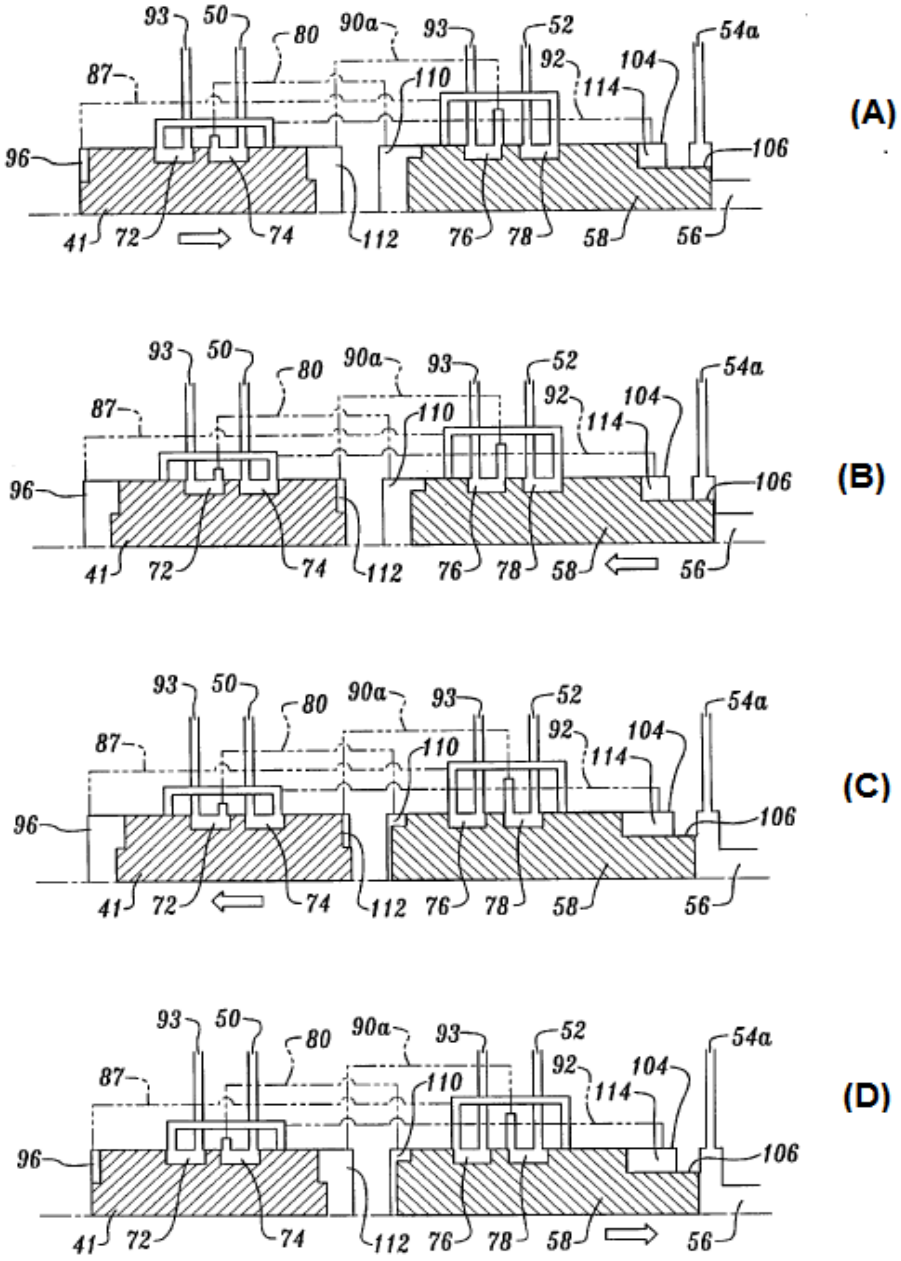

Figure 3.7: Schematic view of four states of Hydropulse valve section during a complete cycle [31]

The exact description of the tool is taken from the tool patent [31]. According to the Figure 3.9A, the first state is when the poppet valve closed. An inlet port (54a) is coupled in

fluid communication with the conduit in the drill-string through which the pressurized drilling fluid is conveyed into the borehole. As shown in figure 3.9A, the poppet valve (58) completely shuts off fluid flow through an outlet port (56).

Another inlet port (50) on the flow interruption valve, which is also coupled in fluid communication with the drill-string conduit conveying pressurized drilling fluid into the borehole, is coupled to a fluid channel (80), which connects into a volume (110) at the back of the poppet valve. The pressurized fluid flowing into volume (110) produces the force that has caused the poppet valve to rapidly close the outlet port (56).

The small volume (114) created by the difference in the diameter between distal end (106) of the poppet valve and housing (104) is connected to a drain channel (93) through a channel (92).

In the next step, pressurized drilling fluid flowing into an inlet port (52) passes through the fluid channel (87) which is coupled to a volume (96) on the back of the main valve. This fluid flow forces the main valve to shift to its second position which is shown in the figure as the second stage. At the same time the fluid at the volume (112) in front of the main valve drains through the channel (93).

Figure 3.9B shows the second states of the valve assembly. As shown in the figure, by shifting the main valve, combination of the flow channels is changed. At this stage, the poppet valve starts to open. Pressurized fluid from inlet (50) flows to the volume (114) in front of the poppet valve through channel (92) and forces the poppet valve to shift back

while fluid in the back of the poppet valve (volume 110) is draining to the outlet port (93). This causes the poppet valve to shift to its open position which is shown in Figure 3.9C.

Again by shifting the poppet valve, the channel combination changes. At this stage which is shown in Figure 3.9C, fluid from inlet (52) flows through channel (90a) to the volume (112). This action forces the main valve back to its first position while fluid in the back of the main valve (volume 96) is being drained through the channel (93). This brings the valve section to the fourth state in which the main valve is at first position and the poppet valve is open. This state is shown in Figure 3.9D.

Again by flow of the fluid inlet (50) and draining the volume (114) through the outlet port (93), the valve combination becomes exactly same as shown in Figure 3.9A.

This cycle repeats as long as fluid is passing through the tool. Momentary interruption of the flow by the poppet valve generates suction pulses that travel down.

This section attempted to describe the Hydropulse tool in the simplest way. The main idea of the operating mechanism of the tool was presented, however, the real embodiment of the tool has so many complications that is out of scope of this research. More details about the Hydropulse operating mechanism are available in the references.

Chapter 4 Distinct Element Method (DEM) modeling of the AGT

This chapter presents the DEM simulations for the AGT in 4 sections. All of the simulations were done by Particle Flow Code (PFC2D) software. The theoretical part of this software was presented in Chapter 2. However, in order to become familiar with software, a brief description of the software is presented in the first section. In Section 2, the rock simulation process and its macroscopic properties such as density, UCS, dampening properties, and etc., are presented. Section 3 presents the simulation scenario for the AGT using a unique method developed in this investigation. Also simulation parameters and their range as well as simulation procedure are presented in this section. Finally, in Section 4, simulation results along with analyses and discussions are presented. DEM simulation of the Hydropulse tool is presented in Chapter 5.

4.1 Brief Description of PFC2D Software

PFC2D is the DEM software used in this investigation and is commercial software licensed by Itasca Consulting Inc.

PFC2D has a variety of applications including simulating drilling rock environments. This software is able to simulate the action of the cutter in a drilling process by creating particles of arbitrary shape and attaching two or more particles together using clump logic, so that each group of particles acts as an autonomous object. This software utilizes a

calculation method of DEM which is a time stepping, explicit scheme. It can operate on any computer running the Windows operating system.

PFC2D provides a particle-flow model containing the following assumptions:

1. The particles are treated as rigid bodies.

2. The contacts occur over a vanishingly small area (i.e., at a point).

3. Behavior at the contacts uses a soft-contact approach, where the rigid particles are allowed to overlap one another at contact points.

4. The magnitude of the overlap is related to the contact force via the force displacement law, and all overlaps are small in relation to particle sizes.

5. Bonds can exist at contacts between particles.

6. All particles are circular. However, clump logic supports the creation of super-particles of arbitrary shape. Each clump consists of a set of overlapping particles that acts as a rigid body with a deformable boundary. [26]

Figure 4.1 shows a typical PFC2D drilling simulation environment. The drilling cutter is simulated using clump logic that allows groups of particles to act together as a rigid body. Wall logic is used to simulate the boundaries of the rock. General walls extend the existing wall logic in PFC2D by providing analytically defined geometric objects that function as walls to apply velocity boundary conditions to particles.

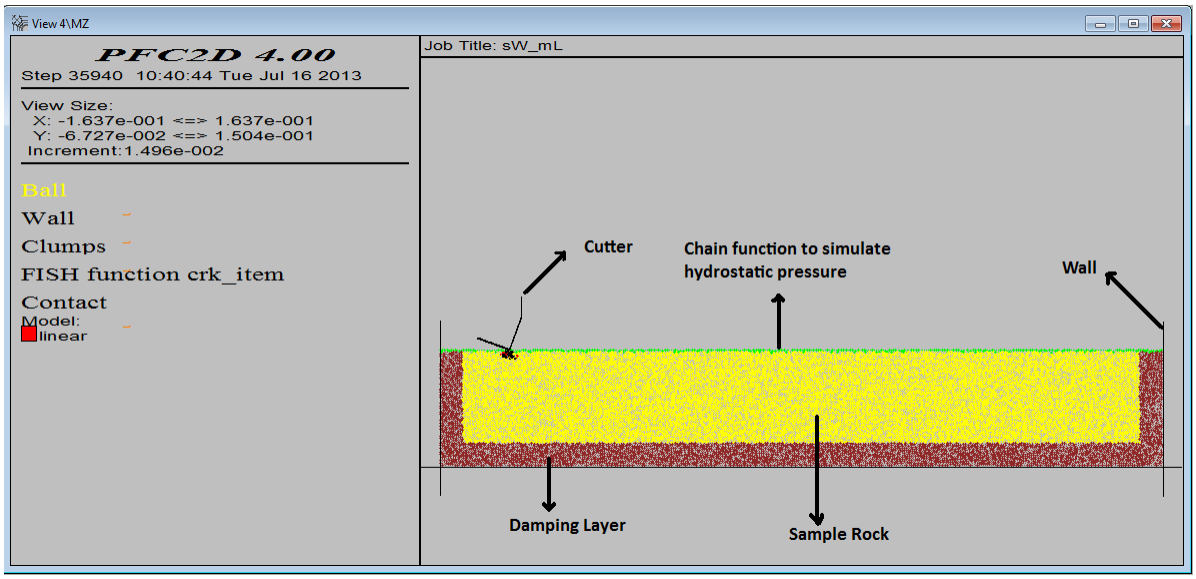

Figure 4.1: Typical PFC2D environment showing drilling process

The Chain Function is provided in the Fish Tank of the PFC2D library that allows the simulation of down-hole hydrostatic pressure in the well. The Chain Function can be seen as a green chain over the rock in Figure 4.1. Chain function simulates down-hole hydrostatic pressure by applying downward force on the rock sample.

PFC2D software can be used in a variety of applications, however, since it only used for drilling process simulation, only the rock generation process and properties dealing with the rock and cutter simulation are discussed in this thesis.

4.2 Simulation of Drilling Rock, Microscopic and Macroscopic Properties

Simulating the rock using the DEM method is a complicated process and the similarity between the simulated and real rock is still under question from different points of view. A common practice in the industry to simulate a rock is to establish equivalence in density, Elastic Modulus, Poisson ratio, Brazilian Strength, UCS and Friction Angle [13]. Any simulated rock needs to be tested for these parameters to be calibrated and used for simulations. However, none of above parameters describes the inelastic properties of the rock such as strain softening and strain hardening that happens in high hydrostatic pressures.

For the simulations of the AGT and Hydropulse tool, the rock that was developed and calibrated by Ledgerwood [13] was used. Ledgerwood conducted series of simulated triaxial tests in order to calibrate his simulated rock with real rock. Table 4.1 shows the micro-properties of the Ledgerwood's simulation rock and Table 4.2 shows the corresponding macro-properties of the rock. Note that in calibrating his simulation rock, Ledgerwood used the idea of Vajdova et al [32] and Wong et al [33] that most rocks exhibit a transition from shear localization at low confining pressure to shear-enhanced compaction at high confining pressures. In the shear localization mode, cracks combine along diagonal shear planes and then large elastic wedges of material slide past each other while in shear-enhanced compaction mode; most of the rock volume is failed [13]. He conducted a series of triaxial tests to confirm these phenomena by PFC2D and he observed the exact patterns that happen in real life.

Table 4.1: Micro-properties of the rock created by Ledgerwood [13]

Property	Magnitude
Ratio of Maximum to Minimum Ball size	1.8
Parallel Bond Shear Strength	44 e6 Pa
Parallel Bond Normal Strength	44 e6 Pa
Minimum Ball Radius	0.35 e-3 m
Ball and Bond Elastic Modulus	40 e9 Pa
Ratio of Normal to Shear Stiffness	2.5
Ball-ball and Ball-wall Friction	0.5

Since this thesis focuses on medium strength rocks (30 MPa<UCS < 80 MPa), this rock is an excellent candidate for drilling simulation of the AGT and Hydropulse tool.

Table 4.2: Macro-properties of the rock created by Ledgerwood [13]

Property	Magnitude
Density	2650 kg/m^3
Porosity	18 %
Normal Damping Ratio	0.2
Shear Damping Ratio	0.2
Local Damping Ratio	0.5
Unconfined Compressive Strength (UCS)	55 Mpa
Young Modulus	40 Gpa

Using the data provided by Ledgerwood [13], the default rock generation code provided in PFC2D FISH Code was developed. Figure 4.2 shows the corresponding simulated rock in the PFC2D environment.

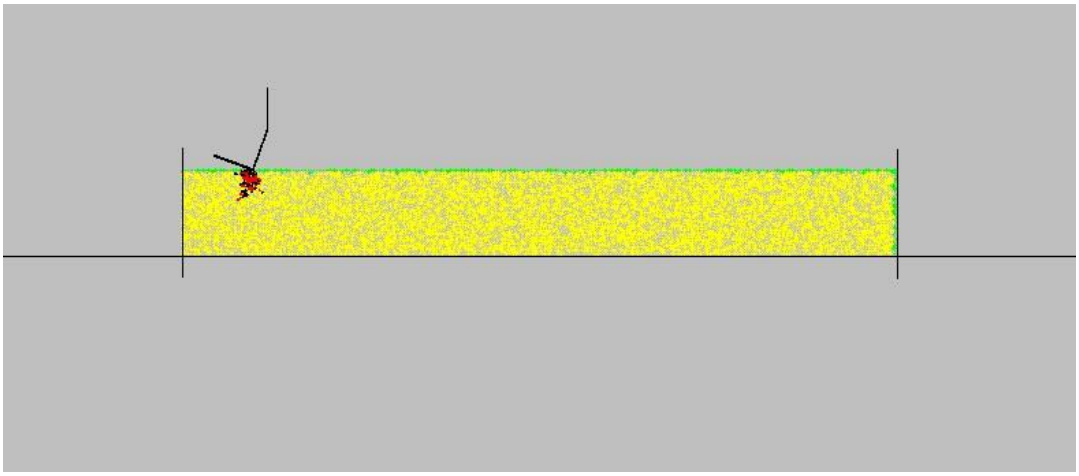

Figure 4.2**: Ledgerwood's simulation** rock with applied hydrostatic pressure (Hydrostatic pressure is in green) [13]

As can be seen in the figure, the rock specimen is surrounded by three walls. These walls don't exert any force on the specimen and their function is to provide a boundary to the rock but they can reflect back elastic waves. As mentioned before, in order to simulate down-hole hydrostatic pressure, the chain function is used. This function employs a topological routine that is run every n^{th} time step which examines the current state of the rock and identifies all the discrete elements on the surface of the cutting and the cut surfaces [13]. It then applies a force representing a hydrostatic pressure to the balls on these surfaces. This pressure chain is more like an impermeable filter cake of mud in real condition [13].

In this study, after conducting a series of preliminary tests, unusual cutter vibrations that didn't match the real condition were observed. These fluctuations were attributed to the wave reflection from the walls. In real life drilling, any compressive wave generated by the

bit, transmits through the rock and travels away from the source and attenuates. But in our simulation process, all of the generated compressive waves reflect back as tensile waves when they reach the walls. These reflected tensile waves exert upward force to the cutter which decrease cutter forces and affect the drilling process. Consequently, a thin dampening layer was added to the model in order to mitigate this problem. This layer has high dampening ratio (0.95) and absorbs almost 95 % of the wave energy and acts as the unlimited boundary rock as in real life. This dampening layer surrounds the rock from three sides. A modified simulation with the dampening layer is shown in Figure 4.3.

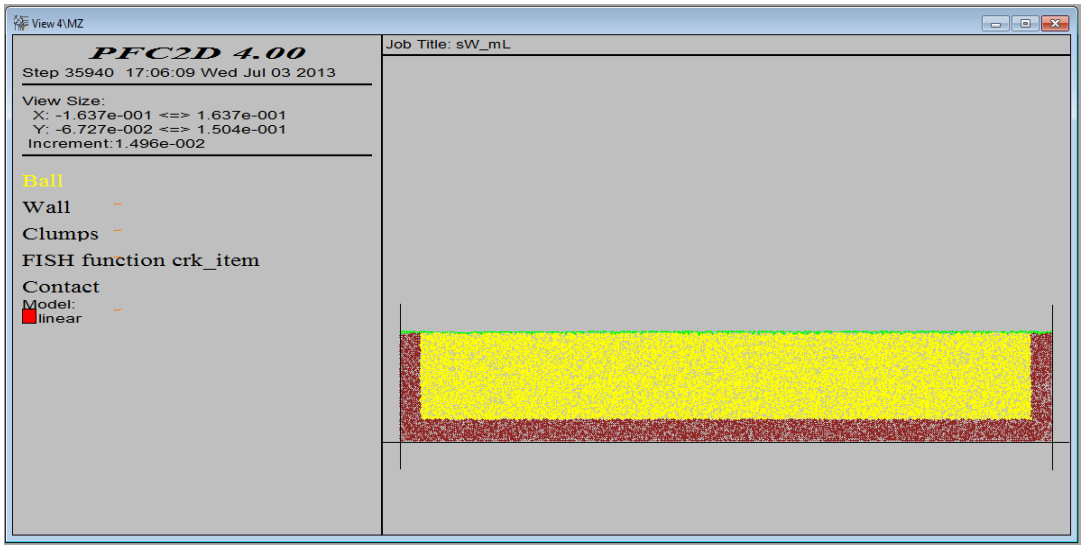

Figure 4.3: Simulation rock with dampening layer (Dampening layer is shown in Maroon color)

The difference in vertical movement of the cutter with and without the dampening layer is shown in Figures 4.4 and 4.5. As the figures show, in the presence of the dampening layer, the cutter penetrates smoothly without jumping up. Figure 4.4 clearly illustrates how the reflected tensile waves push the cutter upward.

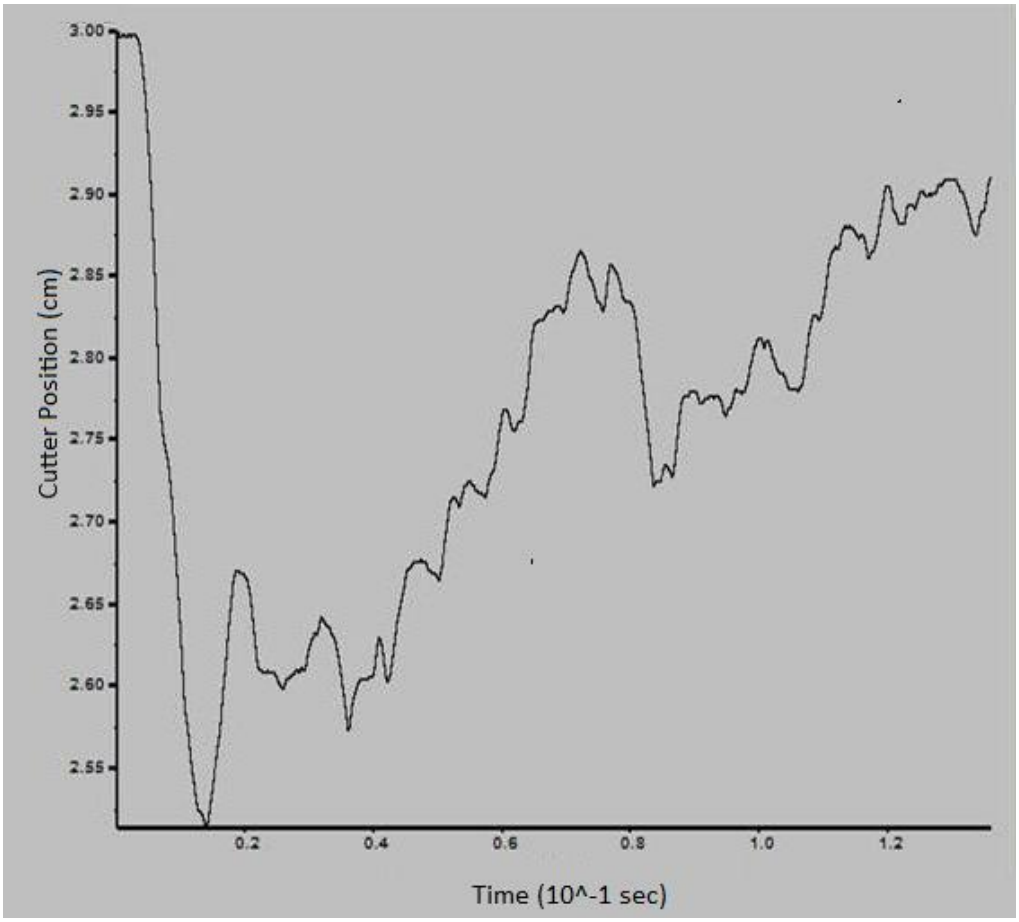

Figure 4.4**: Cutter's vertical position vs. drilling time without dampening layer**

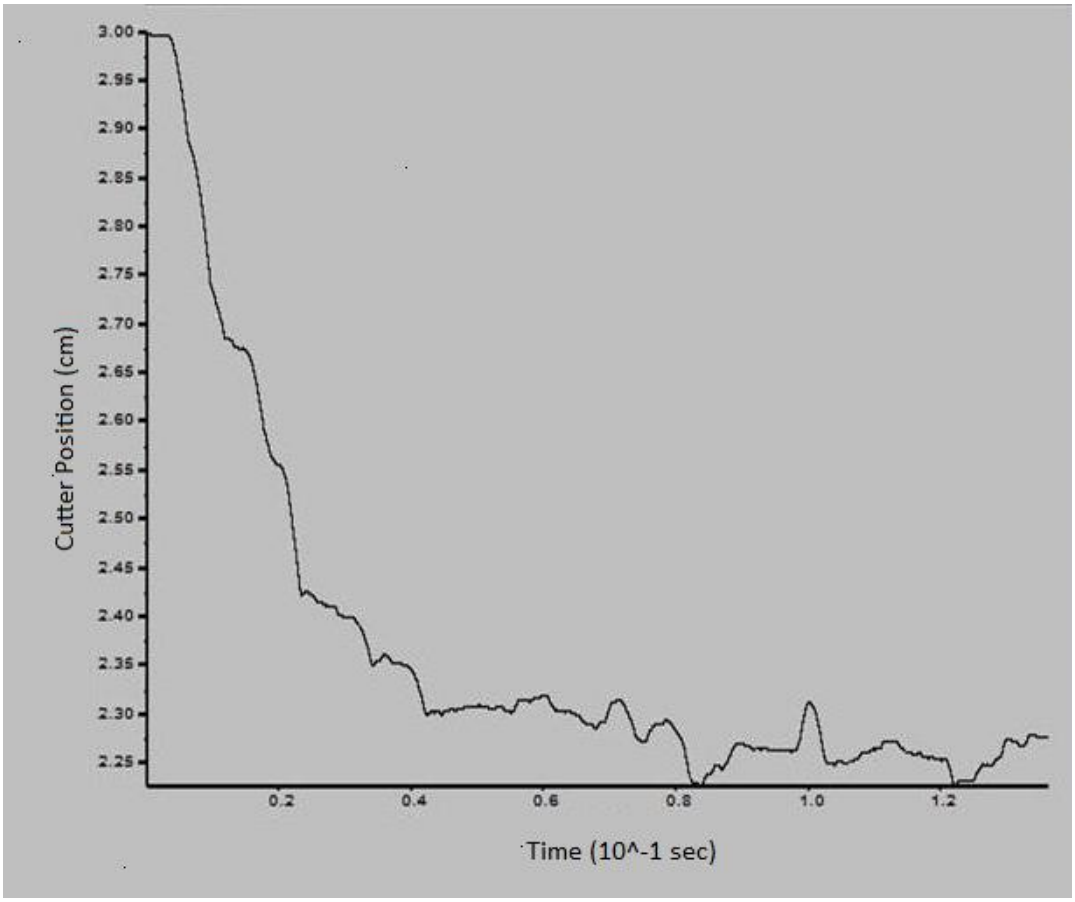

Figure 4.5**: Cutter's vertical position vs. drilling time with dampening layer**

Considering the aforementioned points, the simulation rock was created. This rock was then used in the simulations of both the AGT and the Hydropulse tool. Since the purpose of this thesis is to investigate the performance of these tools and compare them together, the same rock with exactly same properties was used for both simulation sets. The simulation scenarios for the AGT and considerations for parameter selection are presented in the next section. The Hydropulse tool's simulations and results are presented in Chapter 5.

4.3 Simulating the Action of AGT on Single Cutter Penetration

As mentioned earlier, the AGT can be applied behind the bit as a source of variable force to improve ROP. In order to simulate the action of this tool, several different scenarios were examined and finally the best scenario which was very similar to the real conditions was chosen.

In real life drilling, engineers use drill collars to apply static weight on bit. These collars are typically thicker than normal drill pipes and have higher weight per unit length. Figure 4.6 shows the schematic view of typical conventional drilling rig. As shown in the figure, the drill collars are installed above the drill bit and immediately before the down-hole tools. Any down-hole tool such as Measurement While Drilling (MWD) tools or down-hole vibrators are installed between the drill bit and drill collars in the Bottom Hole Assembly (BHA).

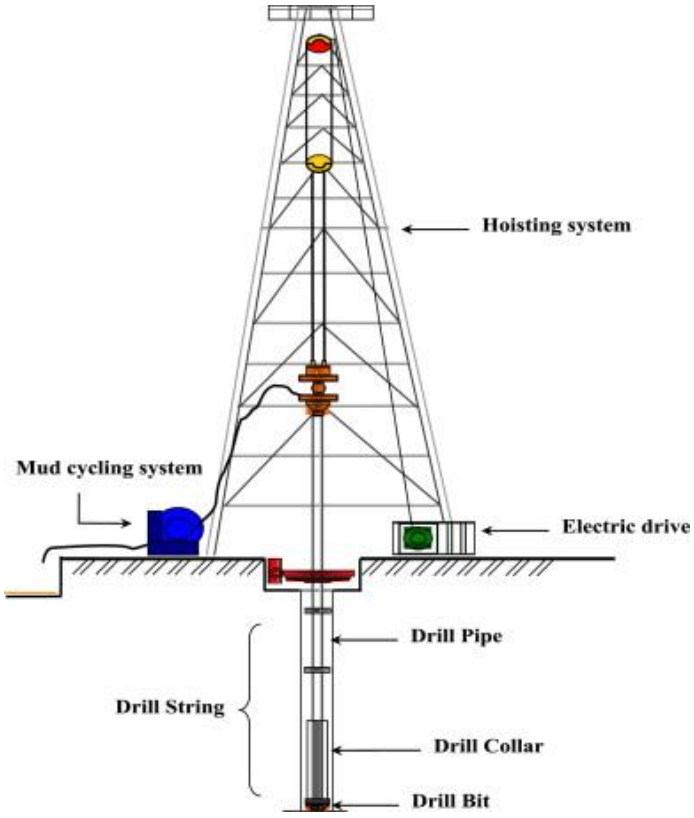

Figure 4.6: Illustration of a rotary drill rig [34]

In case of using the AGT as a down-hole vibrator, it will be installed right behind the bit to transfer the variable force directly to the bit. Engineers typically use a shock tool with specific stiffness to allow the tool to give appropriate displacement to the bit while isolating the drill string from vibration forces. In order to simulate this condition in the DEM environment, the AGT, the shock tool and the drill collars were each represented with one large ball with specific density which defines the mass of the ball. Figure 4.7 schematically represents the scenario.

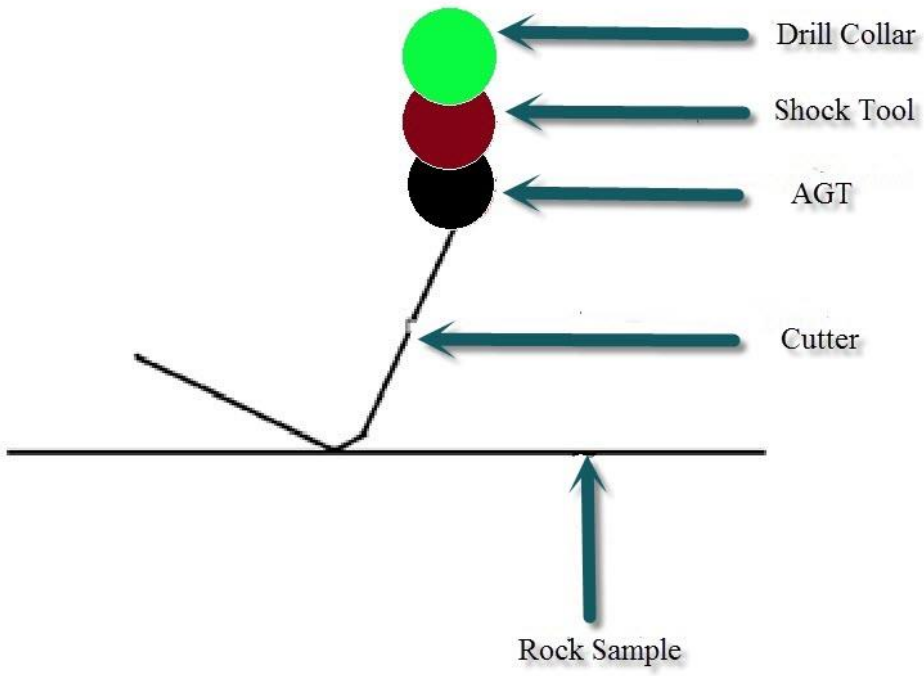

Figure 4.7: Schematic illustration of the drilling scenario including agitator tool, shock tool and drill collar

As can be seen in Figure 4.7, the green ball represents the drill collar behind the bit that provides static weight on the bit (WOB). Its density is adjusted so that its total weight equals the static WOB used in the field for similar cases. The ball in maroon color simulates the action of the shock tool. Its stiffness with the upper and lower ball is adjusted in a way that represents the stiffness of a shock tool spring. It is assumed that the shock sub is isolated from the drill color and drill bit. Entire shock sub acts as a spring between drill bit and drill collar. Finally, the black ball represents the AGT that creates a sinusoidal force behind the

bit. It is attached to the cutter so that the cutter and AGT act as one rigid body. A sinusoidal force profile is given to the red ball that causes the cutter to displace while having the static WOB on the top. Stiffness between the red and green ball and the blue and green ball causes the whole assembly to compress and stretch in a sinusoidal pattern. In the soft contact approach, particles can overlap each other using defined stiffness between them. As mentioned in Chapter 2, PFC2D employs the soft contact approach to simulate granular materials. Therefore, stiffness can be defined between each pair of particles in this software. This ability was used to simulate the shock tool in the DEM environment. According to Figure 4.7, the ball in maroon color is in contact with its upper and lower balls which represent drill collar and AGT, respectively. User-defined stiffness is given to these two bonds so that they simulate the mandrel of the shock tool. The magnitude of stiffness given to these bonds is related to the size of the simulated shock tool. Details of stiffness selection criteria are presented later in this Chapter. Figure 4.8 shows the simulation scenario created in the PFC2D environment. As can be seen from the figure, three balls are overlapping each other which represent the compression of the shock tool in reality.

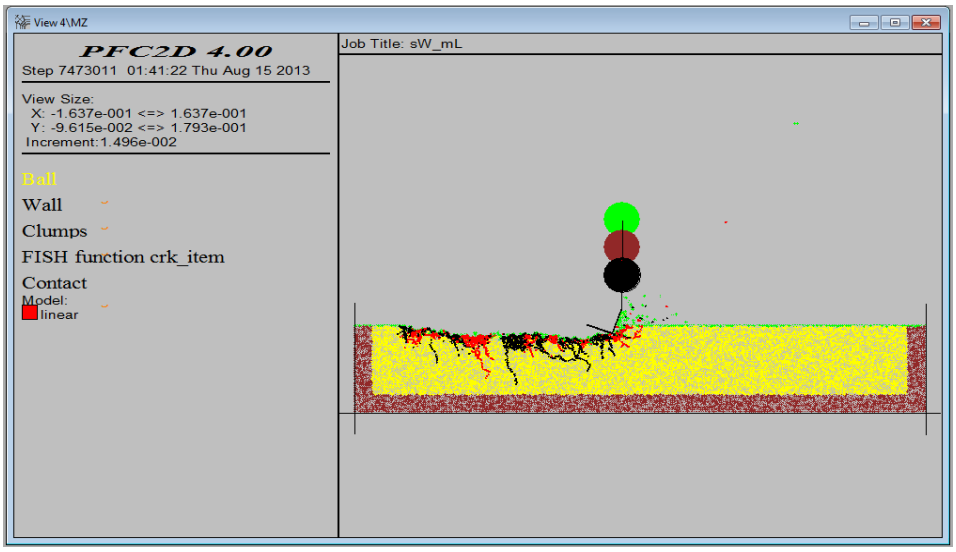

Figure 4.8: Drilling action of agitator tool including shock tool and drill collar

4.3.1 Simulation Considerations and Input Parameters

4.3.1.1 Scaling in PFC2D

PFC2D environment is a two dimensional environment which assumes a unit thickness of 1 m for each ball. Since all units in PFC2D are in the International System of Unit (SI), any input parameter should be converted to SI unit in order to be applied in the simulations.

The calculation system in PFC2D follows the DEM rules in which the Force-Displacement Law and the Law of Motion are used in a cycle to update positions of the particles and forces acting on them. As a result, the parameters are assumed to be related to each other linearly. In other words, if input parameters are increased with specific proportion, the resultant output parameters will be changed in the same proportion.

The cutter created in PFC2D to penetrate the rock specimen has 1 m width as every particle is considered to have 1 m out of plane width in this software. On the other hand, the cutter length of actual PDC bits vary with their diameter. The more the diameter, the more the cutter length. Usually drilling engineers consider total length of face cutters as total cutter length of the bit since only face cutters are in contact with the rock during the entire drilling process. As a result, any parameter obtained for a specific size of PDC bit needs to be scaled to the equivalent PFC2D cutter length to be used in simulations.

4.3.1.2 Input Parameters

For the simulation of both the AGT and the Hydropulse tool, a 6" diameter (150 mm) bit was used as a drilling bit. The cutter length of this bit was found and used as scaling factor to scale up the parameters to be used in the simulations.

In order to clarify the simulation input parameters, each parameter is presented in different section and rationale for selection of the magnitude of each parameter is described in that section. Following are the simulation input parameters to be used in simulation of drilling process using the AGT and accompanying shock tool:

- Vertical force on cutter (WOB + sinusoidal force generated by AGT)
- Frequency of the sinusoidal force

- Rotary Speed
- Axial Compliance (shock tool stiffness)
- Bottom-hole drilling fluid pressure
- Cleaning efficiency

The above parameters are the input parameters to be used in the simulations. Except for two parameters, all the others are constant during the simulations. These two parameters are bottom-hole drilling fluid pressure and the amplitude of the sinusoidal force. Since the frequency of the sinusoidal force is proportional to the amplitude of the oscillation, it also varies during the simulations. Each of these parameters is described below:

(i) Vertical force on the cutter

Vertical force on the cutter is divided into two components.

- Sinusoidal Force
- Static Force

The first component represents the static WOB in reality, while the second component is a variable sinusoidal force that simulates the generated sinusoidal force by the AGT. Overall vertical force to be applied to the cutter is shown in Figure 4.9. Each of these components is described in detail below:

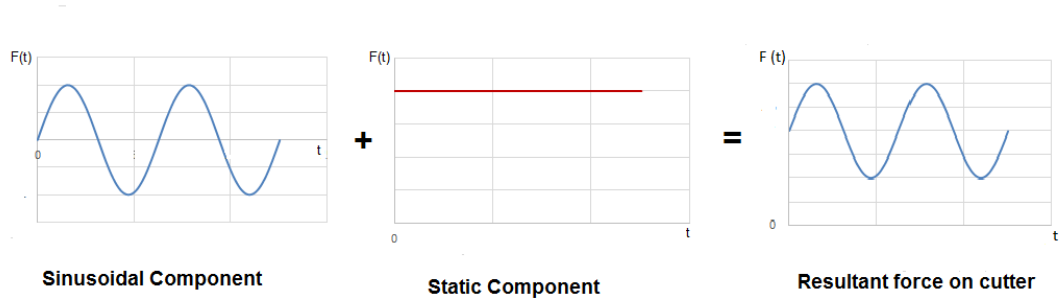

Figure 4.9: Schematic illustration of the components of vertical force applied to the cutter

Sinusoidal Force

The sinusoidal force was selected based on technical tool specification and confirmed using unpublished technical data from AGT experiments. The considerations below were made to select different amplitudes of forces:

As stated before, all of the simulations are based on a 150 mm PDC bit. Table 4.3 summarizes the specifications of the bit that were used in the simulations.

Table 4.3: Specifications of 150 mm M716 PDC bit [7]

Design Specifications	
Total cutters	28
Cutter size	16 mm
Face cutters	21
Blade count	7
Nozzles	3 Standard fixed port
Weight on bit	1 to 10 tonne

According to the table, afformentioned PDC bit has 21 face cutter each having 16 mm length. Therefore, overall cutter length for this bit would be 336 mm.

In this investigation, it is assumed that the outside diameter of AGT is equal to that to drill collar. Therefore, in order to choose proper size of the AGT for a 150 mm bit, suitable collar size needs to be determined. Drill collar selection follows the equation below [35]:

$$D_{ODC} = 2(D_{OCC}) - D_b \qquad (4.1)$$

Where D_{ODC} is the outside diameter of drill collar, D_{OCC} is the outside diameter of casing joint, and D_b is bit diameter.

It is assumed that the outside diameter of the casing joint for the 150 mm bit is 5 ¼". Considering 150 mm bit with 5 ¼" casing joint, Equation 4.1 will give the drill collar with outside diameter of 4.5". According to Figure 3.1, a 4 ¾" AGT tool was selected in order to satisfy this condition. Table 4.4 summarize the amplitude and frequency of oscillation for 4 ¾" AGT in different flow rates taken from AGT unpublished experimental data.

Table 4.4**: Experimental data for 4 ¾"** AGT

Flow rate (GPM)	Amplitude of Oscillation (N)	Frequency of Oscillation (Hz)
100	900	7
175	3430	14
250	6470	20

In order to use the forces in Table 4.4 in simulations of the AGT, they should be scaled up to equivalent PFC2D forces as mentioned before. The idea of weight per millimeter of cutter length was used to scale up the force parameter.

Table 4.4 can be updated to include weight per mm of cutter length using cutter length of the 150 mm PDC bit as calculated earlier. Table 4.5 shows the updated data.

Table 4.5: Updated force and frequency data for AGT size of 4 ¾"

Flow rate (GPM)	Amplitude of Oscillation (N)	Frequency of Oscillation (Hz)	Amplitude of oscillation per mm of cutter (N)
100	900	7	2.7
175	3430	14	10.2
250	6470	20	19.25

Now that amplitudes of force oscillations per millimeter of cutter are known, they can be scaled up for 1 m of cutter length that is used in simulations.

As mentioned earlier, length of PFC2D cutter is 1 m or 1000 mm. On the other hand, amplitudes of force oscillations for the AGT are known in N/mm. as a result, the amplitudes of force oscillations can be calculated for simulation and shown in Table 4.6.

Force to be used in the simulation = 1000 * force per millimeter

Table 4.6: Amplitudes of force oscillations to be used in simulation

Flow rate (GPM)	Amplitude of Oscillation (N)	Frequency of Oscillation (Hz)
100	2700	7
175	10200	14
250	19250	20

Static Force

The static force to be applied in the simulation is the same as static WOB in the real condition. In the drilling process, the amount of weight to be applied on the bit is selected according to the strength of the formation to be drilled and the size of the drilling bit. In order to select the WOB for the simulations, the recommended WOB for the 150 mm M716 PDC bit by Schlumberger Company [7] was used. According to Table 4.3, the recommended WOB for this size of bit varies from 10 to 100 KN (1 to 10 tonne) depending on strength of the formation being drilled. Usually hard formations require higher WOB. As mentioned earlier in this Chapter, the simulation rock has a UCS of 55 MPa which is considered medium strength rock (<80 MPa and >30 MPa). As a result, the lowest fifth of the recommended WOB was selected for the simulations (2 tonne). Weight of the AGT and accompanying shock tool as well as drill bit are all included in static WOB. Consequently, applying the same force conversion procedure as for the sinusoidal force static WOB per mm will be 60 N/mm and finally simulation WOB will be 60 KN.

(ii) Frequency of the sinusoidal force oscillation

The frequency of oscillation for different flow rates are presented in the previous section in Table 4.6. It should be note that the frequency of oscillation is proportional to the flow rate.

(iii) Rotary Speed

Cutters are usually distributed on the bit face symmetrically. As can be seen in Figure 2.1, these cutters are placed along the radius of the bit. Considering a constant Revolution per Minute (RPM) rotary speed of the bit, each of these cutters will have different tangential velocity which is proportional to their distance from the center. The relation between tangential velocity of the cutters and the RPM of the bit is as follow:

$$v\ (m/s) = (\pi/30)RPM\ r \quad (4.1)$$

where v is the tangential velocity of cutter, r is the radius of the bit, and RPM is the rotary speed of the bit.

The input velocity in the simulations is the average tangential velocities of all cutters in corresponding drill bit. The cutter velocity that was selected for the simulations was 0.5 m/s. It was assumed that 1 m cutter length represents the 10" PDC bit. On the other hand, according to Equation 4.1, the tangential velocity of a cutter has linear relationship with the radius of the bit. As a result, average tangential velocity will be the tangential velocity of cutters that are in the middle of the bit (half of the radius). The half of the radius of 10" PDC drill bit is 2.5" (0.0635 m). Using the Equation 4.1 and knowing that the input velocity in the simulations was 0.5 m/s, the RPM of 10" bit can be calculated as follow:

Rotary Speed = (0.5*30) / (0.0635 π) = 75 RPM

Rotary speed of 75 RPM is at lower bound of the field recommended rotary speed. However, due to the simulation limitations (high run time with lower speed), 75 RPM was selected as the simulation rotary speed.

(iv) Compliance

Compliance or shock tool stiffness is determined based on the amplitude of displacement generated in the drilling process. The magnitude of shock tool stiffness (spring rate) for different shock tools are shown in Figure 4.10. As can be inferred from the figure, the spring rate of shock tools varies from 940 to 6100 N/mm depending on size of the tool and the displacement requirement.

Outside Diameter	inches	3-1/8	3-1/2	4-3/4	6-1/4	6-1/2	6-3/4	7
	(mm)	(79)	(89)	(121)	(159)	(165)	(171)	(178)
Inside Diameter	inches	1	1-1/4	2	2	2	2-1/4	2-1/4
	(mm)	(25)	(32)	(51)	(51)	(51)	(57)	(57)
Assembly Number		167	166	155	146	150	147	154
Maximum Recommended Hole Diameter*	inches	n/a	n/a	6-3/4	8-1/2	8-1/2	8-3/4	8-3/4
	(mm)	n/a	n/a	(171)	(216)	(216)	(222)	(222)
Tensile Yield Strength	lbf	150,000	195,000	380,000	555,000	555,000	593,000	593,000
	(N)	(667,200)	(867,400)	(1,690,300)	(2,468,700)	(2,468,700)	(2,637,700)	(2,637,700)
Torsional Yield Strength**	lbf-ft	4,000	4,200	17,000	41,000	50,000	54,000	54,000
	(N-m)	(5,400)	(5,600)	(23,000)	(55,500)	(67,700)	(73,200)	(73,200)
Axial Load to Fully Compress [Down]	lbf	11,000	13,200	74,000	100,000	100,000	100,000	100,000
	(N)	(48,900)	(58,700)	(329,100)	(444,800)	(444,800)	(444,800)	(444,800)
Spring Rate	lb/in	5,400	5,860	29,000	35,000	35,000	35,000	35,000
	(N/mm)	(940)	(1,000)	(5,000)	(6,100)	(6,100)	(6,100)	(6,100)
Opening Travel [Up]	inches	2.0	2.3	1.0	1.8	1.8	1.8	1.8
	(mm)	(51)	(57)	(25)	(44)	(44)	(44)	(44)
Closing Travel [Down]	inches	2.0	2.3	2.5	2.9	2.9	3.0	3.0
	(mm)	(51)	(57)	(64)	(74)	(74)	(76)	(76)
Pump Open Area	in^2	4.0	5.9	11.0	15.9	15.9	17.7	17.7
	(mm^2)	(2,570)	(3,840)	(7,100)	(10,260)	(10,260)	(11,420)	(11,420)
Length	feet	4.6	5.3	8.5	9.4	9.4	9.4	9.4
	(m)	(1.4)	(1.6)	(2.6)	(2.9)	(2.9)	(2.9)	(2.9)
Weight	lb	80	100	380	720	800	850	930
	(kg)	(40)	(50)	(180)	(330)	(370)	(390)	(430)

** Hole Openers not recommended*
*** Torsional Yield Strength rating is based on the yield of the body connections independent of tool joint connections*
**** Pressure Compensated Shock Tools are Assembly Numbers 157, 143, and 113*

Specifications subject to change without notice

Outside Diameter	inches	8	9	9-1/2	10	11	12	14
	(mm)	(203)	(229)	(241)	(254)	(279)	(305)	(356)
Inside Diameter	inches	2-3/4	2-13/16	2-13/16	2-13/16	2-13/16	2-13/16	3
	(mm)	(70)	(71)	(71)	(71)	(71)	(71)	(76)
Assembly Number		160	139	151	138	157***	143***	113***
Maximum Recommended Hole Diameter*	inches	12-1/4	13-3/4	17-1/2	17-1/2	17-1/2	17-1/2	26
	(mm)	(311)	(349)	(445)	(445)	(445)	(445)	(660)
Tensile Yield Strength	lbf	872,000	853,000	1,207,000	1,042,000	808,000	1,337,000	1,865,000
	(N)	(3,878,800)	(3,794,300)	(5,369,000)	(4,635,000)	(3,594,100)	(5,947,200)	(8,295,900)
Torsional Yield Strength**	lbf-ft	79,000	115,000	109,000	157,000	187,000	244,000	400,000
	(N-m)	(107,100)	(155,900)	(147,700)	(212,800)	(253,500)	(330,800)	(542,300)
Axial Load to Fully Compress [Down]	lbf	125,000	110,000	100,000	100,000	100,000	100,000	140,000
	(N)	(556,000)	(489,300)	(444,800)	(444,800)	(444,800)	(444,800)	(622,700)
Spring Rate	lb/in	31,000	35,000	25,000	25,000	15,000	15,000	22,000
	(N/mm)	(5,400)	(6,100)	(4,300)	(4,300)	(2,600)	(2,600)	(3,800)
Opening Travel [Up]	inches	1.8	1.8	3.3	3.3	2.5	2.5	2.0
	(mm)	(44)	(44)	(84)	(84)	(64)	(64)	(51)
Closing Travel [Down]	inches	4.0	3.2	4.0	4.0	7.0	7.0	7.0
	(mm)	(102)	(81)	(102)	(102)	(178)	(178)	(178)
Pump Open Area	in^2	30.7	30.7	38.5	41.3	11.0	11.8	12.6
	(mm^2)	(19,810)	(19,810)	(24,840)	(26,650)	(7,100)	(7,620)	(8,130)
Length	feet	12.5	9.4	10.8	10.8	14.0	12.2	15.0
	(m)	(3.8)	(2.9)	(3.3)	(3.3)	(4.3)	(3.7)	(4.6)
Weight	lb	1,600	1,500	2,200	2,300	3,200	3,400	5,200
	(kg)	(730)	(690)	(1,000)	(1,100)	(1,500)	(1,600)	(2,400)

Figure 4.10: Specifications of different sizes of shock tools [36]

The criteria for the selection of the spring rate of shock tool was based on the AGT operation guideline that the produced bit displacement amplitude should not be more than 3-

4 mm. High bit displacement can cause damage to the bit teeth and finally bit failure. As a result, based on the highest force oscillation that was around 19250 N, spring rate of 4500 N/mm was chosen. This spring rate would create maximum bit displacement of 4 mm during the simulations. Initial compression of the shock tool due to the static WOB was around 11 mm.

(v) Bottom-hole Drilling Fluid Pressure

As mentioned earlier in Chapter 1, drilling performance reduces dramatically with increase in bottom-hole drilling fluid pressure. Cunningham and Eenink [5] plotted ROP as a function of overbalance pressure (pressure difference between formation pressure and hydrostatic pressure of drilling fluid) for wide for different rocks with wide range of permeabilities. Figure 1.1 shows their plot for Indiana limestone. As can be seen from the figure, ROP decreases exponentially with increase in overbalance pressure. However, it should be noted that after pressure of around 2500 psi, no significant decrease in ROP is observed with increase in overbalance pressure. In other word, overbalance pressure cause significant decrease in ROP in lower values of overbalance pressure and if the pressure is high enough, additional increases in overbalance pressure would have minimal effect on ROP.

Considering aforementioned points, five levels of bottom-hole pressure were selected for the simulations. The first level was atmospheric pressure to simulate drilling without any hydrostatic pressure. The other four levels of bottom-hole pressures (100, 200, 1000 and

2000 psi) were simulated in order to investigate the effect of the hydrostatic pressure on drilling performance of the AGT under low and high pressures. Note that higher bottom-hole pressures were not simulated since according to the work of Cunningham and Eenink [4], after hydrostatic pressure of about 2500 psi, no additional effect of bottom-hole pressure on ROP has been observed.

(vi) Cleaning Efficiency

Down-hole cleaning is one of the important factors in the drilling process that can decrease ROP dramatically. If the rate of chip generation is more than the rate of cutting transport, poor cleaning will happen which leads to a well-known phenomenon called the "Chip Hold Down" effect. At this condition, the drill bit crushes the previously formed chips into small fragments which decrease drilling efficiency and increase energy consumption dramatically.

In order to simulate the down-hole cleaning in the DEM environment, a code written by Mozaffari [37] was used that deletes any crushed ball ahead of the cutter during the drilling process. According to this code, there are three levels of down-hole cleaning depends of the number of remaining contacts. Details of these levels are described as follow:

In PFC2D environment, each ball is in contact with several other surrounding balls. During the drilling process, any of these contacts can be broken depending on the position of the ball in the system. The code is written in a way that it attributes a cleaning efficiency of 1, 2 and 3 to the process. Cleaning efficiency of 1 means that any ball that has only 1

remaining contact (three broken contacts) is deleted from the cleaning zone. Accordingly, the cleaning efficiency of 2 means that any ball that has two contacts or lower (two broken) is deleted from the cleaning zone. Finally, a cleaning efficiency of 3 represents a situation in which any ball that has 3 contacts or lower is deleted from the cleaning zone. In the last case, if one contact breaks between two balls, both of them will be deleted.

Cleaning efficiency of 3 is considered too unrealistic since it eliminates approximately half of the balls in the system. As a result, two preliminary runs were conducted to compare the cleaning efficiency of 1 and 2. After completing the runs, it was concluded that cleaning efficiencies of 1 is more realistic and closer to reality. Consequently, this level of cleaning efficiency was selected for the simulations of both tools.

It should be noted that the simple deletion of the particle is assumed to be equivalent of cutting removal in real case scenario. Since it is not possible to introduce hydraulic to the system in PFC2D, flushing of the particles was simulated using simple deletion of the balls. It was assumed that the drilling fluid flushes the particle immediately when the particle is separated from the rock.

4.3.2 Simulation Matrix and Parameters

Table 4.7 illustrates the simulation matrix for the AGT simulations. Two factors (amplitude of the sinusoidal force and bottom-hole pressure) were selected for the simulations as described earlier. Note that one more level (zero amplitude) is added to the

amplitude of sinusoidal force to simulate the conventional drilling without use of the AGT and with no shock tool.

Table 4.7: AGT simulation matrix

Parameter	Levels				
Amplitude of sinusoidal force oscillation (N)	0	2700	10200		19250
Bottom-hole pressure (psi)	0	100	200	1000	2000

It should be noted that frequencies of sinusoidal force oscillations are different for different amplitudes of oscillations as mentioned earlier. For the remainder of this Chapter, for convenience the terms, low, medium and high amplitude of oscillation are used to name the different magnitudes of oscillations. Table 4.8 shows the four levels of sinusoidal forces with their name and frequencies of oscillations.

Table 4.8: Different levels of sinusoidal force oscillations

Amplitude of sinusoidal force (N)	Name attributed	Frequency (Hz)
0	No tool	0
2700	Low amplitude	7
10200	Medium amplitude	14
19250	High amplitude	20

With 4 levels of sinusoidal force amplitudes and 5 levels of bottom-hole pressures, overall 20 runs were conducted and analyzed.

Constant parameters for the simulations were described earlier in this chapter. However, for clarity a summary of these parameters and their magnitudes are presented in Table 4.9.

Table 4.9: Simulation constant parameters

Parameter	Magnitude
Static weight on bit	60 KN
Rotary Speed (RPM)	75
Compliance (N/mm)	4500
Cleaning efficiency	1

4.4 Simulation Results and Discussion

4.4.1 Analyzed Parameters

Considering the simulation matrix presented in the previous section, overall 20 runs were conducted to investigate the performance of the AGT in drilling process with different down-hole hydrostatic pressures. The number of runs and their information are presented in Appendix B.

In the drilling industry, there are different methods to describe and quantify the drilling performance. Three methods of drilling performance evaluation were used in this thesis to analyze the simulation results:

1. Rate of Penetration (ROP)
2. Material Removal Rate (MRR)

3. Mechanical Specific Energy (MSE)

These parameters are described in detail in the following sections:

4.4.1.1 Rate of Penetration (ROP)

The most pronounced and applicable parameter to describe the drilling performance of a specific system (system can include bit, down-hole tool, different type of drilling and etc.) in one formation is a measure of ROP. As mentioned earlier, ROP is the rate at which the drilling bit penetrates the rock and its unit is unit of length per unit of time (L/T). Typical units for ROP are ft/hr and m/hr but in laboratory experiments, researchers sometime use m/s or mm/s. There are two types of ROP measurement: instantaneous ROP and average ROP. Instantaneous ROP is measured by down-hole measurement tools and average ROP is measure over an interval of time. In drilling research, researchers focus on the average ROP rather than the instantaneous ROP. In analyses of the simulation results, the average ROP was used to compare the results of the simulations.

4.4.1.2 Material Removal Rate (MRR)

The second method is the use of factor called Material Removal Rate (MRR). MRR is the volume of removed or crushed rock over a specific period of time. MRR unit is in L^3/T which translates to m^3/s. This parameter is mostly used in literature and research to compare

the results of the laboratory experiments or simulations. MRR doesn't have field application since it is very difficult to measure during the drilling process. However, ROP and MRR are similar in nature and although they give different values for the same drilling process, the overall pattern of results is similar. For clarity in the simulations, MRR values for all runs were calculated and the results were compared.

4.4.1.3 Mechanical Specific Energy (MSE)

Mechanical Specific Energy (MSE) introduced by Teale [38] in 1964 is another method to evaluate the drilling process. MSE is the amount of energy consumed to remove a unit volume of the rock. In most drilling applications, drillers try to increase ROP and MRR values. However, there are some limitations of power consumption. In some cases, ROP or MRR might be higher but overall drilling efficiency is lower due to high power consumption. This changes the definition of optimum drilling which is defined as highest ROP or MRR value with lower power consumption. As a result, it seems that ROP and MRR values are not enough to evaluate the drilling process. Consequently, researchers introduced the MSE value which is independent of any other parameter and can describe the drilling process effectively.

The MSE field unit is ksi (kilo-pound force per square inch). However, other units such as psi or MPa are usually used in research and literature. It has been shown experimentally that the magnitude of MSE in drilling under atmospheric condition is a number very close to the UCS of the rock being drilled [39]. This gives a proper measure to monitor and evaluate

the drilling performance during the drilling process by comparing measured MSE with UCS of the formation being drilled.

As mentioned earlier, different units are used in literature for MSE value. However, J/m^3 (Joule per meter cubed) was used as the MSE unit in this research. For each simulation run, the amount of consumed energy was calculated and divided by the amount of volume removed over a specific period of time. Details of MSE and MRR calculations for different runs are provided in Appendix C.

4.4.2 Simulation Results

After completing all 20 runs for the AGT simulations, a table of runs was produced and corresponding graphs were generated. Table 4.10 shows the MRR results of the AGT simulations.

Table 4.10: MRR results of the AGT simulations (MRR unit is in 10^{-3} m^3/s)

Force Oscillation (N)	Pressure (psi)				
	0	100	200	1000	2000
No tool	4.62	3.48	2.78	1.78	0.8
Low amplitude (2700 N)	5.22	4.87	5.3	2.73	2.06
Medium amplitude (10200 N)	5.09	4.99	4.87	3.05	2.1
High amplitude (19250 N)	5.86	5.22	5.62	4.01	2.23

As can be seen from the table, the MRR values are much lower for conventional drilling than that of vibration drilling. Especially at higher pressures, a more than 100 % increase was obtained when using the AGT in the drilling process. However, MRR values behave inconsistently with different amplitudes of force oscillations. For clarity, the graph of MRR results is presented in Figure 4.11.

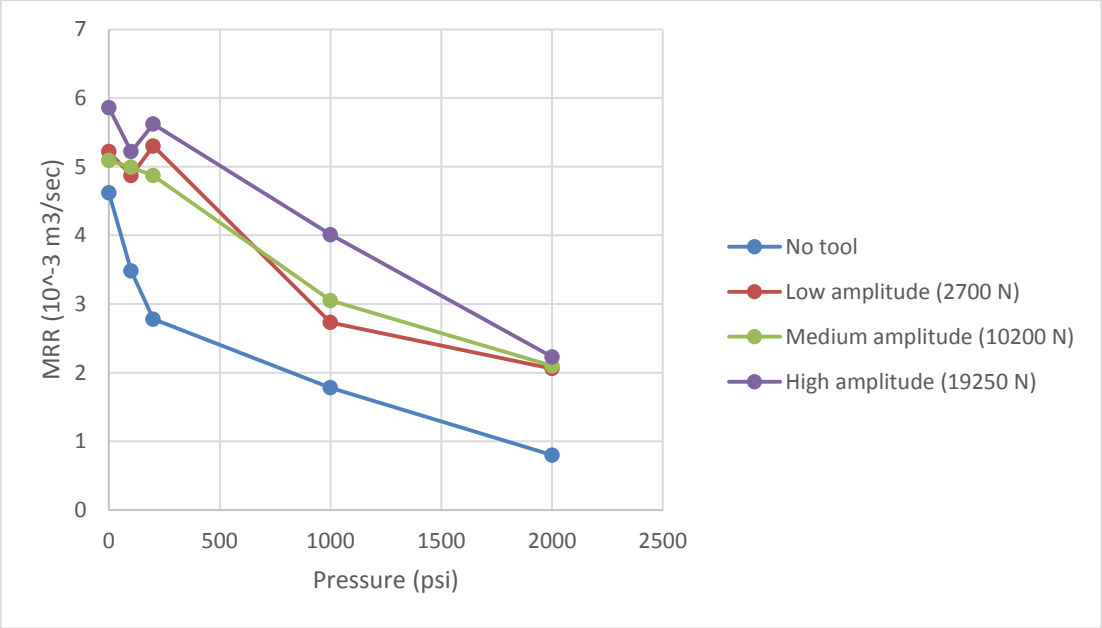

Figure 4.11: Graphical illustration of MRR results for the simulation of the AGT

Figure 4.11 indicates several trends. First is the MRR trend with increase in bottom-hole pressure. As mentioned earlier in this chapter and Chapter 1, ROP or MRR values decrease exponentially with increase in bottom-hole pressure. Since no formation pressure was introduced to the rock specimen, the simulated bottom-hole pressure is the same as overbalance or differential pressure. As can be seen from above figure, MRR value

decreases exponentially with pressure which is in agreement with laboratory experiments [4].

The second trend is the effect of low amplitude vibrations in different bottom-hole pressures. As can be seen from the figure, at higher pressures (around 1000 or 2000 psi) low amplitude force vibrations have significant effect on MRR value (approximately 100 % increase) while this effect decreases to less than 10 % for atmospheric drilling.

The third trend is decrease in MRR values of vibration drilling for the pressure level of 100 psi. This decrease is unusual since MRR values should decrease by increase in bottom-hole pressure. The reason for this is unknown at this point however; MSE results that are presented later in this Chapter give a different trend.

It should be noted however that high amplitude of oscillations has the highest MRR value for all pressure levels. At this point this is believed due to the extra weight that is applied to the bit. As mentioned earlier, higher MRR value doesn't always indicate better performance of the drilling. Analyses of MSE results will indicate whether higher amplitudes of sinusoidal vibration increase drilling performance or not.

Table 4.11 shows the results of ROP calculations for all runs. As can be seen from the table, ROP results are slightly different than MRR results. However, the overall trends are the same.

Table 4.11: ROP (cm/s) results of the AGT simulations

Force Oscillation (N)	Pressure (psi)				
	0	100	200	1000	2000
No tool	3.33	2.28	1.75	1.25	0.675
Low amplitude (2700 N)	5.21	3.57	3.71	3.00	2.2
Medium amplitude (10200 N)	3.175	4.43	3.25	3.52	2.45
High amplitude (19250 N)	3.76	5.23	4.21	4.16	2.75

Figure 4.12 shows the graph of ROP results of the AGT simulations. As mentioned earlier, the overall trend is same as MRR results but some small differences can be seen between two sets of results which are most significant in low pressures.

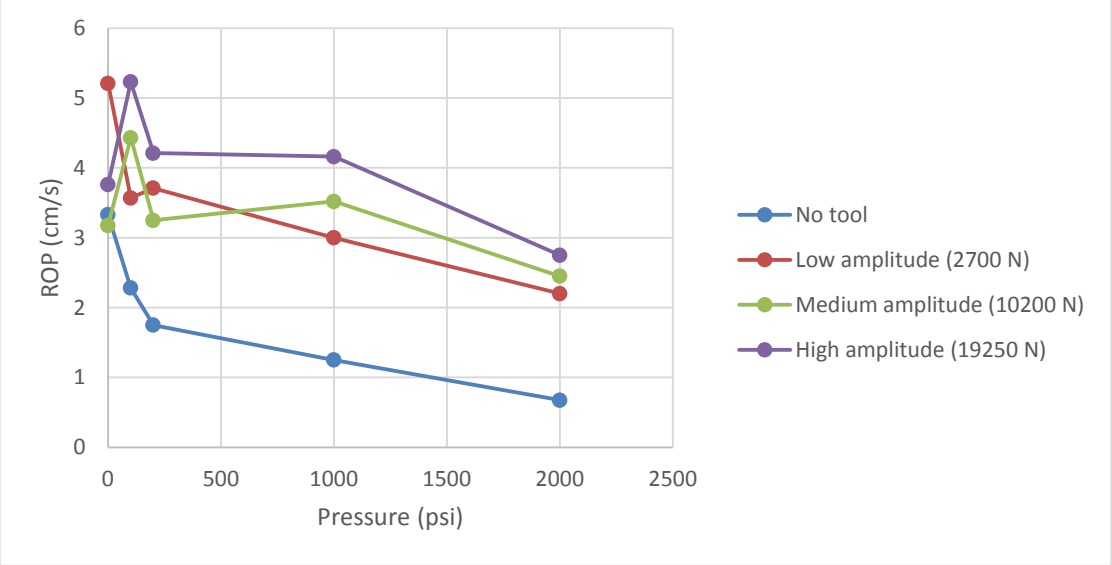

Figure 4.12: Graphical illustration of ROP results for the simulation of the AGT

Table 4.12 shows the MSE results of the AGT simulations. As can be seen from the table, MSE results confirm the results of MRR while eliminating some exceptions that were in the MRR results (e.g. decrease in MRR values at pressure level of 100 psi).

Table 4.12: MSE (KJ/m^3) results of the AGT simulations

Force Oscillation (N)	Pressure (psi)				
	0	100	200	1000	2000
No tool	5850	6490	7550	10700	23700
Low amplitude (2700 N)	6060	6110	5750	8420	13200
Medium amplitude (10200 N)	5840	5050	5640	8530	13000
High amplitude (19250 N)	5010	4900	4950	6880	12500

Figure 4.13 clarifies the MSE results by showing these results in graphical format. As can be seen from the figure, the MSE values increase significantly with increase in bottom-hole pressure. However, the rate of this increase is much lower for vibration drilling. Moreover, vibration drilling has a higher effect on drilling performance at higher pressures. This conclusion was also made by analyzing the MRR results.

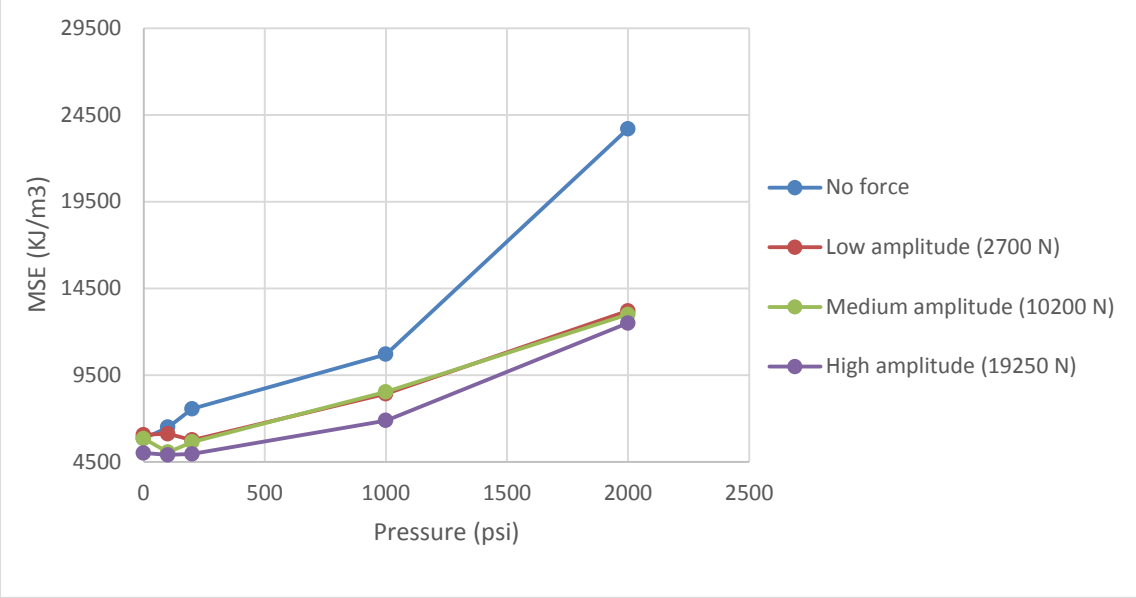

Figure 4.13: Graphical illustration of MSE results for the simulation of the AGT

As mentioned earlier, MSE results show predicted behavior for different amplitudes of vibration in different levels of pressures.

During the analyses of MRR and ROP results, it was found that high amplitude vibrations result in higher MRR values. At first it was thought that this could be because of the extra weight applied to the bit that increased the MRR values. However, after analyzing the MSE results, it was found that high amplitude vibrations also increase drilling performance from the MSE prospective. In other words, through the analyses of MSE results, it was found that the high amplitude of vibrations consumes less energy to drill a unit volume of rock among the other drilling scenarios. An approximately 100 % decrease in MSE value was found in the bottom-hole pressure of 2000 psi by using the AGT and accompanying shock tool.

Analyses of MRR, ROP and MSE values for the simulation runs showed significant increase in drilling performance when using vibration at higher bottom-hole pressures. It seems that vibration drilling is a good candidate to increase the drilling performance in medium strength formations. Besides analyzing drilling performance through the calculation of different parameters, the investigation compared the cutter trace on rock for both conventional and vibration drilling. Figure 4.14 shows the rock surface at the end of the drilling process for both conventional and vibration drilling at bottom-hole pressure of 2000 psi. According to the figure, the sinusoidal trace of the cutter can be seen for the vibration drilling. These peaks and valleys are created by up and down displacement of the cutter as a result of the force fluctuation above the cutter. Stiffness defined for the balls above the cutter translates this force oscillation the displacement which cause bit to move up and down.

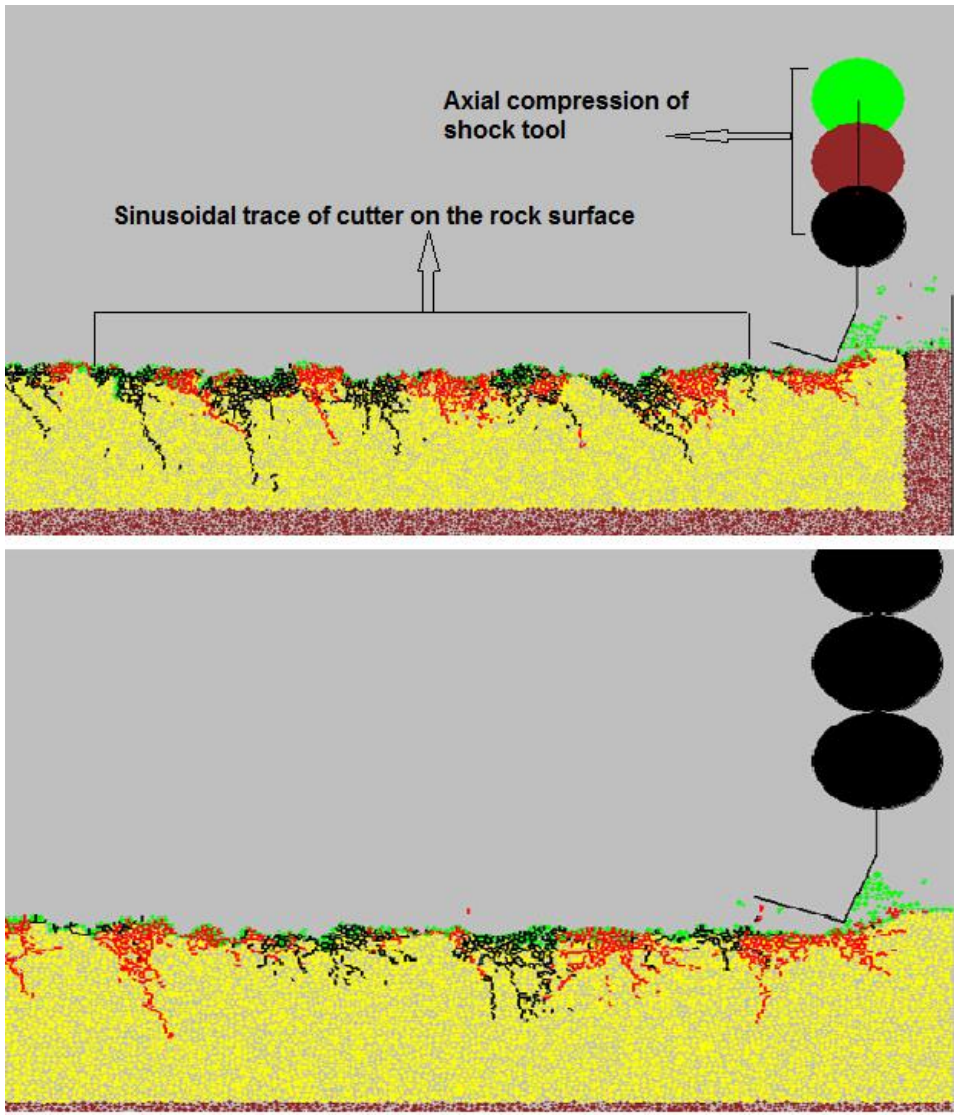

Figure 4.14: Cutter trace on rock for both vibration and conventional drilling (upper: Vibration drilling, lower: Conventional drilling)

Figure 4.15 shows the cutter displacement history for vibration and conventional drilling. As can be seen from this figure, conventional drilling has a smooth curve while the vibration drilling curve fluctuates as it penetrates the rock. The pattern of the cutter displacement was expected to be regular as applied force behind the cutter was sinusoidal

with specific frequency and amplitude. However, the output results for the cutter displacement were not linearly proportional to the applied force. This shows that there are other factors that can affect the cutter displacement.

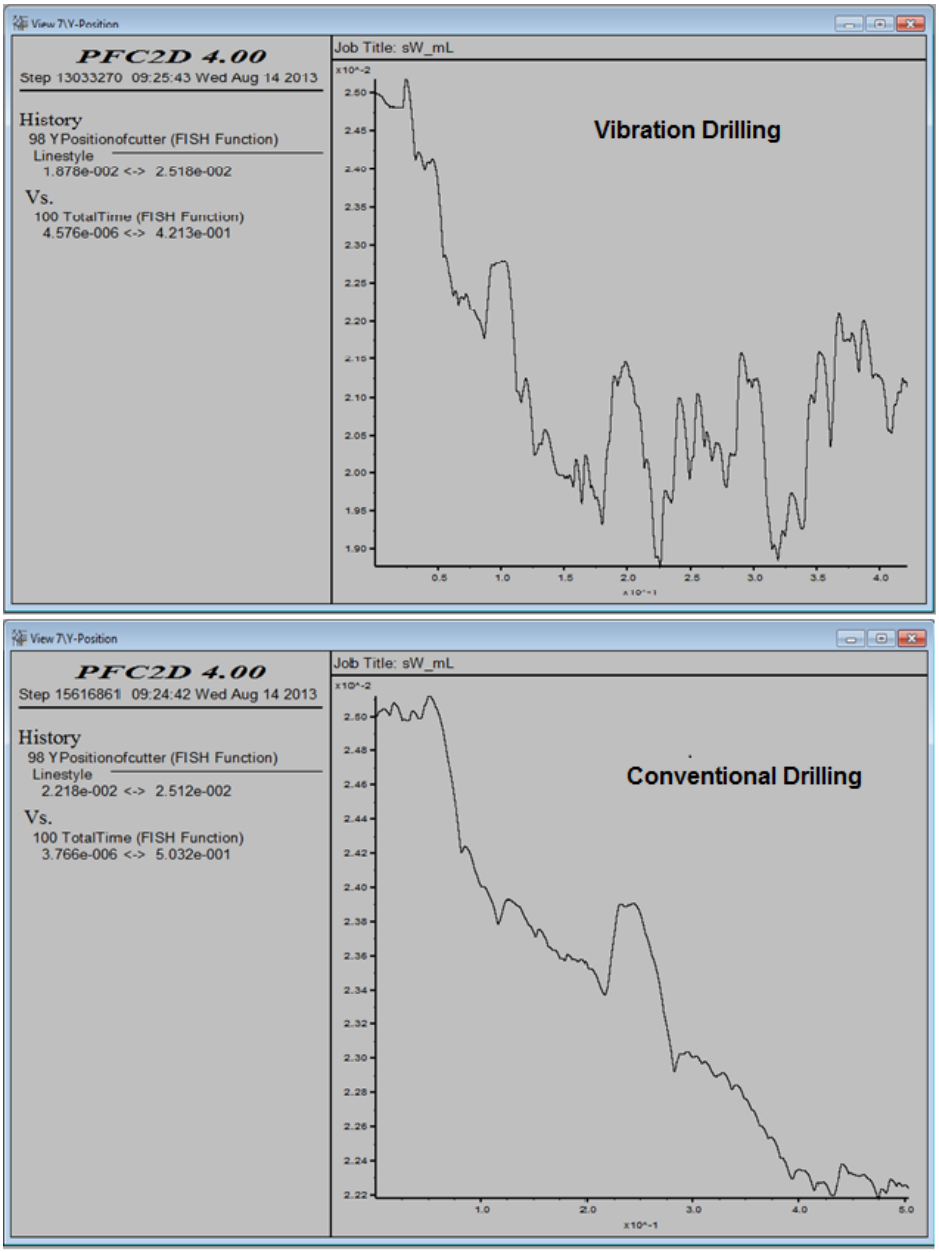

Figure 4.15: Cutter displacement history in vibration and conventional drilling (Bottom-hole pressure is 2000 psi and amplitude of sinusoidal force is 19250N)

One of these factors may be the natural vibration of the cutter when drilling the rock specimen. These vibrations have different frequencies than the frequency of applied force behind the cutter. Therefore, they interfere in the vibrations caused by the AGT and change the pattern of the cutter displacement.

Another factor that may be effective in the cutter displacement pattern is the penetration of the cutter. As the cutter drills the rock specimen, crushed particles are being deleted as the cutter advances. This creates an empty space beneath the cutter which causes vertical advancement of the cutter. This vertical advancement doesn't have a regular pattern. Therefore, similarly to natural vibrations, it affects the cutter vibration and displacement pattern of the cutter. As a result, although the force produced by the AGT behind the bit has regular pattern with specific frequency and amplitude, the output displacement history of the cutter is more irregular with multiple frequencies.

4.5 Conclusion

The use of the AGT and accompanying shock tool behind the bit as a sinusoidal force generator was simulated. The simulation scenario, parameter selection criteria and analyses of the results were presented in this chapter.

The results showed that the sinusoidal force behind the bit increased the drilling performance in medium strength rock. This increase was more significant at higher bottom-hole pressures. The results indicated more than 100 % increase in drilling performance at bottom-hole pressure above 1000 psi. These promising results can validate the use of vibration drilling in medium strength rocks.

The results of MRR and ROP analyses showed that if a proper AGT with suitable shock tool is installed behind the bit, the rate at which the ROP decreases with the bottom-hole pressure (slope of ROP vs. overbalance pressure), will decrease significantly. The results also showed that the amplitude and frequency of the sinusoidal force don't have significant effect on drilling performance.

The effect of shock tool was not investigated in this chapter since the shock tool was applied in all of the simulation runs. However, the influence of drilling without the shock tool was investigated with the results and analyses presented in Chapter 6.

Chapter 5 Discrete Element Method (DEM) Modeling of the Hydropulse Tool

This chapter describes simulating the action of the Hydropulse tool and analyzing the drilling performance when this tool is applied behind the bit. As mentioned in Chapter 3, the Hydropulse tool creates momentary suction pulses that travel down and pass through the bit nozzles which create a sudden pressure drop beneath the bit and effective impulsive load behind the bit. This chapter presents the simulation of this tool and analyses of the simulation results and conclusions on the drilling performance of this tool and consists of three main sections. In the first section, a brief description of the simulation rock is presented. Section 2 is about simulating the action of the Hydropulse tool behind the bit, and finally, in Section 3, the simulation results and discussions are presented.

5.1 Simulation Rock

As described in Chapter 4, the rock to be used in the simulations of both Hydropulse and AGT is same since the objective of this thesis is to investigate and compare the drilling performance of these two tools. Therefore, the simulated rock described in Chapter 4 is used for the simulations in this chapter.

5.2 Simulating the Action of Hydropulse Tool behind the Bit

As described in Chapters 2 and 3, the Hydropulse tool increases drilling performance through generating suction pulses and induced impulsive load, which are shown in Figure 2.8.

The Hydropulse tool is designed to be used in combination with a drilling bit. As can be seen from Figure 2.8, no shock tool is used when drilling with the Hydropulse tool in the field. This prevents bit displacement and applies hammer forces on the bit. The exhaust ports of the Hydropulse tool prevent any upward pressure and force waves in the system which rectifies the pressure and force profile of the tool. The typical pressure profile of the tool is shown in Figure 2.9. As the figure shows, the pressure profile is not sinusoidal and has been termed as "Impact Profile" in this investigation. Since the impulsive load is a result of the bit face pressure acting on the bit effective area, the force profile of the tool would be the same as the pressure profile.

A similar scenario was used to simulate the action of the Hydropulse tool on single cutter penetration. As described thoroughly in Chapter 4, drill string components including drill bit, drill collars and shock tools can be simulated using sets of balls in the PFC2D environment. For this purpose, the described scenario in Chapter 4 was modified to simulate the action of the Hydropulse tool behind the bit. Since no shock tool is involved in drilling with the Hydropulse tool, the simulation scenario for this tool is simpler than for the AGT, and only two balls were used in new scenario to simulate the Hydropulse tool and drill collar behind the bit. Figure 5.1 shows the simulation scenario for the Hydropulse tool.

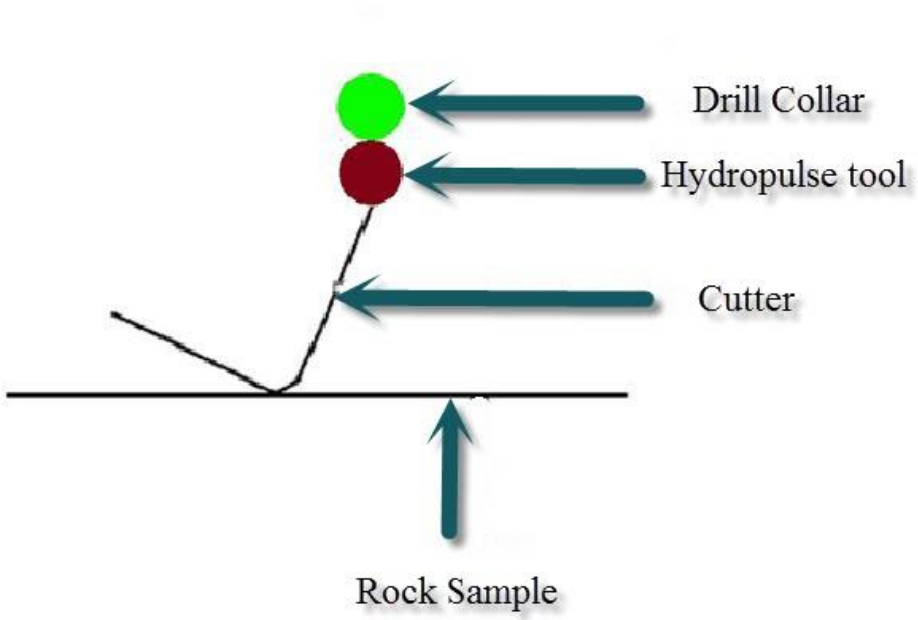

Figure 5.1: Simulation scenario for Hydropulse tool simulations

As can be seen from the figure, no shock tool is used in the simulations. As a result, there will be no axial compliance behind the bit. Figure 5.2 illustrates the simulation scenario in PFC2D environment. As shown in the figure, the green ball which represents the drill collar in real life provides static WOB while the red ball represents the Hydropulse tool and provides variable load.

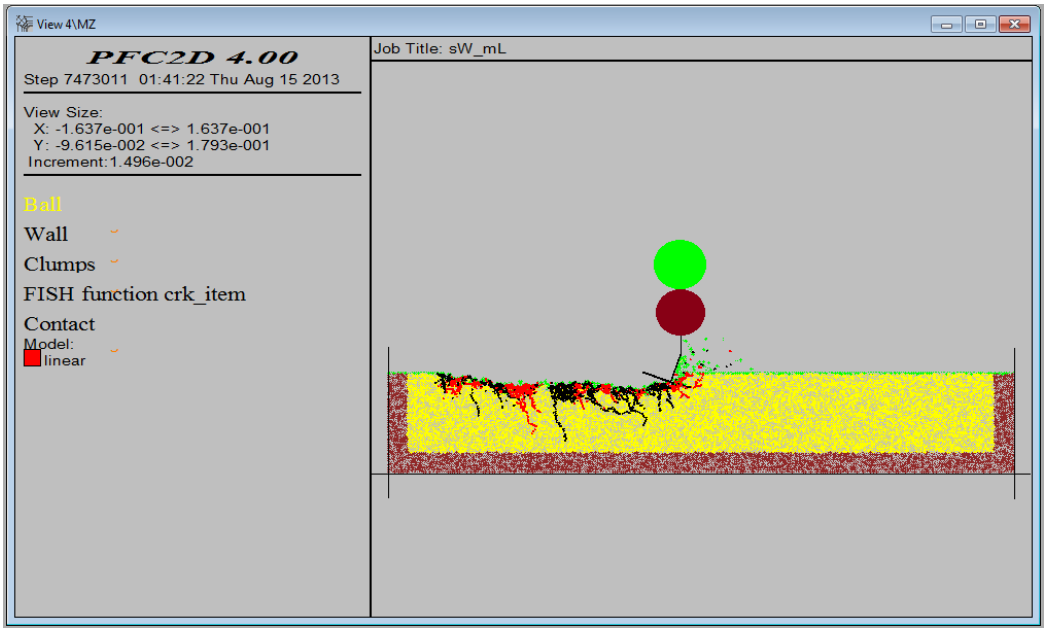

Figure 5.2: Simulation of the Hydropulse tool in DEM environment

5.2.1 Simulation Considerations and Input Parameters

All of the considerations that were presented in Chapter 4 about the simulation of the AGT are also applied to the simulation of the Hydropulse tool.

Input parameters for the Hydropulse tool simulations are very similar to that of AGT and listed as follows:

- Vertical force on cutter (WOB + force generated by the hydropulse tool)
- Frequency pulsation
- Rotary Speed
- Bottom-hole drilling fluid pressure
- Cleaning efficiency

Some of the input parameters are same in magnitude for the simulation of both tools. From above list, WOB, rotary speed and cleaning efficiency are exactly same for the Hydropulse and AGT simulations. These parameters and their selection criteria are described in detail in Chapter 4. However, the other parameters are changed due to the mechanism of the Hydropulse tool. Each of these parameters is discussed in details in the following sections:

(i) Vertical Force

Similar to the vertical force of the AGT simulations, the vertical force for the Hydropulse simulations consists of two components.

- Static WOB
- Dynamic force generated by the Hydropulse tool

Figure 5.3 shows two components of the vertical force for the Hydropulse simulations.

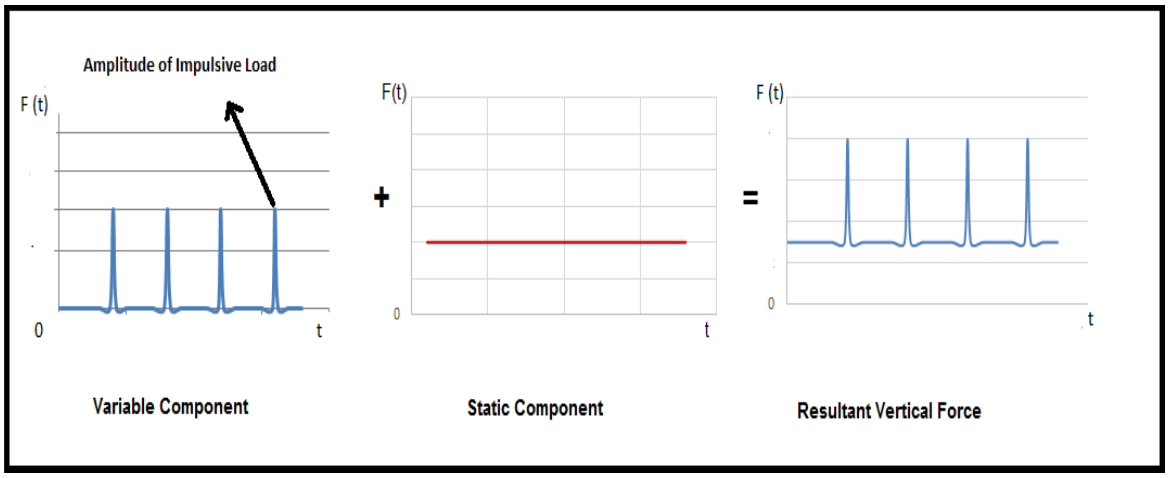

Figure 5.3: Components of the vertical force for Hydropulse simulations

Static WOB

Static WOB was one of the constant parameters for both of the AGT and the Hydropulse simulations. Since the cutter lengths for both of the simulation sets were same (one meter PFC2D cutter length), the static WOB was considered to be same for the both simulation sets. This force was 60 KN as stated in previous chapter.

Variable Force

As mentioned earlier the variable force that the Hydropulse tool generates (impulsive load by suction pulses), is in impact form and its amplitude is dependent on the flow rate of the drilling fluid.

The Hydropulse tool is usually applied behind the bit as an integrated component. It means that the Hydropulse tool is attached to the bit and its diameter is equal to the bit diameter. As a result, the appropriate size of the Hydropulse tool for the 150 mm drilling bit is the same 150 mm bit used for the AGT. Table 5.1 shows the specifications of the 150 mm Hydropulse tool.

Table 5.1: Design specifications for 150 mm Hydropulse tool [16]

Cycling Valve Diameter	150 mm (6")
Cycling Valve Length	600 mm (24")
Volumetric Efficiency	85%
Flow Course Length	1.5 m (60")
Flow Course Area	0.0032 m2 (5.0 in2)

Since the bit size for the both AGT and Hydropulse tool is same, same flow rate levels (100, 175 and 250 USGPM) were used in both simulations.

The mechanism of the Hydropulse tool allows calculation of the magnitude of the produced suction pulse by the Judowsky equation (Equation 2.20). However, this equation is theoretical, and data from real experiments for the Hydropulse tool were used to calibrate and modify the equation. The procedure of calibration is presented in Appendix D.

Calibrated equation is as follow:

$$\Delta P = 0.5\, v\sqrt{\rho k_f} \qquad (5.1)$$

According to Table 5.1, the flow course area for the 150 mm Hydropulse tool is 0.0032 m^2. Assuming water as fluid medium and knowing that the density of water is 1000 kg/m^3

and its bulk modulus is 2.2 GPa [16], Table 5.2 shows the calculated velocities and suction pulse magnitude for different flow rates using Equation 5.1. The reason for the assumption of water as fluid medium is that all laboratory experiments for the Hydropulse tool have been conducted using water as a fluid medium. As a result, in order to compare the results of the simulations with the experimental results this assumption was necessary.

Table 5.2: Suction pulse magnitude for different flow rates of 150 mm Hydropulse tool

Flow rate (USGPM)	Velocity in flow course (m/s)	Magnitude of suction pulse (MPa)
100 (0.0063 m^3/s)	1.97	1.46
175(0.0110 m^3/s)	3.44	2.55
250(0.0158 m^3/s)	4.94	3.66

Calculated suction pulses cause a sudden drop in pressure on the bit face which produces a relative impulsive load downward. The magnitude of this impulsive load can be calculated by simple law of pressure and area. Assuming the bit a circular shape, 150 mm PDC bit will have 0.00182 m^2 area. Using this area and calculated suction pulse magnitudes, Table 5.4 can be updated to include amplitude of variable force (second component of the vertical force). Table 5.3 shows the updated table.

Table 5.3: Updated pressure and force data for 150 mm Hydropulse tool using 150 mm PDC bit

Flow rate (USGPM)	Velocity in flow course (m/s)	Magnitude of suction pulse (MPa)	Amplitude of Impulsive load (KN)
100 (0.0063 m^3/s)	1.97	1.46	26.57
175(0.0110 m^3/s)	3.44	2.55	46.41
250(0.0158 m^3/s)	4.94	3.66	66.61

Above pressures and forces are produced by combined 150 mm Hydropulse tool and PDC bit. However, as mentioned before in Chapter 4, cutter length in PFC2D of 1 m which is much larger than the total sum of the cutters of the 150 mm bit. Applying the same procedure as in Chapter 4, equivalent forces can be calculated as in Table 5.4.

Table 5.4: Simulation variable forces

Flow rate (USGPM)	Magnitude of suction pulse (150 mm Hydropulse) (MPa)	Amplitude of impulsive load (150 mm Hydropulse) (KN)	Simulation force amplitude (scaling factor of 2.97) (KN)
100	1.46	26.57	79.17
175	2.55	46.41	138.3
250	3.66	66.61	198.5

(ii) Frequency of Pulsation

The Hydropulse tool can be configured for a desired frequency of pulsation. To be able to compare the results of the both the AGT and Hydropulse tool, the frequency of oscillation was selected to be same as the AGT. These frequencies are 20, 14 and 7 Hz for 250, 175 and 100 USGPM, respectively.

(iii) Bottom-hole drilling fluid pressure

Bottom-hole drilling fluid pressure for the Hydropulse tool simulations consists of two components. Static pressure which is the bottom-hole drilling fluid pressure, and pulsating pressure which is due to the suction pulses created by the Hydropulse tool. Every time each

of these suction pulses reaches the bottom of the well-bore, it causes a sudden pressure drop which results in a pulsating pressure profile.

Figure 5.4 presents the schematic illustration of two components of down-hole pressure for the Hydropulse simulations.

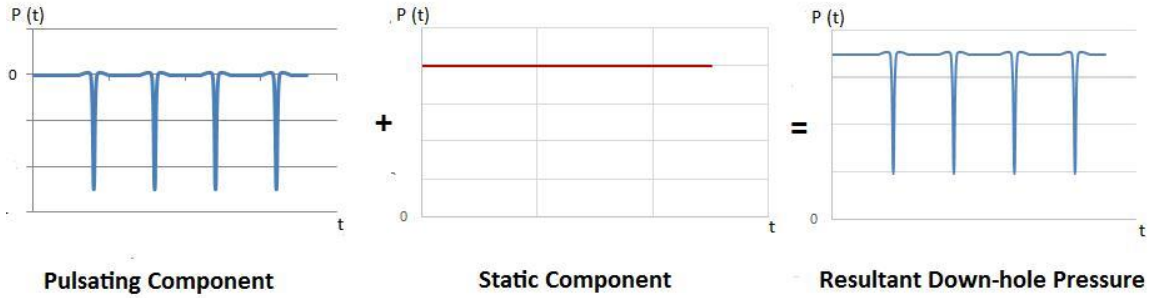

Figure 5.4: Schematic illustration of two components of down-hole pressure for the Hydropulse simulations

The static component of the down-hole pressure was three levels of 0, 1000 and 2000 psi.

The variable component of the down-hole pressure is coming from the tool operation, and is the magnitude of the suction pulses. The magnitude of suction pulse for different flow rates is presented in Table 5.4. The frequency of pulsation is exactly the same as the frequency of oscillation for the variable force, and in fact, impulsive force is a result of these suction pulses. As a result, they happen exactly at the same time.

5.2.2 Simulation Matrix and Parameters

Table 5.5 summarizes the simulation variable and constant parameters that were described in previous section. Note that frequency of pulsation for high, medium and low flow rates are 20, 14 and 7 Hz, respectively. A total of 9 runs were conducted for the simulation of the Hydropulse tool.

Table 5.5: Hydropulse simulation matrix

Variable Parameters	
Amplitude of pulsation (KN)	High (198.5) Medium (138.3) Low (79.17)
Bottom-hole pressure (psi)	0 1000 2000
Constant Parameters	
Static WOB (KN)	60
Rotary speed (RPM)	75
Cleaning efficiency	1

5.3 Simulation Results and Discussion

Overall 9 simulation runs were conducted to investigate the drilling performance of the Hydropulse tool. As mentioned earlier, the simulations were conducted under atmospheric condition and two bottom-hole pressure levels of 1000 and 2000 psi. In this section, results of these simulations are presented by calculating MRR, ROP and MSE value for each run. At the end of this section, simulation results of the Hydropulse tool are compared to those of AGT and related discussions and comments are made.

Table 5.6 shows the calculated MRR values for all of the runs. Note that MRR values for the constant load are taken from the AGT simulations since they represent the same drilling scenario.

Table 5.6: MRR ($10^{-3}m^3/s$) results of the Hydropulse tool simulations

Amplitude of pulsation (KN)	Pressure (psi)			
	0	200	1000	2000
No tool	4.62	2.78	1.78	0.8
High Amplitude (198.5)	6.88	3.13	2.99	1.26
Medium Amplitude (138.3)	4.85	3.69	1.62	1.13
Low amplitude (79.17)	5.99	3.03	1.68	0.98

Figure 5.5 presents the above results graphically. The effect of the Hydropulse action on the cutter performance can be seen more clearly in this figure.

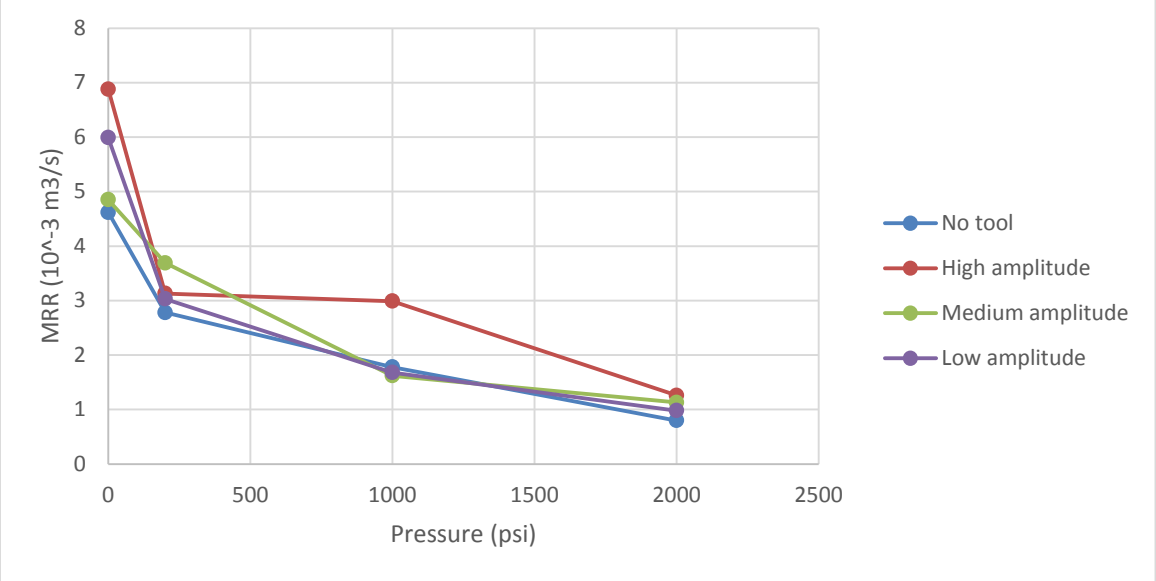

Figure 5.5: Graphical illustration of MRR results of the Hydropulse simulations

As the figure shows, high amplitudes of pulses result in high MRR values which is in agreement with reality (the more force, the more rock removed). According to the calculations, high amplitude of suction pulses which corresponds to the high level of flow rate (250 gpm) can result in an MRR increase of 55 to 65 % depending on the bottom-hole pressure.

In order to verify these results, the ROP values were also calculated for the simulation runs. These values are shown in Table 5.7 and graphically in Figure 5.6.

Table 5.7: ROP (cm/s) results of the Hydropulse simulations

Amplitude of pulsation (KN)	Pressure (psi)			
	0	200	1000	2000
No tool	3.33	1.75	1.25	0.67
High amplitude (198.5)	6.52	3.08	2.28	0.93
Medium amplitude (138.3)	3.67	3.33	1.22	0.86
Low amplitude (79.17)	5.20	3.5	1.14	0.85

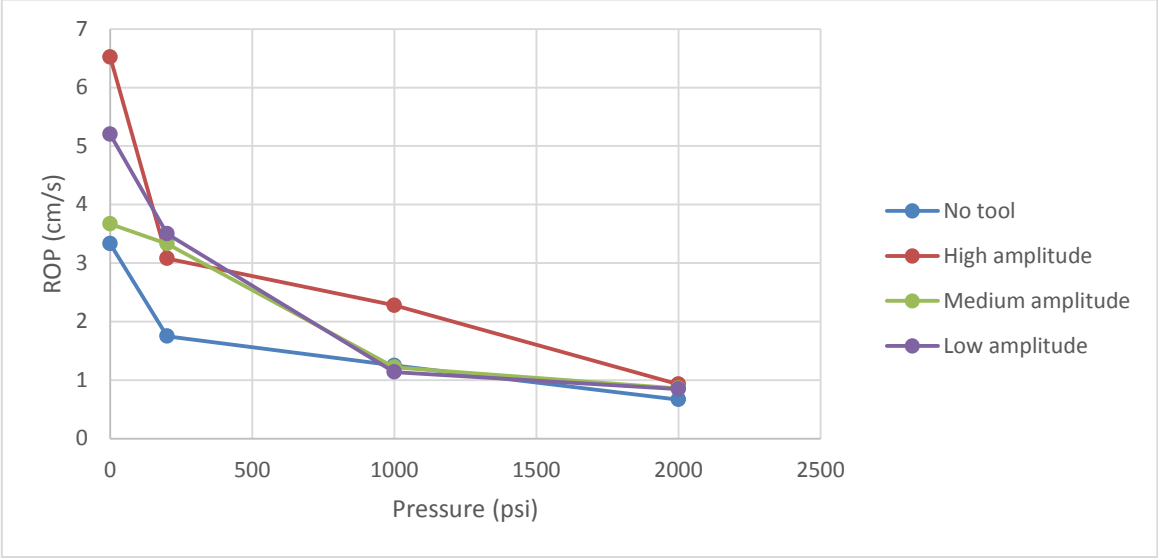

Figure 5.6: Graphical illustration of ROP results of the Hydropulse tool simulations

The ROP results are consistent with the results obtained by calculating MRR values and show the same trend. It can be seen that high amplitude of pulsation has the best performance.

As mentioned earlier in Chapter 4, the MRR and ROP results are not enough to evaluate the drilling performance of a system since the amount of consumed rig power

during drilling is not considered in calculations of these values. The MSE value is a proper indicator of the drilling performance when it comes to total costs of rig and power consumption. Table 5.8 and Figure 5.7 summarize the MSE results of the Hydropulse tool simulations.

Table 5.8: MSE (KJ/m^3) results of the Hydropulse tool simulations

Amplitude of Pulsation (KN)	Pressure (psi)			
	0	200	1000	2000
No tool	5850	7550	10700	23700
High amplitude (198.5)	4120	6880	5870	19500
Medium amplitude (138.3)	5520	5790	12600	19200
Low amplitude (79.17)	4800	7150	11800	22800

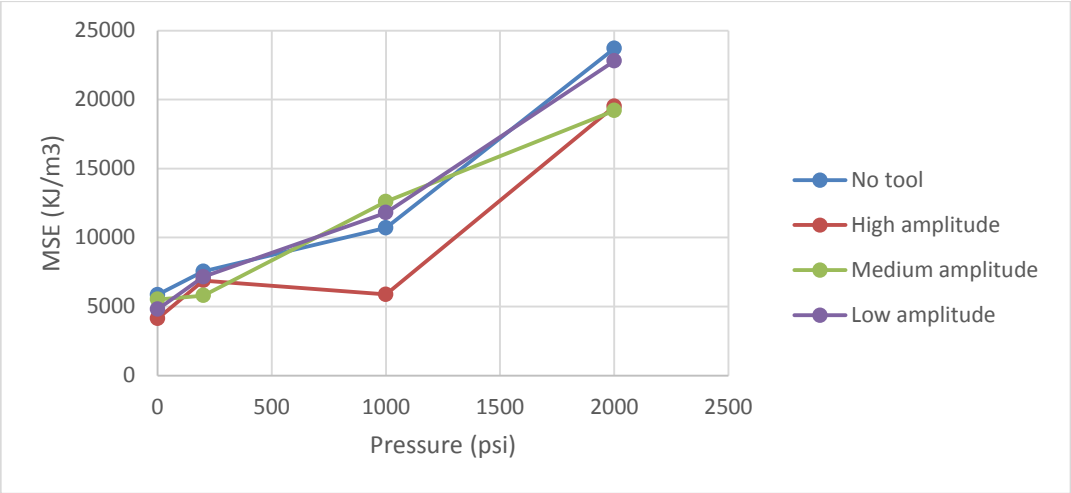

Figure 5.7: Graphical illustration of MSE results of the Hydropulse tool simulations

As the results show, high amplitude of pulsation has better performance compared to others. It causes the MSE values to be decreased by 50 %. However, similar to the MRR and ROP results, the medium and low amplitudes of pulsations do not have significant effect on drilling performance.

5.4 Comparison and Conclusion

Results of the AGT and the Hydropulse tool simulations are compared in this section to find out which tool (i.e. which type of force profile behind the bit) has better performance in drilling medium strength rocks. For this purpose, the MRR and MSE results of both tools in three different bottom-hole pressures (0, 1000 and 2000 psi) are compared to each other and to the conventional drilling scenario with constant static loading on no compliant shock tool. Figure 5.8 shows the MRR results for both tools. As the figure shows, the AGT's overall performance is better than the Hydropulse tool. In particular, at the bottom-hole pressure of 2000 psi, the AGT was shown to increase MRR significantly, which was 200 % better than with the Hydropulse tool and 400 % better than with conventional drilling.

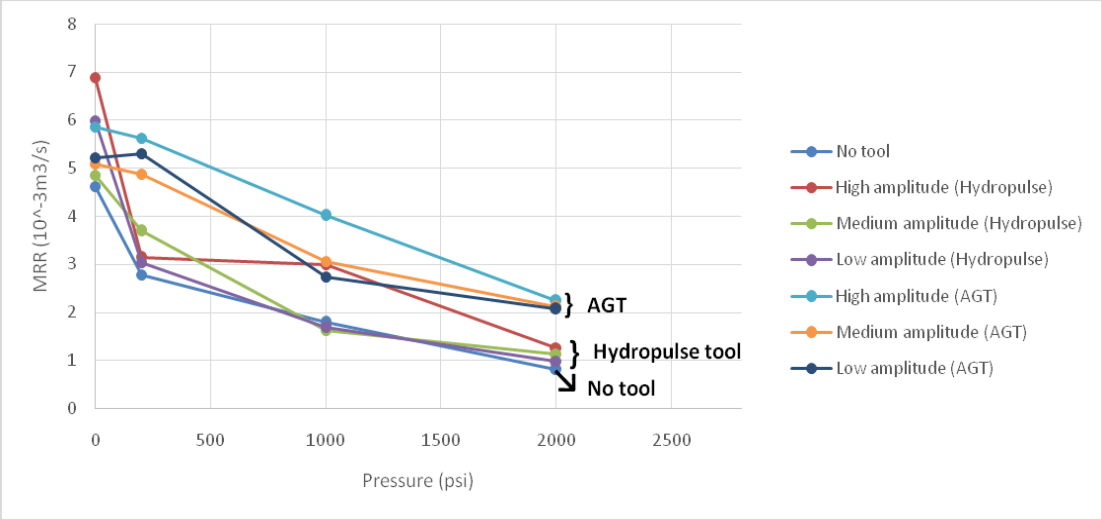

Figure 5.8: MRR comparison of the AGT and the Hydropulse tool

Both tools can increase ROP but the effect of the AGT which represents the vibration drilling (sinusoidal force profile) is much more significant than the effect of the Hydropulse tool (impact force profile). The effects of both tools are not evident in lower pressures but at higher pressures, they influence the MRR value significantly.

In order to compare both tools from cost and power consumption prospectives, the MSE results are presented in Figure 5.9. The figure implies that the AGT has better performance compared to the Hydropulse tool and conventional drilling. The MSE values for the AGT are much lower than those of the Hydropulse tool and conventional drilling (constant static load).

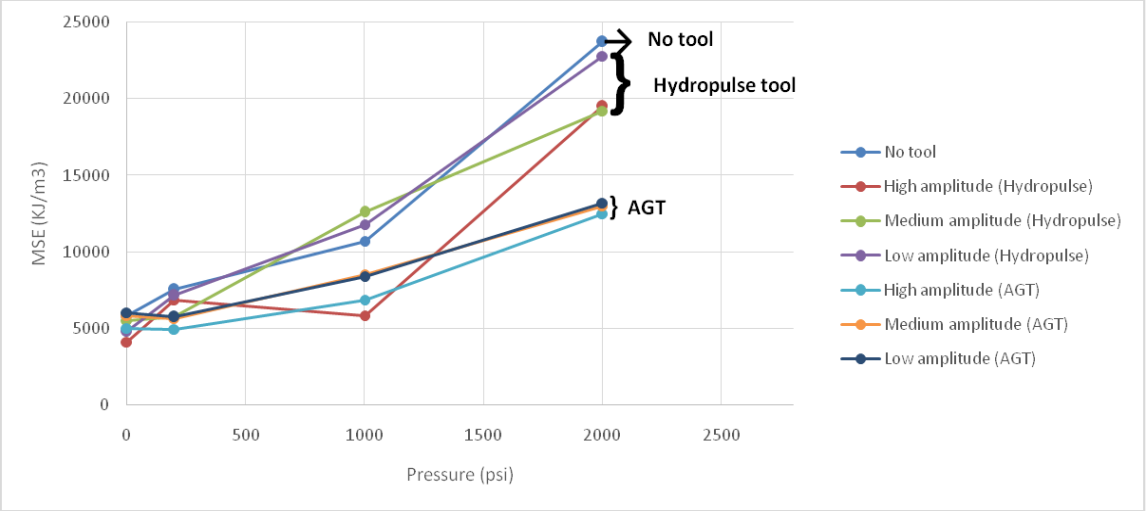

Figure 5.9: MSE comparison of AGT and Hydropulse tool performance

Simulation of the both the AGT and the Hydropulse tool revealed that in order to increase drilling performance in medium strength rocks, use of low amplitude vibration instead of high amplitude impacts is more effective. It should be recalled that the lowest amplitude of pulsation for the Hydropulse simulations was more than the static WOB (79.17 KN). Even this huge amplitude of force couldn't increase penetration rate the same amount that low amplitude vibration (2.7 KN) did. Two main factors are assumed to account for this issue:

The first factor is the profile of applied force. Considering that the force profile of the Hydropulse tool is in impact form, it can be concluded that short duration of pulses in the Hydropulse tool will create impact loads on the cutter which are similar to a rotary percussion hammer drill bit that is known to increase ROP in high strength rocks but have minimal benefit in medium strength rocks [40].

An appropriate analogy of increasing ROP by vibration in medium and weak strength rocks can be imagining a small vibrating object in loose and very fine sand. If the small vibrating object is placed on the top of very fine grain sand and allowed to vibrate, it will penetrate downward after a while. However, if the same object but without vibration is placed at the same area, it will never penetrate downward.

The second factor for the better performance of the AGT may be the existence of the shock tool in its assembly. The effect of shock tool or compliance is explained in detail in Chapter 6 through analyses of additional simulations that were done to see the effect of compliance on drilling performance.

Chapter 6 Effect of Axial Compliance and Conclusion

This chapter presents the conclusions and necessary discussions about the simulations of the AGT and the Hydropulse tool. These simulations were described and analyzed separately in previous chapters. However, a summary of these analyses is presented in this chapter.

As stated earlier, besides comparing the drilling performance of the AGT and Hydropulse tool, this thesis aims to investigate the effect of axial compliance (shock tool) in drilling performance. As a result, one section of this chapter is dedicated to this purpose.

This chapter consists of two main parts. The first part is about the effect of shock tool in the drilling performance of both tools. Besides previous simulations, additional simulations

were conducted to investigate this effect. Results of these simulations with correspondent discussions and conclusions are presented in this part. At the second part, the final conclusion about the drilling performance of the two investigated tools is presented and future investigations are suggested.

6.1 Effect of Axial Compliance

Compliance was mentioned as one of the reasons that affected the drilling performance in Chapter 5. Shock tools are usually used in drilling to isolate the drill string from bit vibrations. The operating mechanism of a shock tool was described in Chapter 3 and simulation scenarios to simulate the effect of the shock tool were described in Chapter 4. In order to investigate the effect of shock tool in drilling performance, two more simulations (one for the AGT and one for the Hydropulse tool) were conducted. It should be noted that shock tool was included in the simulation of the AGT and no shock tool was included in the Hydropulse tool scenario. As a result, additional simulations were conducted for the AGT without the shock tool and for the Hydropulse tool including shock tool. All other parameters are exactly same for both of the simulations. For both of the simulations, the highest level of amplitude was selected (high amplitude of oscillation). Both of the simulations were conducted for a bottom-hole pressure of 1000 psi, with the corresponding MSE and MRR results presented in Table 6.1.

Table 6.1: Simulation results of the AGT without shock tool and the Hydropulse tool with shock tool

AGT without shock tool		Hydropulse tool with shock tool	
MSE (KJ/m^3)	MRR (10^{-3} m^3/s)	MSE (KJ/m^3)	MRR (10^{-3} m^3/s)
338000	0.08	5680	4.88

As can be seen from the table, very low MRR value for the AGT and very high values for the Hydropulse tool and the same results for the MSE values reveals the effect of the shock tool in the process. During the simulation of the AGT without shock tool, the cutter bounced to a level higher than its initial position. As a result, for most of the times, the MRR value for the process was negative. Negative value of MRR means bit bounce in this context. Figures 6.1 and 6.2 show the drilling performance for the both AGT and the Hydropulse tools with and without including the compliance element, respectively. As the figures show, the AGT had very poor performance in the absence of the compliance element. The sinusoidal force exerted to the cutter caused whole assembly to bounce. Consequently, low ROP and at some cases negative penetration was resulted. On the other hand, the Hydropulse tool had excellent performance with very high ROP when used with the shock tool. Further the effect of compliance is greater on the AGT than the Hydropulse tool. As mentioned before, this tool gives negative ROP or MRR value in the absence of the compliant element. Therefore, the effect of compliance behind the bit seems to be much more significant than it was thought before.

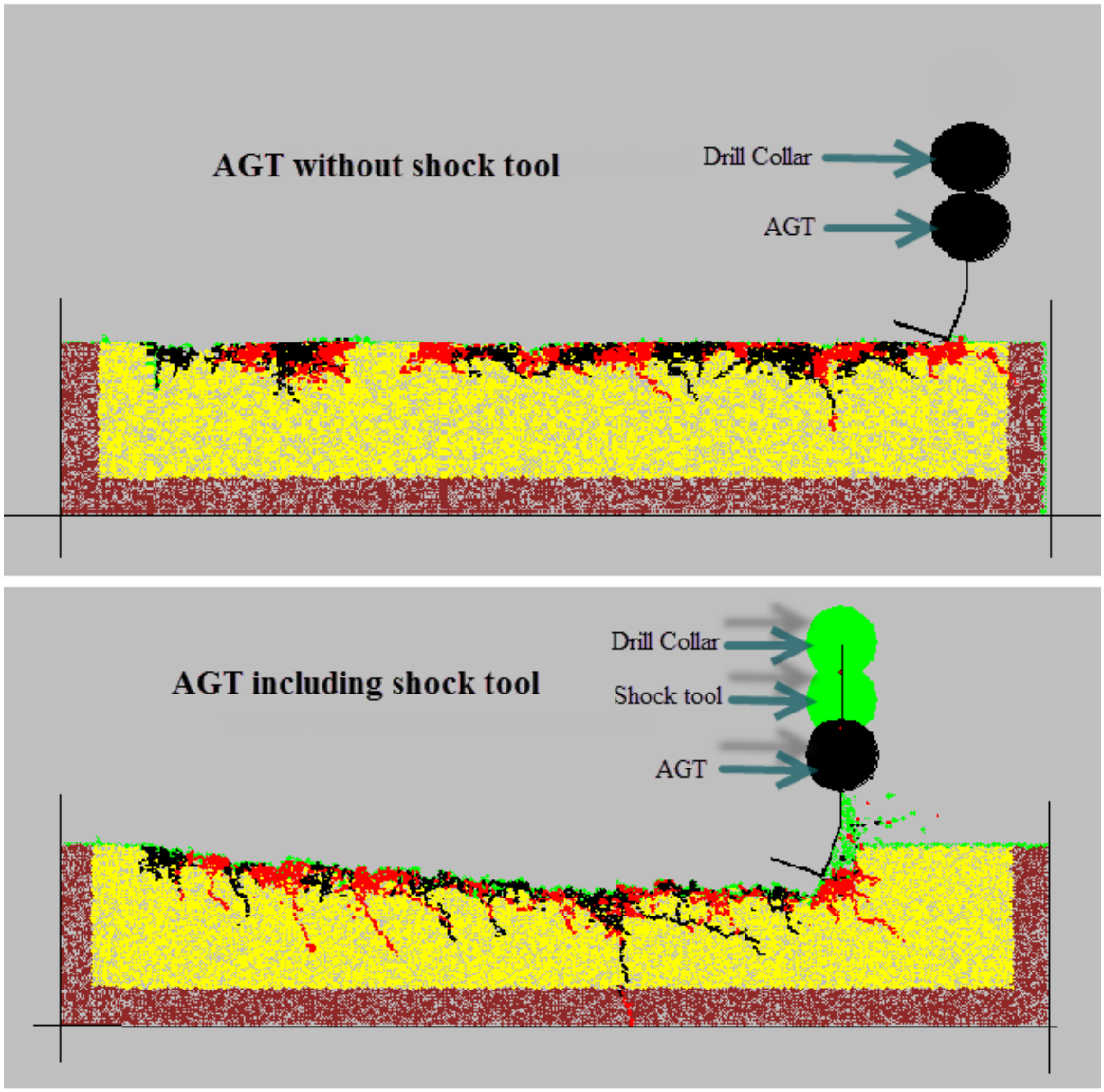

Figure 6.1: Effect of shock tool in drilling performance of the AGT (Bottom-hole pressure of 1000 psi, WOB of 60 KN and sinusoidal force amplitude of 19.25 KN)

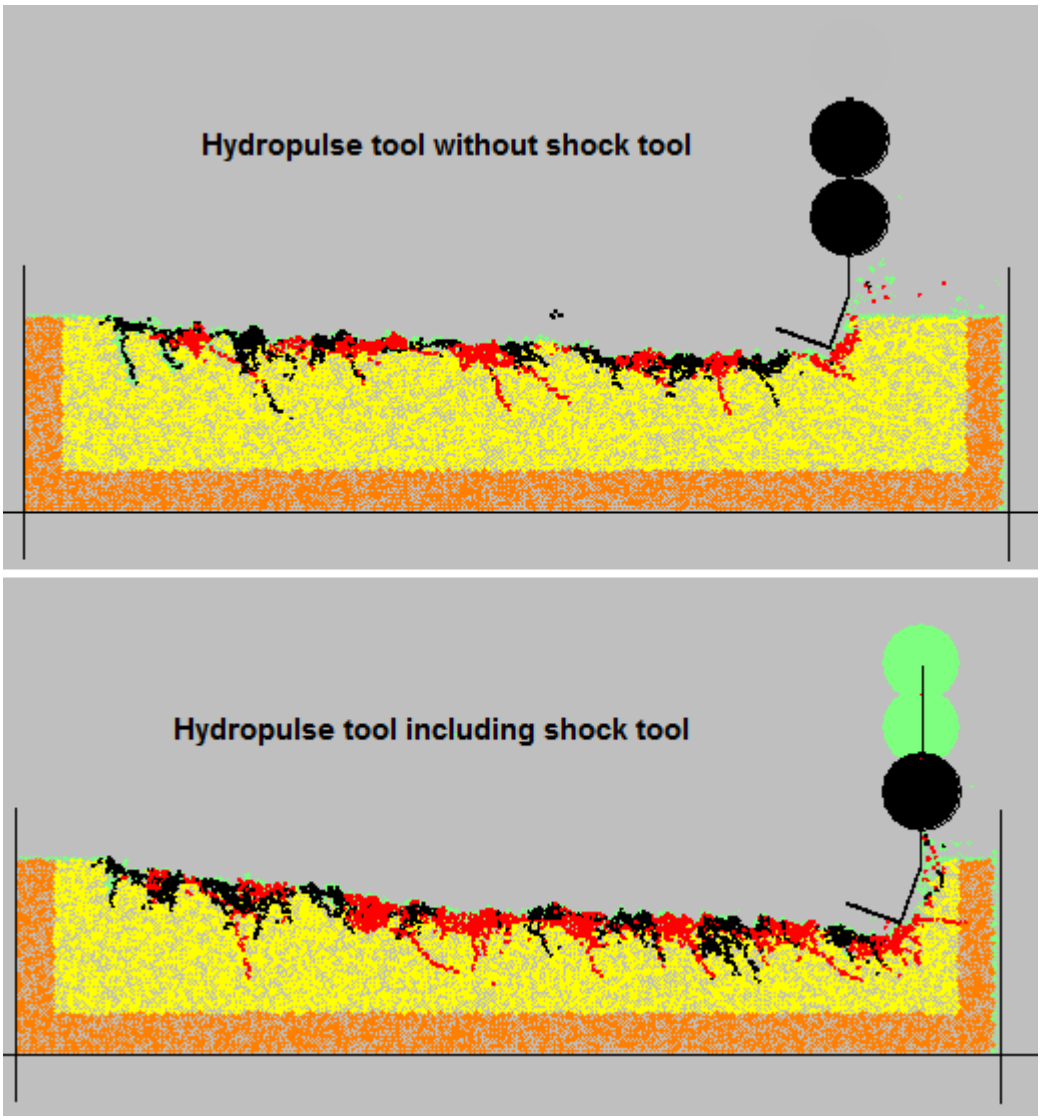

Figure 6.2: Effect of shock tool in drilling performance of the Hydropulse tool (Bottom-hole pressure of 1000 psi, WOB of 60 KN and pulse amplitude of 198.5 KN)

Comparing the drilling performance of the both tools with and without shock tool, it can be concluded that shock tool can increase ROP by more than 100 %. For example, the MRR value for the high amplitude impact force of the Hydropulse tool in the bottom-hole pressure of 1000 psi was around $2.28\times 10^{-3} m^3/s$ while at the same condition with shock tool,

the MRR value of 4.88 × $10^{-3}m^3/s$ was obtained which is more than a 100 % increase. The effect of shock tool is even more significant for the AGT because of the nature of its force profile. Negative forces applied by the tool to the cutter are normally damped by the shock tool but in the absence of the shock tool, these forces cause the whole assembly to bounce.

6.2 Conclusion

This thesis evaluated hydraulic pulsed tools and their potential impact on ROP. An extensive literature review was done about the penetration mechanism of drag bits and different models proposed by well-known authors were introduced. A summary of case studies about different hydraulic pulsed tools was presented and operational mechanism of these tools was described.

DEM modeling was used to simulate the action of the AGT and the Hydropulse tools. A brief overview of the method as well as descriptions about simulation software were presented. Finally, unique simulation scenarios were selected to simulate the action of the AGT and the Hydropulse tool both with and without the accompanying shock tool.

Simulation results showed significant increase in drilling performance when the AGT and Hydropulse tool was deployed. However, the performance of the AGT was better than that of the Hydropulse tool. Simulation parameters were based on a variety of sources including technical tool specifications, operations guidelines and both published and unpublished experimental data. Analyses of results showed that the power required to drill a unit volume of the medium rock is much less in vibration drilling as compared to

conventional drilling. Two main reasons for the poorer performance of the Hydropulse tool were suggested. The first was the duration of the pulses which prevents significant load increase on the cutter, and the second one was the absence of shock tool and corresponding axial compliance in the system.

Results of additional simulations showed significant effect of axial compliance in drilling performance. Calculated MRR and MSE values for simulation of the Hydropulse with shock tool suggested significant increase in drilling performance compared to the same condition without the shock tool. More than a 100 % increase in drilling rate was observed when shock tool was used in the drilling process. On the other hand, the MRR and MSE values for the AGT without shock tool showed poor performance of the tool.

The positive effect of axial compliance on drilling performance was clearly illustrated in this thesis and further investigation in this area should continue.

DEM is an appropriate method to simulate the vibration drilling process. Output results from the DEM software are in a good agreement with real life conditions. For example, the ROP vs. pressure graph obtained from the DEM simulations is compatible with the graph obtained from experiments where an exponential decrease in drilling rate with increase in down-hole differential pressure is observed.

References

[1] Costs for Drilling the Eagle Ford by Trey Cowan. Retrieved from https://www. rigzone.com/news/article.asp?a_id=108179.

[2] Bonham, K. (2007, Dec 28). Drilling horizontal. Grand Forks Herald. Retrieved from http://search.proquest.com/docview/376048898?accountid=13158.

[3] Kolle J.J. "A Model of Dynamic Confinement During Drilling in Pressurized Borholes" Int. J. Rock Mech. Min. Sci. &Geomech. Abstr. Vol.30, No.7, pp. 1215-1218, 1993, Printed in Great Britain.

[4] Adam T. Bourgoyne Jr., et al. (1991). Applied Drilling Engineering. Richardson TX: Society of Petroleum Engineers.

[5] Ledgerwood, L.W., "Efforts to Develop Improved Oilwell Drilling Methods" Presented at first API Drilling Research Symposium, Jan. 13 – 14, 1960.

[6] Rock properties and their importance to stoneworking, carving, and lapidary working of rocks and minerals by the ancient Egyptians by (ArchaeSolenhofen) retrieved from: http://www.oocities.org/unforbidden_geology/rock_properties.htm

[7] Schlumberger PDC Smith Bits Data Sheet. Retrieved from www.slb.com/pdc.

[8] Glowka, David A., SPE, and Sandia Natl. Laboratories, "Use of Single-Cutter Data in the Analyses of PDC bit Designs: Part 1- Development of PDC Cutting Force Model" JPT, August 1989.

[9] Sellami, H., Fairhurst, C., Deliac, E. and Delbast, B., "The Role of In-situ Rock Stresses and Mud Pressure on the Penetration Rate of PDC Bits" ISBN 9061919754, Rock at Great Depth, Maury & Fourmaintraux (eds), 1989

[10] Detournay, E. and Detournay, P. "A Phenomenological Model for the Drilling Action of Drag Bits" International Journal of Rock Mechanic and Mining Science, Vol.29, No.1, pp. 13-23, 1992, Printed in Great Britain.

[11] Detournay, E., Richard, T. and Shepherd, M. "Drilling Response of Drag Bits: Theory and Experiment" International Journal of Rock Mechanic and Mining Science, Vol. 45, pp. 1347-1360, 2008.

[12] Gerbaud, L.,Menand, S., Sellami, H., "PDC Bits: All Comes from the Cutter/Rock Interaction" IADC/SPE 98988, Presented at the IADC/SPE Drilling Conference, 21-23 February 2006.

[13] Ledgerwood III, L.W., "PFC modeling of Rock Cutting under High Pressure Conditions" Hughes Christensen Company, The Woodlands, Texas, USA

[14] Kolle, J.J., "Hydraulic Pulse Drilling: Final Report" Presentation for GTI Natural Gas Technology II Conference, February 8 – 11, 2004.

[15] Erik Trostmann. (1996). Water Hydraulics Control Technology. New York, NY. Danfoss A/S.

[16] Kolle, Jack J., Marvin, and Mark M. "Suction Pulse Drilling System" Results of A Phase I Feasibility Study" Tempress Technologies Inc.

[17] Newman, K., Burnett, T., Pursell, J., Gouasmia, O., and NOV "Modeling the Effect of a Down-hole Vibrator" SPE 121752, Presented at SPE/ICoTA Coiled Tubing and Well Intervention Conference and Exhibition, 31 March – 1 April 2009.

[18] Baker Hughes Incorporated (1998). Navi-Drill Motor Handbook. Baker Hughes Incorporated.

[19] McCarthy, J.P., Stanes, B.H., Clark, K.W., Leuenberger, G.E., Rebellon, J., Grabski, L.E., "A Step Change in Drilling Efficiency: Quantifying the Effects of Adding an Axial Oscillation Tool within Challenging Wellbore Environments" SPE/IADC 119958, presented at the SPE/IADC Drilling Conference and Exhibition, Amsterdam, Netherland, 17-19 March, 2009.

[20] Skyles, Lane P., Amiraslani, Yousef A., National Oil Varco, Wilhoit, James e., and Devan Energy, " Converting Static Friction to Kinetic Friction to Drill Further and Faster in Directional Holes" SPE/IADC 151221 Presented at 2012 SPE/IADC Drilling Conference and Exhibition, 6-8 March 2012.

[21] Robertson, L., Mason, C. J., Sherwood, A. C., Newman, K. R., SPE, Andergauge Ltd. "Dynamic Excitation Tool: Developmental Testing and CTD Field Case histories" SPE 89519, Presented at the SPE/ ICoTA Coiled Tubing Conference and Exhibition, 23 – 24 March 2004.

[22] Rasheed, W., SPE, Andergauge Ltd. "Extending the Reach and Capability of Non-rotating BHAs by Reducing Axial Friction" SPE 68505, Presented at the SPE/ICoTA Coiled Tubing Roundtable, 7 – 8 March 2001.

[23] Thomas, R., Hartwig, D., McKeever, S., ConocoPhillips Alaska, Inc.; Egedahl, D., ASRC Energy Services E&P Technology, Inc.; Patton, J., Holtzman, K., Halliburton–Sperry Drilling Services; Smith, L.,Halliburton-Security DBS/Alaskan Energy Resources "Overcoming Weight Transfer Challenges in Complex, Shallow, Extended Reach Wells on Alaska's North Slope" OTC 19550, Presented at Offshore Technology Conference, 5 – 8 May 2008.

[24] Cheng, R., Ge, Y., Wang, H., SPE, CNPC Drilling Research Institute, Ni, H., Zhang, H., Sun, Q., "Self-Oscillation Pulsed Percussive Rotary Tool Enhances Drilling Through Hard Igneous Formations" IADC/SPE 155784, Presented at IADC/SPE Asia Pacific Drilling Technology Conference and Exhibition, 9 - 11 July 2012.

[25] Luding, S., "Introduction to Discrete Element Method" Multi Scale Mechanics, TS, CTW, UTwnte

[26] "Particle Flow Code Manual", Itasca Consulting Group Inc. 4th edition, November 2008.

[27] "Agitator Tool Operating Guidlines" National Oil well Varco

[28] "Agitator Tool Handbook" National Oil well Varco

[28] Al Ali, A., Barton S., Mohanna A., and National Oil Varco "Unique Axial Oscillation Tool Enhances Performance of Directional Tools in Extended Reach Applications" SPE 143416, Presented at Brasil Offshore Conference and Exhibition, 14-17 June 2011.

[29] Eddison, A. M., Hardie, R. (2001). U. S. Patent No. 6, 279, 670 B1. Washington, DC: Patents and Trademark

[30] Bellville Spring Retrieved from: http://en.wikipedia.org/wiki/Belleville_washer.

[31] Kolle J.J., Marvin, M. H. (1998). U.S. Patent No. 6,237701 B1. Washington, DC: Patents and Trademark

[32] Vajdova, V., Baud, P. & Wong, T.F, 2004, "Compaction, dilatancy, and failure in porous carbonate rocks"Journal of Geophysical Research 109.

[33] Wong, T.F. & Baud, P. 1999, "Mechanical compaction of porous sandstone" Oil and Gas Science and Technology.

[34] Liao, C.M. (2011). Experimental and Numerical Studies of Drill-string Dynamics. (Doctoral Dissertation) Available from University of Maryland website.

[35] Robert F. Mitchell and Stefan Z. Miska. (2011). Fundamentals of Drilling Engineering. Richardson TX: Society of Petroleum Engineers

[36] NOV Griffith Shock tool, Retrieved from:http://www.nov.com/Downhole/Drilling_Tools/Shock_Tools/DRILLING_SHOCK_TOOL.aspx

[37] Mohammad Mozaffari, 2013, DEM Modeling of Bit/Rock Interaction: An Overview of the Developed PFC2D Toolkit [Toolkit presentation], April 29, Online meeting using GotoMeeting

[38] Teale, R., 1965, "the concept of specific energy in rock drilling" Intl. J. Rock Mech. Mining Sci., 2, 57-53.

[39] Rafatian, N., Miska, S., Ledgerwood, L. W., Ahmed, R., "Experimental Study of MSE of a Single PDC Cutter under Simulated Pressurized Conditions" IADC/SPE 119302, presemted at IADC/SPE Drilling Conference and Exhibition, Amsterdam, Netherland, 17-19 March, 2009

[40] Han, G., Bruno, M., Grant, T. "Lab Investigations of Percussion Drilling: from Single Impact to Full Scale Fluid Hammer" ARMA/USRMS 06-962, Presented at 41st U.S. Symposium on Rock Mechanics, Golden, Colorado, 17 – 21 June, 2008

Appendix A

Drilling AGT

Tool Size (OD)	3¾"	4¾" (High Flow)	5" (High TORQUE)	6½"	6¾"	8"	9⅝"
Overall Length	12½ ft	8¾ ft	8¾ ft	6 ft	9 ft	11 ft	12 ft
Weight	240 lbs	310 lbs	498 lbs	900 lbs	1,000 lbs	1,600 lbs	2,000 lbs
Recommended Flow Range	90-140 gpm	150-270 gpm 250-330 gpm	150-270 gpm 250-330 gpm	375-475gpm	400-600 gpm	500-1,000 gpm	600-1100 gpm
Temp Range*	150°C	150°C	150°C	150°C	150°C	150°C	150°C
Operating frequency	26 Hz @ 120 gpm	18-19 Hz @ 250 gpm 16-17 Hz @ 250 gpm	16-17 Hz @ 250 gpm	15 Hz @ 400 gpm	16-17 Hz @ 500 gpm	16 Hz @ 800 gpm	12-13 Hz @ 900 gpm
Operational Pressure drop generated	500 700 psi	550 650 psi	550 650 psi	600 700 psi	600 700 psi	600 800 psi	600 800 psi
Max Pull	230,000 lbs *depending on service connection	260,000 lbs	500,000 lbs	570,000 lbs	570,000 lbs	930,000 lbs	1,145,000 lbs
Connections	2⅜" IF, 2⅞" IF 2⅞" AMOH, 2⅞" REG pin/box	3½" IF pin/box	4" GRANT PRIDECO XT39 pin/box	4½" XH, 4" IF pin/box or NC46 pin/box	4½" IF pin/box	6⅝" REG pin/box or NC-56 pin/box	7⅝" REG box up 7⅝" REG pin down or 05⅛" REG pin down

Coiled Tubing AGT

Tool Size (OD)	2⅛"	2⅜"	2⅞"	2⅞" (HF)	3⅛" (HF)	3⅜"	3-3/8" (HF)
Overall Length	6 ft	6 ft	5¾ ft	7 ft	7 ft	6½ ft	7 ft
Weight	80 lbs	90 lbs	100 lbs	100 lbs	125 lbs	125 lbs	145 lbs
Recommended Flow Range	40-80 gpm	40-80 gpm	40-80 gpm	40-140 gpm	40-140 gpm	90-140 gpm	40-140 gpm
Temp Range*	150°C	150°C	150°C	150°C	150°C	150°C	150°C
Operating frequency	9 Hz @ 40 gpm	9 Hz @ 40 gpm	15 Hz @ 40 gpm	9 Hz @ 120 gpm	9 Hz @ 120 gpm	26 Hz @ 120 gpm	9 Hz @ 120 gpm
Operational Pressure drop generated	600-800 psi	600-800 psi	600-800 psi	500-700 psi	500-700 psi	450-700 psi	500-700 psi
Max Pull	20,000 lbs	20,000 lbs	85,000 lbs	85,000 lbs	130,000 lbs	150,000 lbs	150,000 lbs
Connections	1½" AMMT pin/box	1½" AMMT pin/box	2⅜" PAC pin/box	2⅜" PAC pin/box	2⅜" REG pin/box	2⅜" REG pin/box or 2⅞" REG pin/box	2⅜" REG pin/box or 2⅞" REG pin/box

Appendix B

AGT run sheet and calculated parameters:

Run No.	Down-Hole Pressure (psi)	Magnitude of Force Oscillation (N)	Oscillation Frequency (Hz)	Rate of Penetration (cm/s)	Material Removal Rate (10^{-3} m^3/s)	MSE (KJ/m3)
1	0	540	7	5.21	5.20	5880
2	0	2040	14	3.175	5.00	5830
3	0	3850	20	3.76	5.77	5070
4	100	540	7	3.57	4.81	6120
5	100	2040	14	4.43	4.99	5050
6	100	3850	20	5.23	5.15	6250
7	200	540	7	3.71	5.23	5940
8	200	2040	14	3.25	4.76	5730
9	200	3850	20	4.21	5.49	5000
10	1000	540	7	3.00	2.73	8420
11	1000	2040	14	3.52	3.05	8530
12	1000	3850	20	4.16	4.01	6880
13	2000	540	7	2.2	2.06	13200
14	2000	2040	14	2.45		
15	2000	3850	20	2.75	2.23	12500
16	0	0	0	3.33	4.64	5650
17	100	0	0	2.28	3.48	6490
18	200	0	0	1.75	2.73	7740
19	1000	0	0	1.25	1.76	10700
20	2000	0	0	0.675	0.80	23700

Appendix C

MSE and MRR Calculation

MRR value

In order to calculate MRR value for different runs, simple summation method was used. In this method, area removed by the cutter is divided to a series of rectangles each having one time-step width. Then width and length of each of these rectangles are calculated using the x and y position of the cutter tip throughout the drilling process. Using Excel worksheet, all of the rectangles are then added up to calculate the total volume of removed rock over a specific period of simulation time. By dividing this volume by drilling time, the MRR value for the process is calculated.

MSE Value

Calculation of MSE value was based on MSE definition which is amount of energy consumed to remove specific volume of rock. In order to calculate the amount of energy during the process, concept of work was applied.

$$W = F * d$$

Where W denotes the amount of work that is done by force F over a length of d.

Using above concept, every time-step the amount of energy consumed on the cutter is calculated using cutter displacement and amount of force applied on the cutter. At the end of the process, total energy consumed over the entire process is calculated. Using this energy and the removed volume that was obtained from MRR calculations, the MSE value can be calculated as follow:

MSE = Amount of energy consumed / Amount of rock removed

Both MSE and MRR values for the different simulation runs are calculated using Excel sheet since number of data point (time-step) exceed 200000. Since the time-step is two short for the simulations, the calculated MSE and MRR values can give good approximate of real values.

Appendix D

Calibrated Equation for the Hydropulse Tool

The mechanism of the Hydropulse tool is in a way that the magnitude of the produced suction pulse can be calculated by Judowsky equation provided. However, this equation is theoretical. The data from real experiments for the Hydropulse tool were used to calibrate and modify the equation. Figure below shows the bit face pressure profile obtained in flow loop tests using 9.3 Pound per Gallon (ppg) drilling mud and flow rate of 390 USGPM (0.0246 m^3/s) . Flow area of the tool that was used in this experiment was 9.5 in^2 (0.0061 m^2). As we can see from the figure, suction pulse amplitude of around 450 psi is generated.

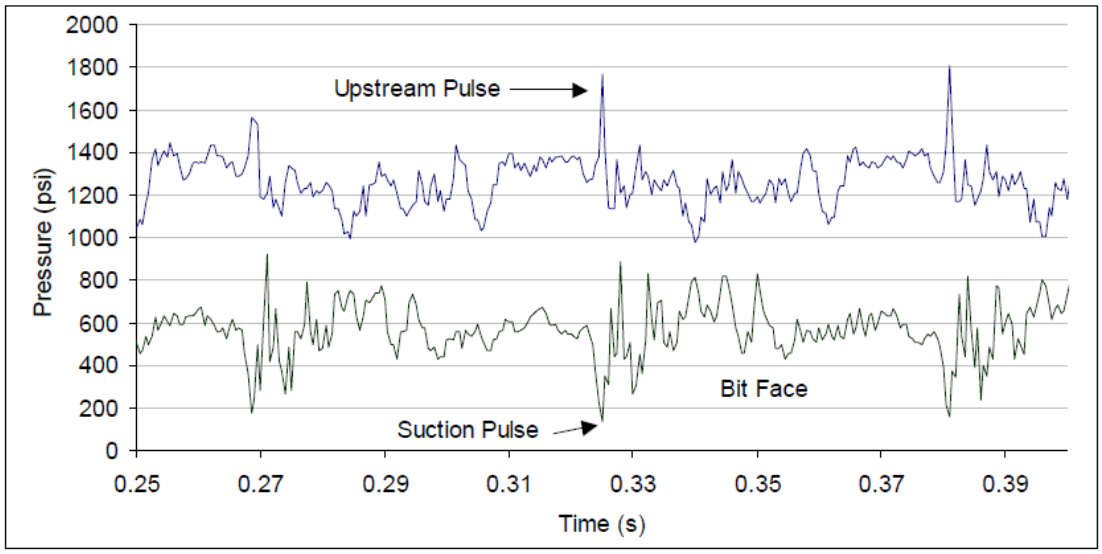

Using provided information the velocity of fluid in flow course can be calculated as follow:

$$v\ (m/s) = Q\ (m^3/s)/\ A\ (m^2) \qquad (5.1)$$

where, v is the velocity of fluid in flow course, Q is the flow rate, and A is the flow course area.

Using above information:

$$v = 0.0246/0.0061 = 4.033\ m/s$$

Using above velocity and knowing that the fluid density is 9.3 ppg (1114 kg/m^3) and assuming the fluid bulk modulus to be same as water (2.2 Gpa), the theoretical amplitude of pressure wave can be calculated using equation 1.1 as follow:

$$\Delta P = 4.033 * \sqrt{1114 * 2.2 * 10^9} = 6.3\ MPa = 915\ psi$$

Obtained theoretical value is approximately two times of the experimental value. As a result, equation 1.1 can be modified to satisfy the experimental values and can be used to predict the pressure pulse magnitudes for the simulations.

$$\Delta P = 0.5\ v\sqrt{\rho k_f}$$